

DISS. ETH NO. 29526

Advanced Polymer Synthesis and Chemical Recycling via Oxygen-Enhanced Controlled Radical Polymerization and Light-Induced Depolymerization Strategies

A thesis submitted to attain the degree of

DOCTOR OF SCIENCES

(Dr. sc. ETH Zurich)

presented by

KONSTANTINOS PARKATZIDIS

MSc, Master in Chemistry, University of Crete

born on *19.11.1992*

accepted on the recommendation of

Prof. Dr. Athina Anastasaki

Prof. Dr. Tae Lim Choi

Prof. Dr. Brent Sumerlin

2023

*This PhD thesis is dedicated to four remarkable teachers who have had a profound influence on my life
and have guided me towards the path I am currently walking.*

To:

Ms. Xrysi-Anna Veroniki

Ms. Diana Stefanidou

Prof. Maria Vamvakaki

Prof. Athina Anastasaki

Dedication

I firmly believe that education holds immense significance in one's life, regardless of the level. I consider myself incredibly fortunate to have had access to education and to have been taught by a diverse range of teachers. Among them, there were four particularly influential educators who made a lasting impact on my educational journey and transformed me as a person.

Starting from the 6th grade in high school, I had an incredible math teacher named Ms. **Chrysi-Anna Veroniki**. She was the first person in my education who taught me a vital lesson. One day, she handed out a sheet of paper with 10 equations and asked us to solve them. Despite not being a fan of math, I found this particular topic to be logical and solving equations came easily to me, unlike memorizing the multiplication table (yes, I still don't know it by heart to this day), so within a few minutes, I handed in my answers. At that point one of my classmates was very upset about not being able to solve the equations first and began to cry. In that moment, I felt a rush of guilt and asked the teacher not to evaluate my "exam" so that the other student wouldn't feel sad. It was on that day that she asked me to stay after the lesson for a talk. She said, "Listen closely, young boy. I don't know what you're going to do in your life, but whatever it is, give it your all! You shouldn't feel guilty for being good at something; you should feel proud. Never pretend to be anything less than what you are just to make someone else feel better, as you'll be doing them a great disservice". That day it became crystal clear that being good at something was perfectly fine.

The second person who had a significant influence on me was my chemistry teacher in the final year of high school, Ms. **Diana Stefanidou**. She was incredibly dedicated to her work and deeply cared about the success of her students. While I had always loved chemistry, I wasn't particularly fond of physical chemistry. One day, during an examination when it was my turn to answer a question, I rebelled and said, "I don't understand why you're so persistent on this part that seems pointless, instead of focusing on more interesting aspects of organic chemistry." To my surprise, she responded, "Oh well, I have failed miserably this year. If you see this part as meaningless, then I have failed to show you the beauty of chemistry." In that moment, I could sense that she truly meant every word she said, and she was disappointed in herself for not being able to convey the beauty of chemistry to me. It was then that I realized the significance of being completely dedicated and passionate about your job.

At university, I had a lot of great professors who deepened my love for science and taught me so many things. However, one of them was my favorite, and she taught us polymer chemistry. Professor **Maria Vamvakaki** was not only my professor for polymer chemistry classes, but also my supervisor for both my bachelor's and master's thesis. I could say endless things about what I gained from interacting with her, but I will try to mention a few that have shaped me academically.

Professor Vamvakaki is a role model for me. Her dedication to work, enthusiasm, and care for what she does had an immense impact on me. Even in the challenging research environment in Greece, she always manages to be exceptional and give her best for research and to her students. As a supervisor, Professor Vamvakaki provides the necessary space for individual growth, yet this

freedom is accompanied by the absolute certainty that she will be there whenever one needs her support. It was the best start I could have wished for on my academic journey. I had the freedom to work and develop my ideas with an absolute sense of support. I felt like a child learning how to walk, unafraid because I knew there would always be a parent around to intervene if necessary. Another characteristic of hers that I greatly admire is her ability to help you improve without making you feel inadequate. I will never forget her comment after my first oral presentation as an undergraduate student in a conference. She was genuinely proud of me and said, "That was an excellent first time. You presented this part and that part very nicely. Next time, try to put more emphasis on and improve this particular aspect." This was her approach, always acknowledging my work and pointing out areas for improvement in a manner that suited me best. Her advice holds significant weight for me. Even 5 years after leaving her group, she is the first person who comes to mind when I have to make an important decision or when I find myself in a difficult situation. I always seek her advice, and I know I will receive her response no later than midnight on the same day. This aspect makes her incredibly special to me and highlights that our connection extends beyond a regular student-advisor relationship. I could never fully express my gratitude to her, so what I strive to do is make her as proud as possible through my actions and by incorporating the work ethic I learned from her.

Last but certainly not least, I must express the immense impact that my PhD advisor, Professor **Athina Anastasaki**, had on me. She is undeniably one of the sharpest minds I have ever encountered. Beyond her intelligence and knowledge, what truly impresses me is her remarkable emotional intelligence and her ability to handle challenging situations. There are countless aspects I could mention about her, but what truly stands out to me is her willingness to adapt her supervisory approach and meet me halfway, resulting in highly productive interactions. This has been an invaluable lesson for me, teaching me how to navigate diverse personalities in a professional setting and fostering my own flexibility. Additionally, her exceptional organizational skills and attention to detail never fail to amaze me. I am constantly surprised by her ability to forecast and plan with such precision. This skill is of paramount importance and makes a tremendous difference. I strive to absorb as much of it as possible, enabling me to concentrate, organize my thoughts, and take actions that lead to productivity. Professor Anastasaki is not only an exceptional mentor, but she is also someone who genuinely supports and takes pride in her students' achievements. It is this unwavering support that acts as a catalyst for our relationship. The admiration, respect, and acceptance I have for her form the foundation of our connection. Furthermore, I have no doubt that she has my best interests at heart and truly desires to see me succeed and grow.

I am well aware that it is challenging to give back even a fraction of what I have gained from their guidance, but I will forever be grateful for their efforts, and I will try to pay back by trying to inspire someone else as much as they have inspired me.

For me, true success in my academic career will be achieved if I will manage to inspire and ignite a passion for science in even one of my students, just as my role models have done for me.

Table of Contents

List of Schemes	7
List of Figures	7
List of Tables	11
Acknowledgments	14
Summary	18
Zusammenfassung	21
Chapter 1: General Introduction	26
Free Radical Polymerization	27
Anionic Polymerization	28
Reversible Deactivation Radical Polymerization	29
Nitroxide-Mediated Polymerization	30
Atom Transfer Radical Polymerization	31
Reversible Addition-Fragmentation Chain-Transfer (RAFT) Polymerization	31
Main Characteristics of Reversible Deactivation Radical Polymerization	32
Recent Developments in Reversible Deactivation Radical Polymerization	34
References	51
Chapter 2: Oxygen-Enhanced Atom Transfer Radical Polymerization through the Formation of a Superoxido Copper Complex	55
Summary	55
Introduction	56
Results and Discussion	58
Discovery of Oxygen-Enhanced Atom Transfer Radical Polymerization	58
Mechanistic Investigation	64
Investigation into the Scope of Oxygen-Enhanced ATRP	67
Synthesis of a Multiblock Copolymer	67
Synthesis of Block Copolymers	68
Synthesis of High Molecular Weight Polymers	69
Polymerization of Different Monomers	71
Polymerization with Copper of Different Levels of Purity	72
Conclusions	73
References	74

Chapter 3: Photocatalytic ATRP Depolymerization: Temporal Control at Low ppm Catalyst Concentration	77
Summary	77
Introduction.....	77
Results and Discussion	81
Conclusion	91
References	91
Chapter 4: Photo-Induced Iron-Catalyzed ATRP of Renewable Monomers in Low-Toxicity Solvents: A Greener Approach	93
Summary	93
Introduction.....	94
Results and Discussion	95
Conclusion	105
References	106
Chapter 5: Transformer-Induced Metamorphosis of Polymeric Nanoparticle Shape at Room Temperature	108
Summary	108
Introduction.....	108
Results and Discussion	112
Conclusion	124
References	125
Curriculum Vitae.....	Error! Bookmark not defined.

List of Schemes

Scheme 1. 1: Simplified mechanism of free radical polymerization.....	28
Scheme 1. 2: Simplified mechanism of anionic polymerization	29
Scheme 1. 3: Simplified mechanism of NMP, ATRP and RAFT polymerization.....	30
Scheme 2. 1: General reaction scheme illustrating the polymerization of MA via ATRP	58
Scheme 2. 2: Schematic representation of conventional ATRP in which the formation of the catalyst occurs under inert atmosphere	58
Scheme 2. 3: Schematic representation of oxygen-enhanced ATRP in which the formation of the catalyst occurs under ambient atmosphere	61
Scheme 2. 4: Proposed oxygen-enhanced ATRP mechanism.....	66
Scheme 3. 1: Proposed mechanism of photocatalytic ATRP depolymerization	86
Scheme 4. 1: Synthesis of sustainable biomass-derived monomers and their corresponding polymers.....	95
Scheme 4. 2: General schematic illustration for the synthesis of renewable monomers.....	95
Scheme 5. 1: Schematic illustration and highlights of transformer-induced metamorphosis (TIM)	113

List of Figures

Figure 1. 1: Main characteristics of RDRP. a) Ability to target specific molecular weight, b) Control over the polymer dispersity by manipulating the activation-deactivation equilibrium, c) Linear relationship between monomer conversion and number average molecular weight, d) High end-group fidelity which can facilitate post-polymerization modifications and <i>in-situ</i> synthesis of block copolymers, e) Compatibility with various solvents and functional groups...	32
Figure 1. 2: Recent developments in RDRP	34
Figure 1. 3: Stimuli-induced RDRP.....	36
Figure 1. 4: Selected examples in sequence-controlled multiblocks, discrete oligomers, and oxygen-tolerant polymerizations.....	41
Figure 1. 5: Polymerization-induced self-assembly	45
Figure 1. 6: Examples of reversing RDRP through depolymerization.....	48
Figure 2. 1: Polymerization kinetic data for conventional ATRP approach of MA under the conditions: $[MA]/[EBiB]/[CuBr]/[Me_6TREN] = 100:1:0.02:0.12$	59
Figure 2. 2: 1H NMR analysis of the polymerization kinetic of MA for conventional ATRP. Data points are acquired during the induction period of the polymerization	60
Figure 2. 3: Polymerization kinetics of MA under the conditions: $[MA]/[EBiB]/[CuBr_2]/[Me_6TREN] = 100:1:0.02:0.12$	60
Figure 2. 4: Polymerization kinetic data for oxygen-enhanced ATRP approach of MA under the conditions: $[MA]/[EBiB]/[CuBr]/[Me_6TREN] = 100:1:0.02:0.12$	62
Figure 2. 5: (a) MALDI-ToF-MS analysis of PMA ₂₅ synthesized by oxygen-enhanced ATRP and (b) <i>In-situ</i> chain-extension experiment. The MALDI-ToF-MS spectrum was acquired by Dr. Richard Whitfield	63

Figure 2. 6: Merged kinetic data comparing oxygen-enhanced ATRP (in purple) and conventional ATRP (in green) and SEC traces of PMA synthesized via oxygen-enhanced ATRP	63
Figure 2. 7: (a) Monitoring of Cu ^{II} formation by UV-Vis spectroscopy as formed in traditional ATRP (i.e. by mixing CuBr with deoxygenated Me ₆ TREN/DMSO under inert atmosphere) (b) Monitoring of Cu ^{II} superoxido complex decay over time by UV-Vis spectroscopy as formed in oxygen-enhanced ATRP (i.e. by mixing CuBr with Me ₆ TREN/DMSO under ambient atmosphere prior to deoxygenation) (c) Raman analysis of the catalyst formed under ambient atmosphere. The Raman spectrum was acquired and analyzed by the inorganic chemistry groups of professor Rübhausen and professor Schindler	64
Figure 2. 8: Oxygen-enhanced polymerization kinetics of MA employing different amount of ligands	67
Figure 2. 9: Synthesis and characterization of a pseudo multiblock copolymer by oxygen-enhanced ATRP, (a) SEC traces of the molar mass distributions for consecutive cycles during the synthesis of a PMA pentablock copolymer and (b) ¹ H NMR spectra for consecutive cycles whereby very high monomer conversions are reached for each iterative monomer addition step (>97 %).....	67
Figure 2. 10: SEC traces of (a) P(MA- <i>b</i> -nBA), (b) P(MA- <i>b</i> -PEGA) and (c) P(MA- <i>b</i> -TFEA) diblock copolymers prepared by oxygen-enhanced ATRP	69
Figure 2. 11: SEC traces of PMA with a range of targeted DPs (25-6400) synthesized via oxygen-enhanced ATRP	69
Figure 2. 12: Monomer scope of oxygen-enhanced ATRP showing the SEC traces of the corresponding polymers	71
Figure 2. 13: Polymerization kinetics of MA via oxygen-enhanced ATRP utilizing: (a) Highly pure CuBr (>99.999%), (b) Less pure CuBr (98% initial purity followed by storage under ambient atmosphere) and (c) Highly oxidized CuBr (90% initial purity followed by storage at ambient atmosphere for 15 years)	72
Figure 3. 1: Schematic illustration and highlights of photocatalytic depolymerization	81
Figure 3. 2: a) Chemical illustration of polymerization of benzyl methacrylate via ARGET ATRP under the following conditions: [ECPA]:[BzMA]:[CuCl ₂]:[PMDTA]:[Sn(EH) ₂] = [1]:[100]:[0.2]:[0.2]:[0.08] in MeCN (1:1.25 solvent to monomer volume ratio) at 70 °C. b) SEC trace of purified PBzMA c) ¹ H NMR spectra of PBzMA before (bottom) and after (top) purification	82
Figure 3. 3: Control experiments in photocatalytic depolymerization of PBzMA. The repeat unit concentration was 50 mM and the samples were taken after 1 h of reaction at 170 °C and under blue light irradiation using 0.05 equivalent of FeCl ₂	82
Figure 3. 4: Comparison of thermal (red) and photothermal (blue) depolymerization of PBzMA at different temperatures using 1 equivalent of catalyst. The repeat unit concentration was 50 mM and the samples were taken after 1 h of reaction	83
Figure 3. 5: Temporal control of depolymerization of PBzMA at 100 °C using 1 equivalent of catalyst.....	84
Figure 3. 6: Comparison of thermal (red) and photothermal (blue) depolymerization of PBzMA at different temperatures using 0.05 equivalent of catalyst. The repeat unit concentration was 50 mM and the samples were taken after 1 h of reaction	85

Figure 3. 7: Temporal control of depolymerization of PBzMA at 100 °C using 0.05 equivalent of catalyst.....	86
Figure 3. 8: Thermal (red) and photothermal (blue) depolymerization of PBzMA at different catalyst concentrations. The repeat unit concentration was 50 mM and the samples were taken after 1 h of reaction at 170 °C	87
Figure 3. 9: Comparison of depolymerization kinetics utilizing FeCl ₂ (red) and FeCl ₃ (purple) catalyst.....	88
Figure 3. 10: Comparison of thermal and photothermal depolymerization of PBzMA at different temperatures using 1 an 0.05 equivalent of FeCl ₃ -catalyst	88
Figure 3. 11: Incubation experiments at different temperatures.....	89
Figure 3. 12: (a-c) Temporal control of depolymerization of PBzMA at 170, 150 and 120 °C using 0.05 equivalent of catalyst, (e-g) ¹ H NMR spectra of the temporal control experiments	90
Figure 4. 1: Demonstration of a sustainable polymerization methodology via photo-induced iron-catalyzed ATRP of bio-based monomers. SEC traces of PPheMA synthesized in three low-toxicity/green solvents.....	96
Figure 4. 2: Demonstration of temporal control during the polymerization of PheMA	98
Figure 4. 3: SEC traces of PPheMA with different degrees of polymerization.....	99
Figure 4. 4: SEC traces of PPheMA synthesized in tetraethylene glycol dimethyl ether, utilizing iron-catalyzed ATRP without any deoxygenation procedure: a) In 50 µl polymerization solution and b) In 100 µl polymerization solution	100
Figure 4. 5: SEC traces showing the chain-extension of PPheMA	100
Figure 4. 6: SEC traces of renewable polymers synthesized via photo-induced iron-catalyzed ATRP: a) PPheMA, b) PCreMA, c) PGuMA, d) PThyMA, e) PVaMA, and f) PSyrMA.....	101
Figure 4. 7: SEC traces of PGuMA macro initiator and its chain-extension, after purification, with PhMA in tetraethylene glycol dimethyl ether, utilizing photo-induced iron-catalyzed ATRP..	102
Figure 4. 8: Polymerization kinetics of PheMA utilizing a-c) Photo-induced iron-catalyzed ATRP and d-f) Conventional thermal RAFT polymerization.....	103
Figure 4. 9: SEC traces of PheMA synthesized in tetraethylen glycol dimethyl ether, utilizing PET-RAFT polymerization	104
Figure 4. 10: SEC traces of PheMA synthesized in tetraethylen glycol dimethyl ether, utilizing a) Iron-catalyzed photo-induced ATRP at 70 °C and b) Thermal RAFT polymerization at 70 °C...	105
Figure 5. 1: a) Chemical scheme of P(DEGMA- <i>co</i> -HPMA) synthesis, b) ¹ H NMR spectrum of purified P(DEGMA- <i>co</i> -HPMA) measured in DMSO- <i>d</i> ₆ and c) SEC trace of the P(DEGMA- <i>co</i> -HPMA).....	114
Figure 5. 2: a) Chemical scheme of P((DEGMA- <i>co</i> -HPMA)- <i>b</i> -styrene) synthesis, b) Optical representation of the emulsion polymerization procedure and c) SEC traces of P(DEGMA- <i>co</i> -HPMA) (left trace) and P((DEGMA- <i>co</i> -HPMA)- <i>b</i> -styrene) (right trace).....	114
Figure 5. 3: TIM of polymeric nanoparticles obtained via emulsion polymerization. a) Schematic representation of RAFT emulsion polymerization, b) TEM images of spheres, wormballs, worms and vesicles, c) SEC traces showing identical molar mass distributions of various morphologies, d) Schematic representation of the morphologies and visualization of change in turbidity of P((DEGMA- <i>co</i> -HPMA)- <i>b</i> -styrene) nanoparticles in water after sequential addition of transformer	115

Figure 5. 4: ^1H NMR spectra of P((DEGMA-*co*-HPMA)-*b*-styrene) after addition of different amounts of toluene to obtain different morphologies. The water dispersions of the polymeric nanoparticles were dried via air purging in order to eliminate the amount of water. The spectra were measured in a mixture of acetone- d_6 : chloroform- d in a 5:1 ratio 116

Figure 5. 5: a) Chemical scheme of GMA (first step) and PGMA (second step) synthesis, b) ^1H NMR spectra of GMA (bottom) and PGMA (top) measured in methanol- d_4 and c) SEC traces of PGMA117

Figure 5. 6: a) Chemical scheme of P(GMA-*b*-GlyMA) synthesis and b) SEC traces of PGlyMA (left trace) and P(GMA-*b*-GlyMA) (right trace) 118

Figure 5. 7: TIM of polymeric nanoparticles obtained via aqueous PISA. a) Schematic representation of RAFT emulsion polymerization, b) TEM images of spheres, worms and vesicles, c) Visual representation of various morphologies d) Small-angle X-ray scattering data confirming the formation of different morphologies in bulk. **The SAXS data were acquired and analyzed by Dr. Lutz-Bueno in the group of professor Mezzenga**..... 119

Figure 5. 8: a) ^1H NMR spectra of P(GMA-*b*-GlyMA), measured, after addition of different amounts of GlyMA to obtain different morphologies. The water dispersions of the polymeric nanoparticles were dried via air purging in order to eliminate the amount of water. The spectra were measured in a methanol- d_4 and b) SEC traces of P(GMA-*b*-GlyMA) after addition of different amounts of GlyMA to obtain different morphologies. SEC analysis was conducted without water removal 120

Figure 5. 9: a) Chemical scheme of P(POEGMA) synthesis, b) ^1H NMR analysis of purified P(POEGMA) measured in chloroform- d and c) SEC trace of P(POEGMA) 121

Figure 5. 10: a) Chemical scheme of P(POEGMA-*b*-styrene) synthesis and b) SEC traces of P(POEGMA) (left trace) and P(POEGMA-*b*-styrene) (right trace)..... 121

Figure 5. 11: TIM of polymeric nanoparticles obtained via organic PISA. a) Schematic representation of RAFT dispersion polymerization, b) TEM images of worms, octopi-like morphology, jellyfish and vesicles respectively, c) Visual representation and cryo-EM of worms and vesicles. **The cryo-EM images were acquired by Dr. Pilkington** 122

Figure 5. 12: a) ^1H NMR spectra of P(POEGMA-*b*-styrene) with (top spectrum) and without (bottom spectrum) addition of toluene. The water dispersions of the polymeric nanoparticles were dried via air purging in order to eliminate the amount of water. The ^1H NMR spectra were recorded in chloroform- d , and b) SEC traces of P(POEGMA-*b*-styrene) before and after addition of toluene. SEC analysis was conducted without water removal..... 123

Figure 5. 13: Addition of different organic molecules into P(POEGMA-*b*-styrene) worm-like nanoparticles/water dispersion 124

Figure 5. 14: Formation of worms via traditional solution self-assembly of P(POEGMA-*b*-styrene) and the morphological transformation of worms to vesicles..... 124

List of Tables

Table 2. 1: ^1H NMR and SEC analysis of polymerization kinetic of MA under the conditions: $[\text{MA}]/[\text{EBiB}]/[\text{CuBr}]/[\text{Me}_6\text{TREN}] = 100:1:0.02:0.12$. The catalyst was formed under conventional ATRP approach.....	59
Table 2. 2: ^1H NMR and SEC analysis of polymerization kinetics of MA under the conditions: $[\text{MA}]/[\text{EBiB}]/[\text{CuBr}_2]/[\text{Me}_6\text{TREN}] = 100:1:0.02:0.12$	61
Table 2. 3: ^1H NMR and SEC analysis of polymerization kinetic of MA under the conditions: $[\text{MA}]/[\text{EBiB}]/[\text{CuBr}]/[\text{Me}_6\text{TREN}] = 100:1:0.02:0.12$. The catalyst was formed under oxygen-enhanced ATRP approach	62
Table 2. 4: ^1H NMR and SEC analysis of the synthesis of a pseudo pentablock copolymer via oxygen-enhanced ATRP	68
Table 2. 5: ^1H NMR and SEC analysis of the PMA with a range of targeted DPs (25-6400) synthesized via oxygen-enhanced ATRP	70
Table 3. 1: Depolymerization of PBzMA at different temperatures using 1 equiv. of catalyst. $[\text{Polymer}]:[\text{FeCl}_2]:[\text{TBABr}] = [1]:[1]:[1]$ in DCB at 50 mM repeat unit concentration. The reactions were stopped after 1 h except the reaction at 100 °C, which was left for 2 h.....	84
Table 3. 2: Depolymerization of PBzMA using different catalyst equivalents at 100 and 170 °C in thermal (red) and photothermal (blue) system. The equivalents of catalyst are calculated in regards to chain end-group. For example 1 eq of catalyst means $[\text{Polymer}]:[\text{FeCl}_2]:[\text{TBABr}] = [1]:[1]:[1]$. The repeat unit concentration was 50 mM and the samples were taken after 1 h of reaction	87
Table 3. 3: Photocatalytic depolymerization of PBzMA at different repeat unit concertation using 1 eq. of FeCl_2 . The samples were taken after 1 h of reaction at 170 °C	90
Table 4. 1: ^1H NMR and SEC analysis for the synthesis of PPhEMA in three different solvents, under otherwise identical conditions, utilizing photo-induced iron-catalyzed ATRP.....	97
Table 4. 2: ^1H NMR analysis showing the temporal control during the polymerization of PheMA, utilizing photo-induced iron-catalyzed ATRP.....	98
Table 4. 3: ^1H NMR and SEC analysis for the synthesis of PPhEMA in tetraethylene glycol dimethyl ether, with targeted different degrees of polymerization, utilizing photo-induced iron-catalyzed ATRP	99
Table 4. 4: ^1H NMR and SEC analysis for the synthesis of PPhEMA macro initiator and its chain-extension, after purification, with PheMA in tetraethylen glycol dimethyl ether, utilizing photo-induced iron-catalyzed ATRP.....	101
Table 4. 5: ^1H NMR and SEC analysis for the polymerization of different renewable monomers, utilizing photo-induced iron-catalyzed ATRP. For the polymerization of solid monomers (VaMA and SyrMA) 1:1.5 monomer-to-solvent (tetraethylen glycol dimethyl ether) ratio was used while for the rest liquid monomer the ratio was 1:1.....	102

Abbreviations

AIBN	Azobisisobutyronitrile
ARGET	Activators Regenerated by Electron Transfer
ATRP	Atom Transfer Radical Polymerization
BzMA	Benzyl Methacrylate
CTA	Chain Transfer Agent
DMSO	Dimethylsulfoxide
DP	Degree of Polymerization
eATRP	Electrochemical ATRP
EBiB	Ethyl Bromoisobutyrate
FRP	Free Radical Polymerization
GOx	Glucose Oxidase
ICAR	Initiators for Continuous Activator Regeneration
IUPAC	International Union of Pure and Applied Chemistry
LED	Light-Emitting Diode
MA	Methyl Acrylate
MALDI-ToF MS	Matrix-Assisted Laser Desorption/Ionization Time-of Flight Mass Spectrometry
NMP	Nitroxide-Mediated Polymerization
NMR	Nuclear Magnetic Resonance
PBMA	Poly(butyl methacrylate)
PBzMA	Poly(benzyl methacrylate)

PET	Photoinduced Electron/Energy Transfer
PISA	Polymerization-Induced Self-Assembly
PMA	Poly(methyl acrylate)
PMDETA	N,N,N',N'',N'''-Pentamethyldiethylenetriamine
PMMA	Poly(methyl methacrylate)
POEGMA	Poly(oligo ethylene glycol methyl ether methacrylate)
P(PDMSMA)	Poly(poly(dimethylsiloxane) methacrylate))
ppm	Parts per million
PS	Poly(styrene)
RAFT	Reversible Addition Fragmentation Chain Transfer
RDRP	Reversible Deactivation Radical Polymerization
SARA	Supplemental activation reducing agent
SEC	Size Exclusion Chromatography
St	Styrene
TPMA	Tris(2-pyridylmethyl)amine
UHMW	Ultra-High Molecular Weight
UV	Ultraviolet

Acknowledgments

Back in January 9, 2019, I left Greece and headed to Switzerland to start my PhD adventure. When I left my study city, Heraklion, the temperature was surprisingly low for that place, only 16°C. And guess what? I arrived in Zurich, and it was a freezing -5°C (talk about a 21-degree difference!). I didn't know anyone there except Athina, whom I had met once before during a couple of interviews. Luckily, I joined a brand-new lab that was just getting started, and it gave me some awesome and one-of-a-kind experiences.

Looking back now, I realize how lucky I was to be among the first batch of students in that lab. We had a ton of work to do, but we also enjoyed privileges of close communication and collaboration. The best part was that we could build and shape the lab the way we wanted to. We poured our hearts into it to make, as Manon would have said, "our baby to walk". Besides work, we were all in the same boat – coming from different countries, without friends or family in Zurich. We had to figure out how to make the lab function smoothly. The funniest part? None of us spoke a word of German, which made communication a bit more challenging at first. But you know what? That strange situation actually brought us closer together and helped us build amazing relationships.

First of all, I want to give a big thank you to Professor **Athina Anastasaki** for having faith in me and choosing me as one of her first three PhD students. Getting selected for a PhD is always a confidence booster, but being part of the founding crew adds some extra weight to the mix. So, a huge thank you to Athina for taking a chance on me when embarking on her journey as a professor. We definitely had our fair share of arguments and not everything was smooth sailing. But we managed to build a relationship based on acceptance and mutual respect that carried us through this adventure. I could go on and on, filling up pages with gratitude for Athina, but the biggest thing I want to thank her for is giving me the space to grow and evolve as an individual. She's always been there to support me and provide guidance, whether directly or indirectly. And that's something I truly appreciate. I've got to say, I've learned so much on different levels throughout my journey with her. It's not just about the intellectual growth; our relationship has helped me evolve as a person too. Like Athina says, we're like family now. Sure, we've had our ups and downs (and I guess we will have in the future as well), but there's always genuine care for each other, no matter what happens.

I consider myself incredibly lucky because, over the course of these five years, I've had the opportunity to work with various individuals, and out of all of them, two have become true friends. One of them is "**Dr. Manon Rolland**", my PhD partner in crime. We've experienced some truly unique situations together that are hard to come by again. My relationship with Manon has gone through different stages, as any genuine connection does. We started off being super close (let's be honest, we didn't have many other options in our small lab), then we had a phase where we needed to navigate the fine line between personal friendship and professional relationship. Fortunately, we managed to find that sweet spot of true acceptance and care for each other that wasn't affected by our work-based relationships. Having Manon in my life brings me extreme happiness. I'm not only grateful for her being an amazing friend but also for all the valuable life lessons she has taught me along the way.

Now, next person who joined the lab a year later and holds a very special place in my heart is: **Dr.-to-be Hyun Suk Wang**. Our friendship has gone through its own unique stages until it blossomed into what it is today. This guy is an incredibly supportive individual, and I feel truly grateful to have someone like him to lean on both in my work and personal life. One thing that stands out about Hyun is how the interaction with him pushes me to become a better scientist. Honestly, by my standards, he's incredibly intelligent (way better than me), and I can't help but admire him without a hint of jealousy. It's inspiring to be around him and to be influenced by him.

I want to express my heartfelt gratitude to all the students I had the privilege of supervising. First and foremost, a big thank to **Silja Boner**, who was my very first student. She initially worked on her master semester project with me and then honored me by choosing to do her master thesis under my guidance. Next one was **Leonardo de Haro Amez**, who also completed his semester project with me. Even though he worked only for a couple of months his hard work was a catalyst for the project to lead to a very interesting publication. **Asimina Michos** deserves a special mention for conducting her Master's thesis (first master thesis) with me as well. And last but not least, **Sina Della Casa**, who entrusted me with her bachelor's project and did an amazing job, which guaranteed her a publication. Their success makes me incredibly happy and proud. I am truly grateful to all of these exceptional individuals as I learned so much from them! Supervising these students provided me with a remarkable opportunity for growth. It allowed me to communicate effectively, to enhance my ability to explain complex concepts, and to realize where I had gaps in my own knowledge. It also gave me the chance to make mistakes, to guide,

and to succeed alongside them. I would also like to acknowledge the more senior students in the lab, **Stella Mountaki** and **Valentina Bellotti**, whom I had the privilege of supporting during their early days in the lab. It was a unique experience from which I learned a great deal.

I would also like to extend my gratitude to **Dr. Nghia Truong** for his constant help and guidance throughout my PhD journey. His critical opinions and feedback were invaluable in pushing me to progress and evolve. I am truly thankful for his contributions.

Furthermore, I should acknowledge **Dr. Richard Whitfield**, who was part of the initial group that established the lab. Working alongside him and engaging in discussions has been a valuable experience. I've learned a great deal from him, and I appreciate the shared experiences we've had within the lab.

Next one is **Dr. Nethmi De Alwis**. She is one of the politest and most respectful individuals I have met in this lab. Not only did we share the lab space, but we also shared an office. Nethmi has been incredibly helpful, supportive, and inspiring. She truly exemplifies the idea of doing good and making a positive impact on as many people as possible. Thank you, Nethmi, and keep spreading your kindness and goodness in the world.

I also want to give a big thank you to all the current and alumni members of the team who have contributed to creating a positive and productive working environment. Big thank you to, **Maria Nefeli Antonopoulou** (thank you for always having and being willing to share anything one can imagine, from medication to food spices. Also, thank you for all the hugs you gave me when you were worried about the bad dreams you had of me.), **Victoria Lohmann** (besides all the other things, thank you for being a personal German translator), **Dr. Glen Jones** (thank you for nice collaboration and for making my English better!), **Stella Mountaki** (we know each other since our undergraduate studies. Thank you for all the experiences we have shared and have made us wiser) **Valentina Bellotti** (thank you for being a person who makes a difference!) as well as **Nguyen Thi Nguyen** (thank you for being such a special person. We also did share a lot of experiences at the beginning that I will always remember), **Dr. Daniel Messmer** (thank you for helping us out in our initial period at ETH), **Dr. Gregor Hofer** (thank you for helping me with your simulations), and **Manuel Reiter** (thank you for nice time in and out of the lab). Each and every one of them has taught me valuable lessons and I have learned so much from their diverse

perspectives and experiences. Their presence and contributions have made the journey even more enriching.

I would like to express my heartfelt appreciation to all the collaborators I had the privilege to work with. Their expertise and collaboration have been instrumental in expanding and deepening my knowledge. I am grateful for the opportunities I've had to learn from them and to benefit from their valuable insights. Working together with such talented individuals has truly enriched my experience and contributed to my growth. One of my dreams was to meet Professor **Matyjaszewski**. Not only did my dream come true but at the end I had the great honour to have a paper with one of the best polymer chemists in the world. I was truly impressed to see how he knows and remembers everything. Such an inspirational polymer chemist! I was also privileged to work with Professor **Konkolewicz** in three different projects. It was always fascinating talking to him and getting some of his impressive knowledge in polymer chemistry. Working with Professor **Schindler** helped me understand more about inorganic chemistry. It was also my pleasure to collaborate with Dr. **Harrisson** and had great conversations about the ATRP mechanism. Professor **Mezzenga** and Dr. **Lutz-Bueno** helped me in getting a glimpse of SAXS characterization of polymeric particles.

Moreover, I want to extend my gratitude to the examination committee for generously dedicating their time and agreeing to be part of it. A special thank you goes to Professor **Brent Sumerlin**, Professor **Tae-Lim Choi** and Professor **Jan Vermant**.

Additionally, I would like to acknowledge the Onassis Foundation for partially funding my PhD via a scholarship. I am very proud to be among the recipients of this scholarship.

Last but certainly not least, I want to express my deepest love to my partner, friends, and family. Their unwavering support and presence in my life throughout these past five years have been truly transformative. I am incredibly grateful for their love, understanding, and belief in me. Thank you for making a profound impact on my life. Love you guys!!!!

Summary

This dissertation describes advances in the field of reversible deactivation radical polymerization (RDRP).

In **Chapter 1**, I provide a brief introduction about the development and mechanism of reversible deactivation radical polymerization, as well as review the recent advancements in the field. The aim of this chapter is to highlight the strengths and weaknesses of these recent achievements in the field of RDRP and demonstrate how these discoveries have expanded the possibilities of creating tailor-made polymeric materials.

In **Chapter 2**, I discuss a new atom transfer radical polymerization (ATRP) approach I have developed which, paradoxically, is enhanced by oxygen.

RDRP has revolutionized the field of polymer chemistry by allowing access to the synthesis of a wide range of materials with controlled molecular weight, dispersity, architecture and end-group fidelity. In a typical RDRP, oxygen is considered an undesirable component, often yielding terminated polymer chains or deactivated catalysts. In this work, I describe an unusual ATRP in which the oxygen reacts with CuBr/L to form a very reactive superoxido complex at room temperature. It is noted that it is the first time that these reactive superoxido complexes have been detected at room temperature. Owing to the high reactivity of this complex, a very fast superoxido-catalyzed ATRP mechanism takes place exhibiting an instant consumption of the ATRP initiator and significantly faster reaction rates when compared to conventional ATRP. Notably, this system exhibits a number of advantages when compared to conventional ATRP. For instance, exceptional end-group fidelity is shown through the one pot synthesis of block and multiblock copolymers and the synthesis of high molecular weight polymers in the presence of only 4.5 ppm of copper. In addition, a number of monomers can be successfully polymerized thus significantly expanding the scope of our methodology. Overcoming the problem of purifying CuBr in traditional ATRP, I also demonstrate that even a brown highly oxidized 15-year old CuBr reagent can efficiently trigger a superoxido-ATRP mechanism yielding narrow molar mass distributions ($D = 1.07$). This work not only advances the fundamental understanding of ATRP by offering intriguing mechanistic aspects but also expands the potential of polymers made by RDRP through an user-friendly approach.

In **Chapter 3**, I present a reverse process of RDRP; developing photocatalytic ATRP depolymerization which enables temporal control at low ppm catalyst concentration.

Recently, the use of external stimuli to regulate the activation-deactivation equilibrium between active and dormant species has attracted considerable attention in the field of RDRP. Light in particular is one of the most attractive stimuli as it inherently possesses a number of unique properties and characteristics such as high abundance, wide availability, and low cost while providing further possibilities for temporal and spatial control leading to its implementation in 3D and 4D printing. In addition, photo-mediated polymerizations offer significant advantages over traditional thermal approaches including faster reaction times and higher conversions. Although these advantages have been extensively exploited for polymerizations, they have been rarely employed to facilitate efficient depolymerizations. Inspired by the pioneering work on photo-mediated polymerizations, I developed a photocatalytic ATRP depolymerization which enables excellent temporal control. At high concentration of low-toxicity iron-based catalysts and under visible light irradiation, very high depolymerization conversions could be achieved (up to 90%) within just 5 min of reaction time. However, minimal temporal control could be obtained in this system which was primarily attributed to the high concentration of polymer radicals generated that can also act as reducing agents. To overcome this challenge, I subsequently employed ppm concentrations of either FeCl_2 or FeCl_3 and I was able to modulate the rate of the depolymerization by turning the light “on” and “off” thus demonstrating the first example of perfect temporal control in the chemical recycling of polymers made by controlled radical polymerization. It is worth highlighting that the methodology was able to maintain high end-group fidelity throughout the reaction, in stark contrast to previous approaches which suffered from detrimental side-reactions and as such exhibited limited conversions. The depolymerizations could be conducted at high polymer loadings (up to 2M) and the versatility of our strategy was further exemplified by its compatibility with various polymers and light sources.

In **Chapter 4**, I present the iron-catalyzed photo-ATRP of renewable monomers in non-toxic solvents.

The sustainable synthesis of polymeric materials has become a paramount topic for research, both in academia and industry. Currently, the vast majority of monomers used in the synthesis of polymeric materials are based on fossil fuel feedstock, making it an urgent priority to find alternative ways to synthesize monomers and corresponding polymers. In this regard, biomass-

derived materials are promising as an alternative and renewable resource for the synthesis of monomers/polymers. Equally urgent is the goal of achieving high control over the polymerization of such unique monomers in a sustainable, non-toxic manner. In this work, I present the synthesis of monomers obtained from renewable resources (lignin and terpenes) and their polymerization, employing an environmentally friendly photo-induced iron-catalyzed ATRP in green solvents. Iron ATRP is arguably one of the most sustainable RDRP methodologies as iron is one of the most abundant metals on Earth, is inexpensive, non-toxic, and has been shown to be biocompatible. To further develop iron ATRP into a sustainable polymerization methodology, I employed low-toxicity/green solvents and light (rather than heat) to conduct the polymerization. The versatility of the approach was further highlighted by the possibility of temporal control as evidenced by intermittent “on/off” cycles, the controlled polymerization of a variety of monomers and targeted degrees of polymerization, oxygen-tolerance, and high end-group fidelity exemplified by the synthesis of block copolymers. A very important aspect of this project is the demonstration of the superiority of photo-induced iron-catalyzed ATRP over reversible addition-fragmentation chain-transfer (RAFT) polymerization. I show that, using photo-induced iron-catalyzed ATRP, renewable monomers can be successfully polymerized into polymers with low dispersity and good control over the molecular weight (dispersity (\mathcal{D}) as low as 1.17). This is in contrast to RAFT polymerization, arguably the most commonly employed method for bio-based monomers, which results in polymers with poorer molecular weight control and much higher dispersities ($\mathcal{D} \sim 1.4$).

Finally, in **Chapter 5**, I present a technique I developed to tune the morphology of polymeric nanoparticles.

RDRP can produce polymers with high end-group fidelity thereby enabling the production of polymeric nanoparticles with controlled morphology. Many groups have reported remarkable breakthroughs for the synthesis of polymers and polymeric nanoparticles through controlled polymerization strategies coupled with transformation strategies. However, all current protocols to produce polymeric nanoparticles are limited in polymer scope, often alter the chemical structure, operate at high temperatures, and can be fairly tedious and time-consuming. In this project, I was able to alleviate these challenges by introducing a rapid and versatile morphological transformation strategy which operates at ambient temperature and without impairing the chemical structure of the resulting morphologies. By simply adding a small amount

of a molecular transformer (i.e. small organic molecule) in an aqueous solution of polymeric nanoparticles, a rapid evolution to the next high-ordered morphology was observed within seconds, yielding a range of nanoparticles morphology from the same starting material. Significantly, this approach can be applied to nanoparticles produced by disparate block copolymers (i.e. with different cores and coronae) obtained by various synthesis techniques, including emulsion controlled radical polymerization, polymerization-induced self-assembly and traditional solution self-assembly. The method is also highly reproducible and can access a wide range of highly pure polymeric morphologies in a controlled fashion thus significantly expanding the toolbox and availability of controlled radical polymerization and its tailored-made polymeric nanomaterials.

Zusammenfassung

Diese Dissertation beschreibt Fortschritte im Bereich der Radikalpolymerisation mit reversibler Deaktivierung.

In **Kapitel 1** gebe ich eine kurze Einführung in den Prozess der Radikalpolymerisation mit reversibler Deaktivierung (RDRP), die Mechanismen, denen sie folgt, und einen Überblick über die neuesten Fortschritte auf diesem Gebiet. Das Ziel war es, Stärken und Schwächen der jüngsten Errungenschaften im Bereich der RDRP herauszustellen und aufzuzeigen, wie diese Entdeckungen den Umfang maßgeschneiderter polymerer Materialien erweitert haben.

Im **Kapitel 2** stelle ich einen von uns entwickelten, neuen Ansatz zur radikalische Atomtransferpolymerisation (ATRP) vor, der paradoxerweise durch Sauerstoff beschleunigt wird.

RDRP hat das Gebiet der Polymerchemie revolutioniert, indem es die Synthese einer breiten Palette von Materialien mit kontrolliertem Molekulargewicht, Dispersität, Architektur und Endgruppenfunktionalität ermöglicht. In einer typischen RDRP gilt Sauerstoff als unerwünschte Komponente, da er häufig zu terminierten Polymerketten oder deaktivierten Katalysatoren führt. In dieser Arbeit haben wir über eine ungewöhnliche ATRP berichtet, bei der Sauerstoff mit CuBr/L reagiert, um einen sehr reaktiven Superoxidokomplex bei Raumtemperatur zu bilden. Es sei darauf hingewiesen, dass dies das erste Mal ist, dass solche reaktiven Superoxidokomplexe bei Raumtemperatur nachgewiesen wurden. Aufgrund der hohen Reaktivität dieses Komplexes

findet ein sehr schneller, durch Superoxid katalysierter ATRP-Mechanismus statt, der einen sofortigen Verbrauch des ATRP-Initiators und signifikant schnellere Reaktionsgeschwindigkeiten im Vergleich zur konventionellen ATRP aufweist. Dieses System weist eine Reihe von Vorteilen gegenüber der konventionellen ATRP auf. Zum Beispiel wird eine außergewöhnliche Endgruppenfunktionalität durch die Ein-Topf-Reaktion von Block- und Mehrblockcopolymeren und die Synthese von Hochmolekulargewichtspolymeren in Gegenwart von nur 4,5 ppm Kupfer gezeigt. Darüber hinaus können verschiedene Monomerfamilien erfolgreich polymerisiert werden, einschließlich Acrylaten, Methacrylaten und Styrol, wodurch der Anwendungsbereich unserer Methodik erheblich erweitert wird. Dass keine Notwendigkeit zur Reinigung von CuBr wie in herkömmlicher ATRP besteht, zeigen wir mit einer erfolgreichen Auslösung eines Super-ATRP-Mechanismus durch eine 15 Jahre alte braunen, stark oxidierte CuBr-Reagenz, die schmale Molmassenverteilungen (1,07) liefert. Wir sind der Überzeugung, dass diese Arbeit nicht nur das grundlegende Verständnis der ATRP durch faszinierende mechanistische Aspekte voranbringt, sondern auch das Potenzial von Polymeren, die durch RDRP hergestellt werden, durch einen wirtschaftlichen und benutzerfreundlichen Ansatz erweitert.

In **Kapitel 3** präsentiere ich eine Umkehr des RDRP-Prozesses, bei dem eine photokatalytische ATRP-Depolymerisation entwickelt wurde, die eine zeitliche Steuerung bei geringen ppm-Katalysatorkonzentrationen ermöglicht.

In letzter Zeit hat die Verwendung externer Stimuli zur Regulierung des Aktivierungs-Deaktivierungs-Gleichgewichts zwischen aktiven und ruhenden Spezies im Bereich der RDRP beträchtliche Aufmerksamkeit erregt. Insbesondere Licht ist einer der attraktivsten Stimuli, da es eine Reihe einzigartiger Eigenschaften und Merkmale wie breite Verfügbarkeit, hohe Nutzbarkeit und geringe Kosten aufweist und zusätzliche Möglichkeiten für eine zeitliche und räumliche Steuerung bietet, was auch zu weiterer Anwendung in 3D- und 4D-Druck führt. Darüber hinaus bieten photovermittelte Polymerisationen gegenüber traditionellen thermischen Ansätzen erhebliche Vorteile wie schnellere Reaktionszeiten und höhere Monomer Umsetzungen. Obwohl diese Vorteile für Polymerisationen voll ausgenutzt wurden, wurden sie selten zur Unterstützung effizienter Depolymerisationen eingesetzt. Inspiriert von den bahnbrechenden Arbeiten zu photovermittelten Polymerisationen haben wir eine photokatalytische ATRP-Depolymerisation entwickelt, die eine ausgezeichnete zeitliche

Steuerung ermöglicht. Bei hoher Konzentration von gering toxischen, eisenbasierten Katalysatoren und unter sichtbarer Lichtbestrahlung konnten sehr hohe Monomerumsätze (bis zu 90%) innerhalb von nur 5 Minuten Reaktionszeit erreicht werden. Allerdings konnte in diesem System nur eine minimale zeitliche Steuerung erzielt werden, was hauptsächlich auf die hohe Konzentration an Polymerradikalen zurückzuführen war, die auch als Reduktionsmittel wirken können. Um diese Herausforderung zu überwinden, verwendeten wir anschließend ppm-Konzentrationen von entweder FeCl_2 oder FeCl_3 , und wir konnten die Rate der Depolymerisation durch Ein- und Ausschalten des Lichts steuern, was das erste Beispiel einer perfekten zeitlichen Steuerung bei der chemischen Wiederverwertung von Polymeren, die durch kontrollierte radikalische Polymerisation hergestellt wurden, darstellt. Es ist erwähnenswert, dass unsere Methodik eine hohe Endgruppenfunktionalität während der Reaktion aufrechterhalten konnte, im Gegensatz zu früheren Ansätzen, bei denen schädliche Nebenreaktionen auftraten und daher nur begrenzte Umsetzungen erreicht wurden. Die Depolymerisationen konnten bei hohen Polymerbeladungen (bis zu 2M) durchgeführt werden, und die Vielseitigkeit unserer Strategie wurde durch ihre Kompatibilität mit verschiedenen Polymeren und Lichtquellen weiter verdeutlicht.

Im **Kapitel 4** präsentiere ich eine Arbeit über die eisenkatalysierte foto-ATRP von erneuerbaren Monomeren in ungiftigen Lösungsmitteln.

Die nachhaltige Synthese polymerer Materialien ist sowohl in der Wissenschaft als auch in der Industrie ein wichtiges Thema geworden. Derzeit basieren die meisten Monomere, die bei der Synthese polymerer Materialien verwendet werden, auf fossilen Rohstoffen, so dass es dringend erforderlich ist, alternative Wege zur Synthese des Monomers und des entsprechenden Polymers zu finden. In diesem Zusammenhang sind aus Biomasse gewonnene Materialien vielversprechend als alternative und erneuerbare Ressource für die Synthese von Monomeren/ Polymeren. Ebenso dringend ist das Ziel, eine hohe Kontrolle über die Polymerisation solcher einzigartigen Monomere in einer nachhaltigen, ungiftigen Weise zu erreichen. In dieser Arbeit präsentieren wir die Synthese von Monomeren, die aus erneuerbaren Ressourcen (Lignin und Terpene) gewonnen wurden, und ihre Polymerisation unter Verwendung einer umweltfreundlichen fotoinduzierten, eisenkatalysierten, radikalen Atomtransferpolymerisation (ATRP) in grünen Lösungsmitteln. Eine der nachhaltigsten RDRP-Methoden ist sicherlich die Eisen-ATRP. Eisen ist eines der häufigsten Metalle auf der Erde und kostengünstig,

erwiesenermaßen ungiftig und biokompatibel. Um die Eisen-ATRP weiter zu einer nachhaltigen Polymerisationsmethode zu entwickeln, verwendeten wir ungiftige/grüne Lösungsmittel und Licht (anstatt Wärme) zur Durchführung der Polymerisation. Die Vielseitigkeit unseres Ansatzes wurde weiterhin durch die Möglichkeit der zeitlichen Steuerung- nachgewiesen durch intermittierende "Ein/Aus"-Zyklen- die kontrollierte Polymerisation verschiedener Monomere und Kettenlängen, die Sauerstofftoleranz der Polymerisation und die hohe Endgruppenfunktionalität- veranschaulicht durch die Synthese von Blockcopolymeren- belegt. Ein sehr wichtiger Aspekt der vorliegenden Publikation ist die Demonstration der Überlegenheit der fotoinduzierten eisenkatalysierten ATRP gegenüber der reversiblen Additions-Fragmentierungs-Kettenübertragungs-Polymerisation (RAFT). Wir zeigen, dass unter Verwendung der fotoinduzierten eisenkatalysierten ATRP erneuerbare Monomere erfolgreich in Polymere mit niedriger Dispersität und guter Kontrolle über das Molekulargewicht polymerisiert werden können (Dispersität von bis zu 1,17). Dies steht im Gegensatz zur RAFT-Polymerisation, die möglicherweise am häufigsten für diese bio-basierten Monomere verwendet wird und zu Polymeren mit geringerer Kontrolle über das Molekulargewicht und viel höheren Dispersitäten (~1,4) führt.

Schließlich präsentiere ich in **Kapitel 5** eine von uns entwickelte Technik zur Steuerung der Morphologie von polymeren Nanopartikeln.

RDRP kann Polymere mit hoher Endgruppenfunktionalität erzeugen, was die Herstellung von polymeren Nanopartikeln mit kontrollierter Morphologie ermöglicht. Viele Forschungsgruppen haben bemerkenswerte Durchbrüche bei der Herstellung von polymeren Nanopartikeln durch die Verbindung von kontrollierte Polymerisationstechniken mit Transformationsstrategien. Alle diese Methoden haben aber Limitierungen wie auf wenige Polymere begrenzte Anwendbarkeit, Veränderung der chemischen Struktur bei der Transformation, Durchführung bei hohen Temperaturen, beschwerlicher Arbeitsaufwand oder großer Zeitaufwand. In dieser Arbeit präsentieren wir einen neuen und effizienten Weg zur gezielten Kontrolle der Morphologie von polymeren Nanopartikeln durch die Entwicklung einer schnellen und vielseitigen Strategie ohne chemische Veränderung bei Raumtemperatur. Dabei wird eine kleine Menge molekularer Transformer (kleine organische Moleküle) in eine wässrige Lösung der Nanopartikel geben, was eine prompte Evolution zur nächsthöheren Morphologie zur Folge hat. Aus dem gleichen Ausgangspolymer konnten so verschiedene Nanopartikelformen gewonnen werden. Der

maßgebliche Vorteil dabei ist die Anwendbarkeit auf Nanopartikeln aus Blockcopolymeren, die durch die verschiedensten Synthesemethoden, wie kontrollierte Emulsionsradikalpolymerisation, polymerisationsinduzierte Selbstassemblierung und traditioneller Selbstassemblierung in Lösung, hergestellt wurden. Diese Methode weist exzellente Reproduzierbarkeit auf und ermöglicht die kontrollierte Herstellung von sehr reiner Partikelmorphologie und erweitert damit die Anwendung von kontrollierten Radikalpolymerisationen und den zugehörigen maßgeschneiderten Nanomaterialien.

Chapter 1: General Introduction

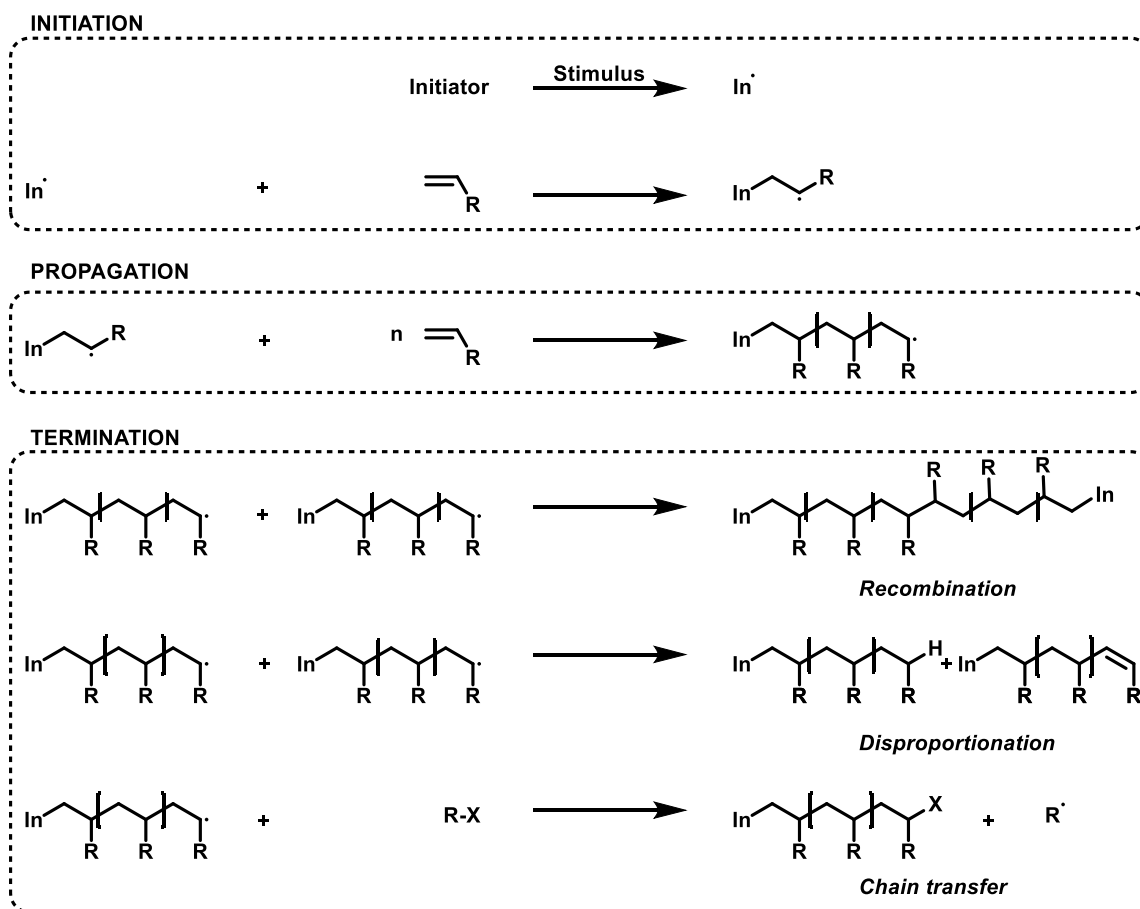
Part of this chapter has been published in Chem and I was the lead/first author (K. Parkatzidis, H. S. Wang, N. P. Truong, A. Anastasaki, Recent Developments and Future Challenges in Controlled Radical Polymerization: A 2020 Update, Chem, 2020, 6, 1575). Permission was obtained from the publisher (Elsevier).

Nature, as the most brilliant chemist, has provided us with a plethora of natural polymers such as DNA, proteins, cellulose, etc. However, it was not until almost one and a half centuries ago that human chemists started making polymers, thereby bringing us to the era of synthetic polymers. The first fully synthetic polymeric material (a thermoset), was a phenol formaldehyde resin known as Bakelite which was produced in 1907 by Baekeland through the polycondensation of phenol with formaldehyde. However, the concept of synthetic polymers and the field of polymer chemistry was established by Hermann Staudinger in 1920, who received the Nobel Prize in 1953 for his world-changing ideas.¹

103 years after the landmark publication by Staudinger², it would not be an exaggeration to say that synthetic polymers have changed the everyday life of modern society. Polymeric materials are used in every aspect of life, with some of them being ubiquitous like polyesters, polystyrene, polyethylene, etc., while others are less known, like those used in medical applications. New polymeric materials are being developed daily, and the increased demand for more advanced materials is pushing the boundaries of research. Finding new or improved polymer-based materials requires advances in synthetic polymer chemistry that will enable the tailoring of important properties such as biocompatibility, degradability, mechanical strength, etc. However, it should be mentioned that the majority of commercial polymers are produced via conventional step growth or chain growth polymerizations with limited ability to impart fine control over macromolecular structure. In this introduction, I will briefly discuss free radical polymerization and controlled/living polymerization. However, the primary focus will be on reversible radical polymerization and the recent advancements that the field has experienced.³

Free Radical Polymerization

One of the most commonly used chain growth polymerization methodology is free radical polymerization (FRP), which allows for the synthesis of a wide range of polymers via a simple and robust synthetic protocol. Mechanistically, FRP can be divided into three main steps (**scheme 1.1**): i) initiation, where there is a generation of an active initiating species (radical) upon application of a stimulus (e.g. heat, light irradiation, etc.), from a labile molecule referred to as initiators. The generated radicals can either react with a monomer or terminate via side reactions or via biradical coupling/disproportionation. The efficiency of the initiator is defined as the ratio between radicals that add to monomer over those that undergo side reactions. ii) Propagation is the chain growth process wherein the radicals react the vinyl π -bonds of monomers, resulting in the formation of polymeric radicals which grow with every addition of monomer. Propagation of individual chains is typically a very rapid step (< 1 second), and can produce polymer chains with up to tens of thousands of monomer units. iii) Termination, in which propagating polymer chains terminate through two pathways which can be either bi-radical combination, disproportionation or chain transfer. In the first case, two polymeric radicals couple together, resulting a single polymer chain with a chain length equal to the sum of the two initially propagating radical chains. In the second case, hydrogen abstraction takes place, producing one saturated and one unsaturated polymer chain, without altering their molecular weights. The unavoidable and irreversible termination events in FRP lead to broad chain length distributions and inactive ("dead") polymer chains that cannot undergo further chain growth or other modification reactions. Thus, the tuning of the properties of materials synthesized by FRP is rather limited. To overcome the limitations caused by the termination effects in FRP, techniques that can eliminate or minimize irreversible termination have been developed, advancing polymer synthesis.⁴



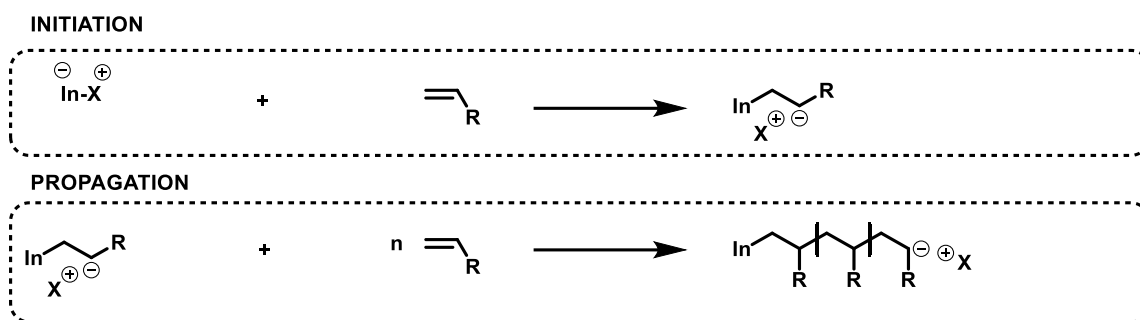
Scheme 1. 1: Simplified mechanism of free radical polymerization.

Anionic Polymerization

The first example of anionic polymerization was the groundbreaking research conducted by Szwarc, which elucidated the concept of living anionic polymerizations. In living polymerization, termination events by combination or disproportionation, as in the case of FRP, are eliminated as the polymerization propagates through an ionic species rather than a radical (**scheme 1.2**).⁵ Szwarc's demonstration of anionic polymerization led to three significant implications. Firstly, in anionic polymerization the number-average molecular weight (M_n) of the resulting polymer could be calculated based on the amount of monomer consumed and the initiator utilized in the polymerization process. The degree of polymerization (DP) could be theoretically determined as the molar ratio of reacted monomer to the initiator. Secondly, it established that all chains within the system would propagate at an equal rate and achieve similar lengths after a given time interval. This behaviour would lead to linear growth of polymer chains relative to the monomer concentration. Thirdly, it revealed that polymer chains possessed active end-groups capable of

further polymerization if additional monomer was introduced. These three characteristics enable a controlled polymerization in terms of molecular weight, narrow distribution of polymer chains, and facilitate the synthesis of more intricate polymeric materials such as block copolymers.

It should be though noted that the success of an anionic polymerization is highly dependant on the purity of the reagents and the reaction conditions as they can cause severe side reactions that can prevent polymerization altogether. Additionally, the polymerization's tolerance to functional groups of the monomers as well as solvents is rather limited, minimizing the scope of the technique.



Scheme 1. 2: Simplified mechanism of anionic polymerization.

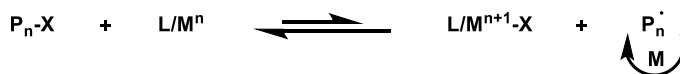
Reversible Deactivation Radical Polymerization

To overcome the limitations of living ionic polymerizations while keeping the majority of their advantages, “living” radical polymerization, today referred to as reversible deactivation radical polymerization (RDRP), was developed. The golden decade in RDRP was the 1990s in which the three most important techniques were discovered. Starting with the discovery of nitroxide-mediated polymerization (NMP) in 1986,⁶ other RDRP methodologies were subsequently discovered including atom transfer radical polymerization (ATRP) in 1995,^{7,8} and reversible addition–fragmentation chain-transfer (RAFT) polymerization in 1998.⁹

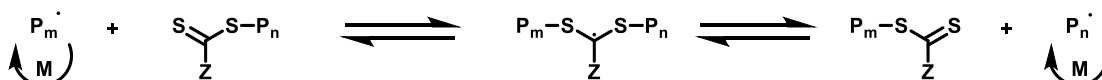
NITROXIDE-MEDIATED POLYMERIZATION (NMP)



ATOM TRANSFER RADICAL POLYMERIZATION (ATRP)



REVERSIBLE ADDITION-FRAGMENTATION CHAIN-TRANSFER (RAFT) POLYMERIZATION



Scheme 1. 3: Simplified mechanism of NMP, ATRP and RAFT polymerization.

Nitroxide-Mediated Polymerization

In the mid-1980s, an RDRP process was patented at the commonwealth scientific and industrial research organization (CSIRO) that exploited stable aminoxyl radicals to reversibly deactivate propagating radical species. This method, now referred to as nitroxide-mediated polymerization (NMP), began attracting increasing attention in academia in the early 1990s when Georges and colleagues applied NMP to produce low-dispersity polystyrene.¹⁰ This method was further developed by Hawker¹¹ and others,^{12,13} through the discovery of more versatile nitroxides capable of mediating effective RDRP of a wider range of monomer families. Mechanistically, NMP is based on a reversible termination mechanism between the growing propagating (macro)radical and the nitroxide (**scheme 1.3**), acting as a control agent, to yield a (macro)alkoxyamine as the predominant species. By raising the temperature, the alkoxyamine bond can cleave, producing a macro(radical) which can propagate through the reaction with vinyl monomers, and a stable alkoxyamine radical. The two types of radicals can recombine, producing a dormant polymer chain. Selecting an appropriate temperature allows for the establishment of an equilibrium between the dormant and active species, known as the activation-deactivation equilibrium.

Atom Transfer Radical Polymerization

In 1994-1995, Matyjaszewski and Sawamoto, independently presented new metal catalyzed RDRP processes that operates through an atom-transfer radical addition process.^{7,8} The system developed by Sawamoto employed ruthenium as a metal catalyst in conjunction with a Lewis acid to mediate the polymerization while Matyjaszewski used a copper complex as the metal catalyst in the absence of a Lewis acid.

ATRP operates by utilizing a transition metal to first trigger and then mediate the polymerization (**scheme 1.3**). In conventional ATRP, the metal in its low oxidation state (e.g. Cu^I) coordinates to an amine ligand (e.g. Cu^I/L) forming a complex which acts as a catalyst. The catalyst activates the carbon-halogen bond of an alkyl halide initiator generating a radical and a metal complex in a higher oxidation state (e.g. Cu^{II}/L), known as the deactivator. The generated propagating radical can be either immediately deactivated by the catalyst in the higher oxidation state, propagate by reacting with one or more vinyl monomers before being deactivated, or undergo an irreversible reaction with another radical. The latter leads to the accumulation of Cu^{II} during the polymerization and is responsible for the control over the polymerization through the persistent radical effect. As a result, conventional ATRP necessitates a certain extent of termination prior to gaining control over the molar mass distributions. In addition, high amounts of catalyst are typically needed for a successful polymerization.¹⁴

Reversible Addition-Fragmentation Chain-Transfer (RAFT) Polymerization

Reversible addition-fragmentation chain-transfer (RAFT) polymerization was developed at CSIRO in 1998.⁶ The process uses a free radical initiator which, upon the application of stimuli, can generate radicals that will react with the monomer to form the first propagating radicals. The propagating radicals can then add to the thiocarbonylthio group of the RAFT agent, forming intermediate radicals. In these species, the weak C-S bond can then fragment, forming dormant thiocarbonylthio-capped polymer chains and new propagating radicals (**scheme 1.3**). Thus, the role of the raft agent is to deactivate the propagating radical via a chain-transfer mechanism. Successful polymerization can be achieved if the intermediate radical species fragments rapidly, allowing all chains in the mixture to grow uniformly. In an ideal scenario, less than one monomer is inserted per activation cycle before the propagating radical is capped again. As in the case of other FRP and RDRP methodologies, termination events are also unavoidable in RAFT and the

precise extent of termination can be theoretically calculated based on the concentration of the free radical initiator used for the polymerization.¹⁵

Main Characteristics of Reversible Deactivation Radical Polymerization

Overall, and regardless of the mechanism, RDRP offers several revolutionary characteristics which combine the advantages of living polymerization with the versatility of FRP (**figure 1.1**).^{3,16}

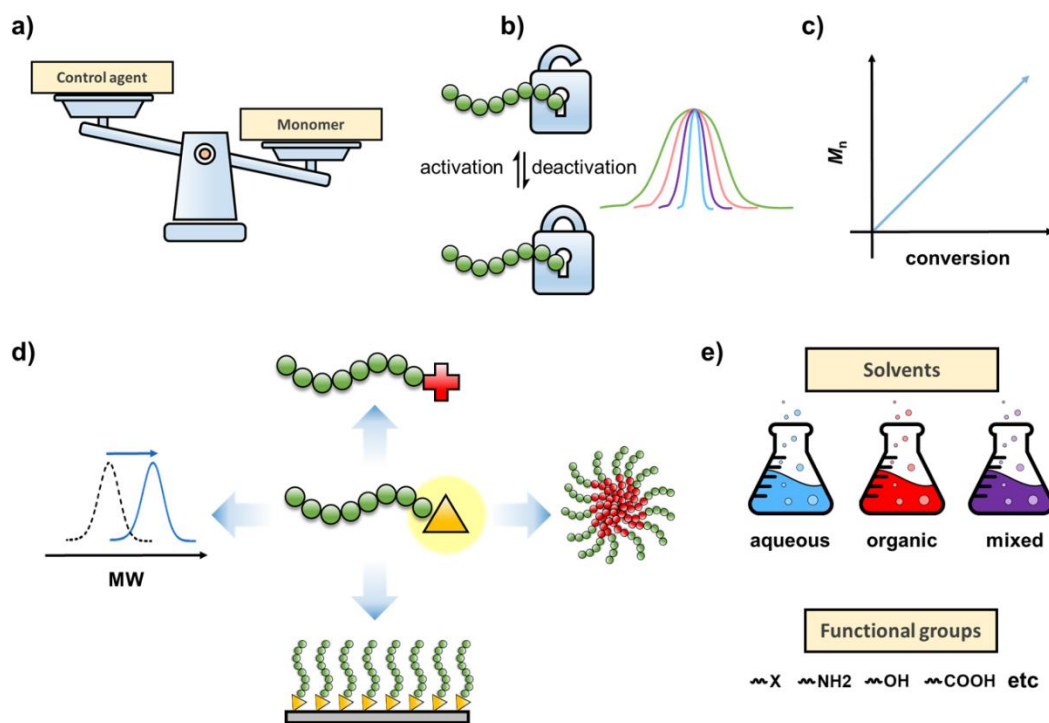


Figure 1. 1: Main characteristics of RDRP. a) ability to target specific molecular weight, b) control over the polymer dispersity by manipulating the activation-deactivation equilibrium, c) linear relationship between monomer conversion and number average molecular weight, d) high end-group fidelity which can facilitate post-polymerization modifications and *in-situ* synthesis of block copolymers, e) compatibility with various solvents and functional groups.

1. RDRP allows precise control over polymerization processes, resulting in predefined molecular weight and controlled dispersity, similar to living polymerizations. This control enables the synthesis of polymers with well-defined molecular weights and dispersities, allowing for the design of specific properties and desired functionality. The molecular weight of the polymers can be altered by changing the ratio of the monomer to alkoxyamine initiator or ATRP initiator or RAFT agent, and the dispersity can be tuned via the precise control of the activation-deactivation equilibrium.

2. RDRP techniques often result in polymer chains with dormant functional groups at the chain-ends (also referred to as living chains). This "living" nature allows for subsequent modification of the polymer chains, enabling the introduction of specific chemical groups, crosslinking, or attachment to surfaces. Additionally, the preservation of these functional end-groups, along with the ability of RDRP to achieve full monomer conversions, allows for the addition of a second monomer batch and further polymerization to result in more intricate polymers without the need for any intermediate purification steps.
3. RDRP methods can be applied under a wide range of reaction conditions, similar to FRP and in contrast to living polymerization. The reactions can take place either in bulk or solution, with the media being aqueous, organic, or mixed. RDRP methods generally have a broader monomer scope compared to living polymerization techniques and can polymerize a wide range of monomers, including those that are challenging or incompatible with living polymerization methods (acidic, basic, or functional monomers). The reactions usually operate under mild reaction conditions, such as ambient or near-ambient temperatures (50-70 °C) and moderate pressures. This mildness in reaction conditions is advantageous for the synthesis of temperature-sensitive monomers or polymers, and for reducing energy consumption and processing costs. Importantly, RDRP uses fairly simple catalysts and chemical reagents, without the need for any tedious reagent purification steps.
4. RDRP techniques minimize side reactions and undesired termination events compared to traditional FRP. This reduction in side reactions leads to better control over the polymerization process and improves the uniformity of the chain growth.

While FRP and living polymerizations have their own merits, RDRP offers distinct advantages that make it a valuable tool in the field of polymer and materials science.

Recent Developments in Reversible Deactivation Radical Polymerization

Since the discovery of RDRP techniques, the field of polymer science has experienced significant advancements. Summarizing all the developments in a thesis introduction can be challenging, so I will attempt to cover the advancements that have occurred in the last decade, starting from 2010 onwards (figure 1.2).

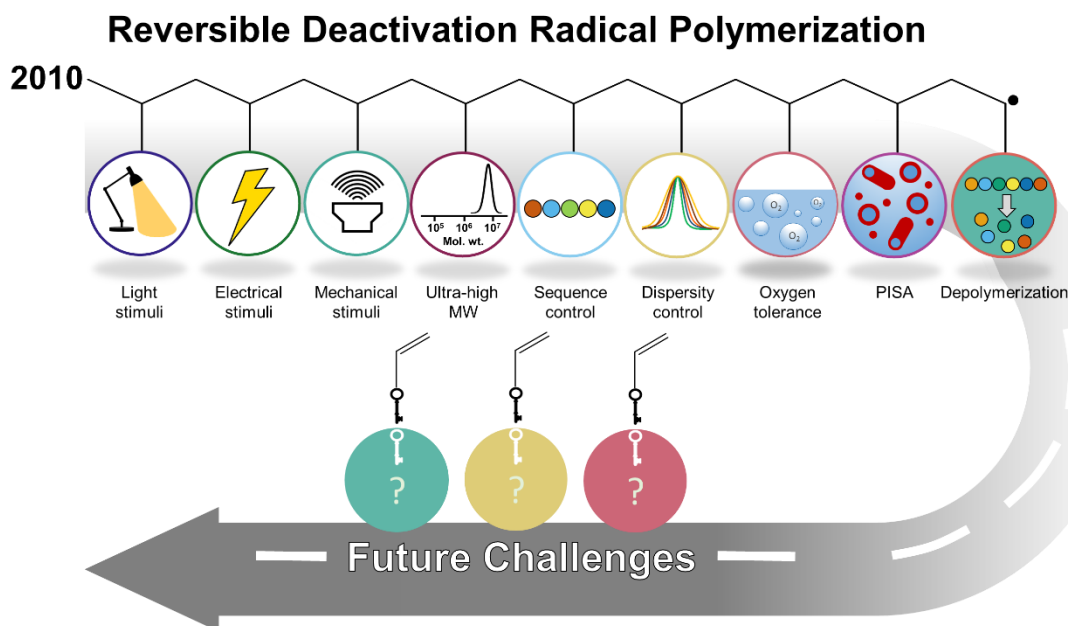


Figure 1. 2: Recent developments in RDRP.

Using Light as an External Stimulus

Amongst various stimuli, light is perhaps the most attractive due to its abundance, wide availability, mild nature, low cost and environmental benignity while it offers tremendous possibilities for temporal and spatial control. In addition, light-mediated polymerizations might offer additional opportunities as they do not require high temperatures which may facilitate side reactions and/or depolymerization. At the same time, however, light-mediated polymerizations suffer from limited depth penetration and scalability issues, although these have been considerably addressed through the development of flow photochemistry which allows for faster polymerizations, enhanced control over the molecular weight distributions and can also be combined with on/in-line monitoring characterization techniques (the reader is referred to a recent review in flow chemistry polymerization).¹⁷ Furthermore, certain wavelengths and intensities may be disadvantageous for various biological systems. Currently, there are two main

developments in this area, namely photo-ATRP (including metal-mediated and metal-free ATRP) and photoinduced electron/energy transfer RAFT (PET-RAFT) polymerization (**figure 1.3 A and D**). Both have revolutionized polymer chemistry from both a synthetic and an applications standpoint. Elegant achievements on photo-NMP and photo-RAFT will not be reviewed here, as those developments have emerged mostly during previous decades.

Photo-ATRP

The first example of the significance of light in ATRP (in the absence of conventional photo-initiators or dye sensitizers) was published in 2000 by Guan and Smart who discovered that in the presence of visible light the polymerization rate of methyl methacrylate (MMA) during conventional ATRP (CuCl used as the catalyst) was accelerated.¹⁸ However, it was not until 2011 that Yagci and co-workers reported the first publication on UV-mediated ATRP of MMA in bulk, during which CuBr₂ was reduced *in-situ* to CuBr which subsequently mediated the polymerization.¹⁹ In 2012, the group of Mosnacek demonstrated that photo-ATRP was possible even with ppm amounts of CuBr₂ enabling the controlled polymerization of MMA in a variety of different wavelengths.²⁰ In the same year, Matyjaszewski and co-workers reported controlled polymerization of both acrylates and methacrylates using ppm concentration of CuBr₂ under visible and sunlight irradiation.²¹ Two years later, in 2014, Haddleton and co-workers utilized a CuBr₂/Me₆TREN (Me₆TREN = tris[2-(dimethylamino)ethyl]amine) complex to mediate the polymerization of a range of acrylic monomers under UV irradiation reporting for the first time quantitative monomer conversions for different degrees of polymerization (**figure 1.3 B**), very fast rates (~2 h to reach completion in dimethyl sulfoxide (DMSO)) and *in-situ* block copolymers.²² Aside from copper-mediated polymerizations, another significant development in photo-ATRP was reported in 2012 by Fors and Hawker who exploited an iridium (Ir)-based photoredox catalyst that facilitates the controlled polymerization of methacrylates.²³ Since these landmark discoveries, photo-ATRP has been widely utilized by many groups for a number of reasons. Aside from advantages associated with the use of light (e.g., mild reaction conditions, modulation of reaction kinetics through different wavelengths, temporal control, etc.), another major improvement of photo-ATRP over conventional ATRP is that it allows for polymers with increased livingness (owing to the use of low ppm concentrations of catalyst), efficient synthesis of a wide range of architectures including block copolymers, bottle brushes²⁴ and star polymers²⁵ as well as faster polymerization rates. Those attributes have proven beneficial towards the synthesis of hybrid materials including protein-polymer bioconjugates under mild conditions

(e.g. blue light), as elegantly demonstrated by Matyjaszewski and co-workers.²⁶ Such hybrid materials have been comprehensively covered in a recent review by Maynard and co-workers.²⁷ Currently, photo-ATRP is widely reported to operate in a near ideal manner (i.e. high end-group fidelity at high conversions) for the polymerization of acrylates while there are significantly fewer reports on the polymerization of methacrylates. Other monomers, including styrenics and (meth)acrylamides or monomers with functional moieties are more difficult to polymerize and remain a challenge. Another limitation hindering the extensive use of photo-ATRP is the fact that different light sources (wavelengths) are required for each respective ligand, thus the discovery of a universal catalytic system which would be compatible with a range of ligands and monomers would be highly beneficial. In addition, perfect temporal control cannot be attained due to the increased lifetime of the active catalyst, although this has been partly addressed recently.²⁸ Furthermore, due to the use of homemade light boxes with various intensities, exact reproducibility of polymerization rates in different groups can also be a challenge.

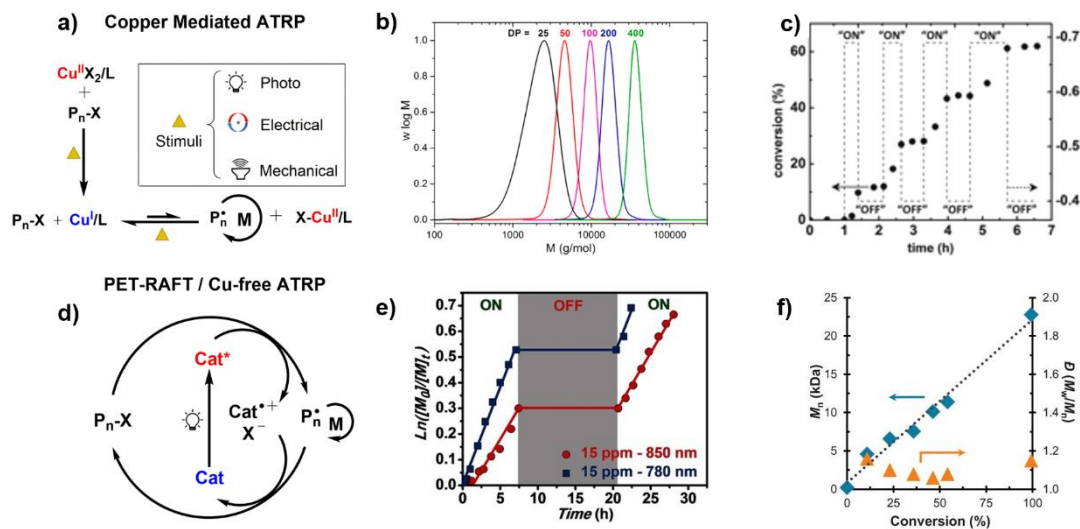


Figure 1. 3: Stimuli-induced RDRP. A) Simplified mechanisms of a Cu-mediated ATRP, B) Photo-ATRP: SEC traces of PMA with various DP (25-400) prepared by photo-mediated polymerization in the presence of UV light ($\lambda_{max} \approx 360$ nm), C) e-ATRP: Conversion (solid circles) and applied potential (dashed line) with respect to time. D) Simplified mechanisms of a PET-RAFT/Metal-free ATRP, E) PET-RAFT: Dependence of $\ln([M]_0/[M]_t)$ on the exposure time under NIR (red circles) and far-red (blue squares) irradiation that was switched on and off, and F) Organocatalyzed ATRP: Plot of M_n and \bar{D} versus monomer conversion for the polymerization of MMA under continuous irradiation.

Despite the advantages of photo-ATRP, the metal contamination of the final polymers may limit potential applications. To address this, Hawker's and Miyake's groups independently reported the first examples of metal-free ATRP, also referred to as organocatalyzed ATRP. In particular,

Hawker, Fors and co-workers used the photoredox catalyst 10-phenylphenothiazine under 380 nm irradiation at room temperature to polymerize methacrylic monomers in a controlled fashion, yielding polymers with high end-group fidelity and low dispersities.²⁹ In parallel, Miyake's group utilized perylene as an organic visible-light photocatalyst to mediate the polymerization of MMA.³⁰ However, upon monitoring the polymerization kinetics, it was noticed that the weight-average molecular weight slightly decreased during the polymerization which suggests a deviation from a controlled polymerization. Nevertheless, block copolymers were still reported, albeit exhibiting higher dispersity values compared to those synthesized by PTH polymerization. To improve this system the same group, guided by computational simulations, subsequently reported the use of diaryl dihydrophenazine photo redox catalysts which allowed for the controlled polymerization of methacrylic monomers, reaching low dispersity values (as low as $\bar{D} = 1.10$) even at high monomer conversions (**figure 1.3 F**).³¹ The synthesis of diblock copolymers was also possible, although higher dispersity values were obtained ($\bar{D} = 1.37-1.63$). Apart from omitting the use of metals, these metal-free or organocatalyzed ATRP methodologies are advantageous in that they exhibit perfect temporal control due to the limited lifetime of the excited state of the photocatalyst. However, good control over the polymerization is reported mostly for methacrylates while the polymerization of acrylic and styrenic monomers leads to less control over the molar mass distributions. In a recent promising publication, the controlled metal-free ATRP polymerization of acrylic monomers was reported by Miyake's group.³² In addition, end-group fidelity is not as high as in the metal-mediated photo-ATRP encouraging further research in the area. Moreover, the range of currently available catalysts is rather limited, thus hindering the widespread use of these methodologies. Another remaining challenge in the area is the limited number of solvents reported which, in turn, narrows down the scope of accessible monomers. Last but not least, despite avoiding the use of metals, tedious purification of the organic catalyst is also required. It is also unclear whether in the presence of the organic catalyst, such materials can be used directly for bio-applications or cases in which intense visible color is not preferred. As such, organic photocatalysts that would yield colorless polymers would also be highly beneficial.

PET-RAFT Polymerization

In 2014, Boyer and co-workers developed the first example of PET-RAFT polymerization.³³ By using very low concentrations of the photoredox catalyst *fac*-[Ir(ppy)₃] (~1 ppm to monomers), the polymerization of both conjugated and unconjugated monomers was feasible through the use of low-energy visible light-emitting diode (LED) as the light source ($\lambda = 435$ nm). Impressively, this method also gave access to ultra-high molecular weight homopolymers (up to 2,000 kDa), well-defined block copolymers and *in-situ* sequence-controlled multiblocks with excellent temporal control. Boyer, Xu and co-workers further expanded the scope of the initial photocatalyst by exploring various metalloporphyrins.³⁴ This enabled the use of a broader range of wavelengths (from 435 nm to 655 nm) while allowed to manipulate the reaction rate. In particular, they discovered that zinc porphyrins could selectively activate the PET-RAFT polymerization with trithiocarbonate compounds to control the polymerization of a wide range of monomers. In contrast, other thiocarbonylthio compounds (e.g., dithiobenzoate, dithiocarmamate, xanthate) could not be activated in an efficient manner. Importantly, the use of organic dyes was also investigated, expanding the possibilities of PET-RAFT polymerization in the absence of metal photocatalysts.³⁵ The Boyer group subsequently introduced far-red light and near-infrared (NIR) to mediate the polymerization through the use of Bacteriochlorophyll as a photoredox catalyst (**figure 1.3 E**).³⁶ Although PET-RAFT polymerization was just discovered six years ago, it has already been implemented in a range of additional developments such as surface PET-RAFT polymerization from DNA³⁷ and living cells³⁸ and 3D/4D printing systems.³⁹ Perhaps the most significant advantage of PET-RAFT polymerization is the use of low-intensity light sources which do not degrade the RAFT agents (in contrast to other photo-RAFT polymerization techniques). Another important advantage is that the use of a conventional free radical initiator (e.g., azobisisobutyronitrile =AIBN) is avoided, thus leading to polymers with improved livingness. As opposed to conventional RAFT processes where high temperatures are employed, PET-RAFT polymerization is considered a greener alternative due to the low temperatures employed which also leads to the reduction, or even elimination of by-products and side reactions. Finally, PET-RAFT can tolerate significant amounts of oxygen (see further section on oxygen-tolerant polymerizations) and exhibits perfect temporal control. Despite these impressive developments, there are still challenges that need to be addressed. For instance, the discovery of additional efficient and selective photocatalysts would be highly desirable for applications in which orthogonality is beneficial. In addition, the development of a

universal photocatalyst compatible with a range of monomers, RAFT agents and wavelengths is also needed. Moreover, the scope of the compatible solvents also needs to be expanded in order to maximize the benefits of this versatile polymerization methodology (DMSO is by far the most used solvent). Finally, although initial computational studies to identify suitable photocatalysts have been conducted,⁴⁰ further correlation between experimental and theoretical/predictive studies is required.

Electrochemically Mediated Controlled Radical Polymerization

Electrochemical stimulus has a number of benefits including temporal control (**figure 1.3 C**), ppm catalyst concentrations and manipulation of polymerization rate by adjusting the applied current or voltage. Such processes can also be environmentally friendly because of the possibility to eliminate reducing agents while leveraging electrodeposition as a facile removal/recycle process. Matyjaszewski and co-workers pioneered this field and reported the first example of copper-mediated e-ATRP by using an externally applied electrochemical potential to *in-situ* reduce CuBr_2 to CuBr and fine-tune the ratio between activator and deactivator.⁴¹ In the original publication, methyl acrylate (MA) was successfully polymerized in acetonitrile using ppm concentrations of catalyst (~50 ppm) yielding a well-defined polymer with narrow distribution of molar masses ($\mathcal{D} \sim 1.06$) and good agreement between theoretical and experimental values. Perhaps two limitations on this original report were the complicated set-up and the limited scope of solvents. These constraints were circumvented by the same group who developed a further simplification of the e-ATRP set-up which allowed much easier access to rapid and controlled polymerizations.⁴² Today, e-ATRP is possible for acrylic, methacrylic and acrylamide-based monomers while the technique is compatible with a range of solvents including aqueous media. In addition, e-ATRP enables the polymerization of functional monomers such as methacrylic acid.⁴³ The possibility to control the polymerization of further functional and less activated monomers would be one of the next exciting directions in the area. Apart from copper-mediated e-ATRP, Fe-mediated e-ATRP is also possible as elegantly reported by Amatore, Labbe and co-workers, although it has not been expanded significantly since the first report in 2009.⁴⁴ Given the versatility and broad monomer scope of RAFT polymerization, e-RAFT could be an attractive development. However, to date this concept has not been fully realized due to a number of limitations such as the irreversible redox processes involved in a RAFT polymerization and the decomposition of the RAFT agents.

Other External Stimuli

In 2017, Esser-Kahn and co-workers described the first mechanically controlled radical polymerization. The authors utilized piezoelectric BaTiO₃ nanoparticles and ultrasound to *in-situ* reduce CuBr₂ to CuBr, thus enabling a controlled radical polymerization. Despite this pioneering development, only polymers of relatively low molecular weight were explored.⁴⁵ The system was further expanded by the groups of Matyjaszewski and Xia who demonstrated good temporal control and the synthesis of higher molecular weight polymers through the use of ppm concentrations of copper catalyst, reduced amounts of BaTiO₃ nanoparticles and a low-intensity ultrasound bath.⁴⁶ In early 2018, the groups of Matyjaszewski/Xia and Qiao independently published the first examples of sono-ATRP in aqueous media.^{47,48} In particular, by exposing the polymerization mixture to ultrasonication at room temperature, water-soluble monomers could be polymerized in a controlled fashion. However, solvolysis of water yielded reactive hydroxyl radicals which in turn could create additional polymer chains. It is noted that the temporal control for these systems was not ideal as the polymerization was continued even during the “off” periods. Another challenge in the area is the polymerization of hydrophobic moieties and the possibility to reach higher molecular weights (>50 kDa) while maintaining monomodal molar mass distributions. In parallel with the ATRP developments, sono-RAFT was also reported in 2017 by Qiao, Ashokkumar and co-workers.⁴⁹ In the original publication, ultrasound was used as an external stimulus to produce initiating radicals (hydroxyl radicals and hydrogen atoms) in aqueous media. This sono-RAFT is environmentally friendly, also referred to as a “green” process, as it is conducted at ambient conditions (e.g., room temperature) and aqueous media. It is also noted that high frequencies were employed (400 kHz/40 W), conditions under which the chemical effect dominates and shear force is eliminated. In particular, water-soluble acrylates and acrylamides were successfully polymerized reaching relatively high molecular weights (>50 kDa) and very low dispersity. Excellent temporal control was also maintained in this system. The concept was then transferred to organic media, although much more specialized conditions and tedious optimizations were required for selecting suitable monomers and solvents.⁵⁰ Overall, the aqueous system appears to function better as opposed to the organic counterpart in terms of control over the polymerization and final dispersities. Nevertheless, sono-RAFT still requires extensive optimization and design of specific conditions such as the monomer concentration, the vapour pressure of both monomer and solvent and the need for varied frequencies depending on the structure of monomer/solvent. A potentially interesting future direction would be to assess

the potential of such systems to undergo efficient block formation and target various architectures.

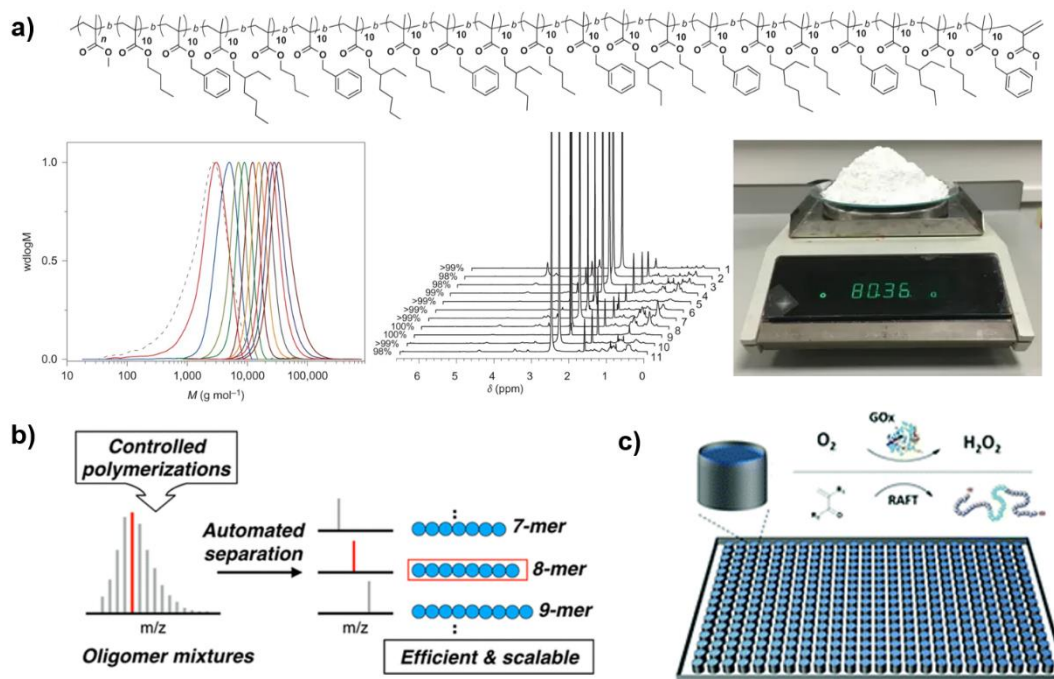


Figure 1. 4: Selected examples in sequence-controlled multiblocks, discrete oligomers, and oxygen-tolerant polymerizations. A) Scalable synthesis of methacrylic sequence-controlled multiblocks via sulphur-free RAFT emulsion polymerization, B) Isolation of discrete polymers via automated flash chromatography and C) Oxygen consumption via enzyme glucose oxidase (GOx) during a RAFT polymerization.

Ultra-High Molecular Weight Polymers (UHMW)

Access to ultra-high molecular weight polymers has always been a target for polymer chemists to not only unlock further applications but to also demonstrate the capability of a given system to maintain high livingness and afford the synthesis of high molecular weight polymers. This concept has been mostly realized in aqueous media and/or using high k_p monomers such as acrylamides. Following seminal work by Percec and co-workers in 2006 who synthesized several UHMW polymers in protic solvents,⁵¹ many groups significantly expanded the scope of accessing such materials. For instance, Sumerlin and co-workers utilized light and iniferter chemistry to produce polyacrylamides in aqueous media exhibiting fast polymerization rates (in particular when using xanthates), low dispersity values ($\mathcal{D} \sim 1.03-1.43$) with final molecular weights up to 8 MDa.⁵² The Qiao group also employed similar chemistry to yield UHMW star polymers with high livingness and suppressed side-reactions.⁵³ UHMW polymers have also been achieved by other

groups mainly using RAFT polymerization and emulsion processes and have been critically reviewed recently by An.⁵⁴ It should be mentioned that the synthesis of UHMW is dominated by RAFT polymerization with significantly less examples reported on ATRP. Arguably, a main limitation here is that low k_p monomers are much more challenging to reach UHMW, in particular when polymerized in organic solvents. More recently, the Sumerlin group published the synthesis of a range of ULMW polymer classes in organic solvents thus showing great promise towards this direction.⁵⁵ UHMW block copolymers maintaining high end-group fidelity are also difficult to produce, although some examples were recently demonstrated.⁵² It should also be highlighted that the characterization of such materials is not trivial, thus limiting further research in the area. Following this, determining the exact nature of the end-groups of such materials is impossible by currently available analytical techniques and should be a focus of future studies.

Sequence-Controlled Multiblock Copolymers

Sequence-defined polymers (truly monodisperse materials) are not covered herein; the reader is referred to a recent review.⁵⁶ In addition, polymers with controlled monomer sequence (i.e. precise insertion of maleimide monomers leads to polymer folding) will not be discussed as they were mainly developed in the previous decade.⁵⁷ In this section, sequence-controlled multiblocks are defined as polydisperse polymers obtained by regulating the monomer sequence in RDRP. In the early days of RDRP, high monomer conversions were avoided to ensure high end-group fidelity which would subsequently facilitate the efficient synthesis of block copolymers. In 2011, Whittaker and co-workers utilized Cu(0)-mediated radical polymerization and reported the first example of one pot sequence-controlled multiblock copolymers comprising very short blocks (degree of polymerization DP = 2) without the need for purification between each block formation.⁵⁸ Following this seminal work, Haddleton and co-workers reported higher molecular weight decablock copolymers via copper mediated photoinduced radical polymerization achieving near-quantitative monomer conversion and very high end-group fidelity per block.⁵⁹ In another contribution from the same group, the *in-situ* disproportionation of CuBr/Me₆TREN in aqueous media was exploited yielding acrylamide-based hexablock copolymers.⁶⁰ Besides the contribution of this one-pot approach to multiblocks this is also one of the fastest approaches to polymerize the challenging acrylamide class by copper-mediated polymerization in aqueous media. In 2013, Perrier and co-workers enabled the synthesis of an impressive icosablock copolymer via a scalable and optimized conventional RAFT polymerization approach in which extremely low amounts of free radical initiator were employed in aqueous media.⁶¹ It is noted

that this strategy is particularly efficient for high k_p monomers such as acrylamides and acrylates. The first example of the challenging methacrylic sequence-controlled multiblocks was published in 2017 by Haddleton, Davis, Anastasaki and co-workers who exploited sulphur-free emulsion RAFT polymerization yielding heneicosablock copolymers in the absence of either sulphur or copper contamination (**figure 1.4 A**).⁶² More recently, Zetterlund and co-workers employed sulphur RAFT emulsion polymerization to also produce methacrylic multiblock copolymers in a controlled fashion.⁶³ A critical work in the area was published by Harrisson and co-workers who showed that the statistical nature of RDRP may limit the control possible in sequence-controlled multiblocks. In particular, his study concluded that for lower DP multiblocks (< 6 units per block), defective chains dominate and thus the purity of the materials is compromised.⁶⁴ An important limitation in this area is that each individual method is capable of controlling the polymerization of one monomer family. For instance, the sulphur-free RAFT methodology only works for methacrylic monomers while the vast majority of conventional RAFT and ATRP reports focus on acrylates and acrylamides. Thus, the development of a universal system allowing for sequence-controlled multiblocks from different monomer families (separately and all together) is urgently required. In addition, obtaining higher molecular weight multiblocks (>50/100 kDa per block) and multiblocks consisting of functional moieties is also challenging. The progress in the development of these materials has considerably simplified polymerization protocols allowing for complex multiblock copolymers to be obtained in a facile manner. However, current applications of these materials is rather limited and should be the focus of future research.

From Monodisperse to Polydisperse Materials

Due to the statistical nature of RDRP, monodisperse polymers ($\mathcal{D} \sim 1$) are currently impossible to directly synthesize. Recently, Hawker and co-workers used automated flash chromatography to isolate discrete polymers ($\mathcal{D} \sim 1$) from higher dispersity polymers made by RDRP (**figure 1.4 B**).⁶⁵ Although this methodology is highly reproducible, it is quite tedious and time-consuming and limited to low molecular weight polymers (typically, polymers of up to DP = 15 can be isolated) and specific polymer types, making them important challenges in the area. Until very recently, low-dispersity polymers were the main focus of RDRP following a common misconception that only such materials are associated with high end-group fidelity/livingness. However, it has been recently shown that both low and high-dispersity polymers exhibit unique characteristics and functions and even high-dispersity materials can have impressively high end-group fidelity. Such reports have led to the development of further strategies to tune both the dispersity and the

shape of molar mass distributions. For example, Fors and co-workers employed a novel temporal initiation regulation method that allows deterministic control over the molar mass distribution.⁶⁶ Apart from engineering approaches, chemical methods have also been developed allowing for the efficient tailoring of polymer dispersity.^{67,68} Such methods not only enable the synthesis of a range of polymers with different dispersities in a controlled fashion, which in turn are useful for a number of applications, but may also increase our fundamental understanding in RDRP. Current challenges here include the potential of a specific approach to control the dispersity and the shape of molar mass distributions (in both a symmetric and asymmetric way) for a wide range of molecular weights, different polymer classes and architectures.

Oxygen-Tolerant Polymerization

For many years, RDRP was conducted under strictly deoxygenated conditions as oxygen is a well-known radical scavenger. One of the first examples of oxygen-tolerant polymerization in RDRP was published by Matyjaszewski and co-workers back in 1998. In a sealed vessel and in the presence of Cu(0) as a reducing agent, low-dispersity polymers were obtained in the absence of any deoxygenation method.⁶⁹ Although the development of activator (re)generated by electron transfer (A(R)GET)-ATRP enabled further studies in the area during the first decade of the millennium, it was not until the last decade that oxygen-tolerant polymerization has gained increased attention and popularity. In particular, oxygen-tolerant polymerizations are now a reality for a number of ATRP variations including supplemental activation reducing agent (SARA)-ATRP, photo-ATRP and e-ATRP in which the oxygen is being consumed before the start of the polymerization by the reaction components (e.g., typically by the initiating/propagating radicals or the catalyst/ligand).⁷⁰ In RAFT polymerization, it was also known early in 2000 that the presence of large amounts of free radical initiator can eliminate the presence of oxygen.⁷⁰ A noteworthy publication utilizing this approach in the last decade was in 2015 by Perrier, Gody and co-workers who reported the impressive synthesis of multiblock copolymers in the presence of air.⁷¹ Following a completely different approach, Stevens, Chapman and co-workers employed the enzyme glucose oxidase (GOx) to consume the oxygen during a RAFT polymerization (**figure 1.4 C**).⁷² In the same year, Boyer's group paved the way for oxygen-tolerant polymerizations by leveraging PET-RAFT, where the oxygen was consumed mainly by the photoredox catalyst.³³ Importantly, oxygen-tolerant polymerizations have also significantly simplified the synthesis of polymer-protein bioconjugates^{26,73} and surface polymerizations⁷⁴ which can now operate under extremely mild conditions. Overall, oxygen-tolerant polymerization strategies have simplified

RDRP processes by allowing facile access to the synthesis of large libraries of well-defined polymers. Perhaps the main limitation of some of these approaches is the longer induction periods, the use of excess of catalysts or reducing agents and the low initiator efficiency (the latter one holds true for ATRP cases). In addition, the synthesis of block copolymers via ATRP methodologies in the presence of air is more limited. Another challenge is the in-depth understanding of the mechanism of oxygen-tolerant RDRP approaches which will further assist in the optimization of the reaction conditions. Despite the development of oxygen-tolerant approaches, oxygen is still commonly regarded as an undesirable component in polymerization processes, and it is typically consumed prior to polymerization through various pathways. However, harnessing the potential of oxygen is an unconventional approach, and it will be demonstrated in Chapter 2.

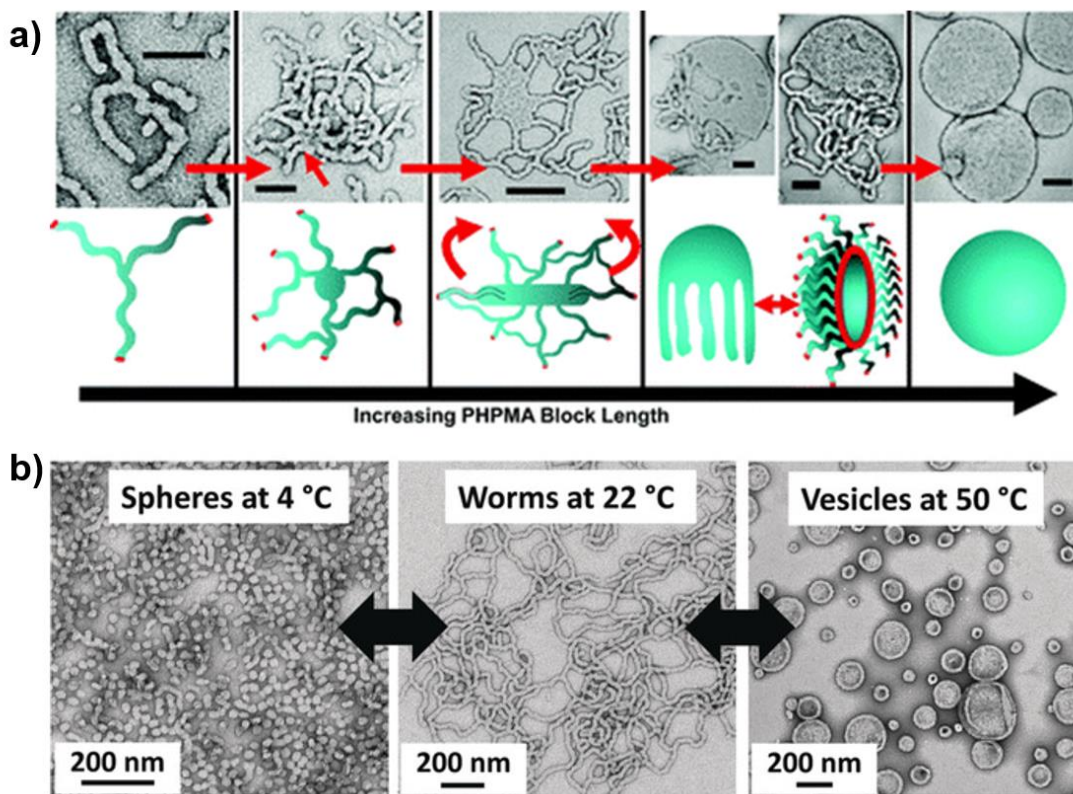


Figure 1. 5: Polymerization-induced self-assembly. A) Suggested mechanism for the polymerization-induced worm-to-vesicle transformation. B) Thermo-responsive order-to-order morphological transformation.

PISA

Polymerization-induced self-assembly (PISA) is a technique that was used in the past few decades to provide access to the concurrent synthesis of polymeric nanoparticles. At the early stages, the vast majority of the reported nanoparticles possessed a spherical shape. However, the shape of nanomaterials is of paramount importance for many applications ranging from catalysis to nanoengineering and biomedicine. During the last decade, PISA has been extensively evolved as a methodology to produce nanomaterials of various shapes.⁷⁵ The first example deviating from a spherical morphology was reported by Charleux, Delaittre and co-workers in 2009 who observed the formation of vesicles and worm-like micelles during the NMP of 4-vinylpyridine from a polyacrylic acid macroalkoxyamine.⁷⁶ The vast majority of the subsequent publications focused on PISA-RAFT dispersion polymerization, of which the first was published also in 2009 by Pan and co-workers who obtained both spherical and worm-like morphologies during the synthesis of poly(4-vinylpyridine)-*b*-polystyrene in methanol.⁷⁷ It is noted that this system relies on extremely high feed ratio of monomer (>5000 targeted DP of styrene). The excess of unreacted monomer acts as a good solvent for the polystyrene, thus allowing for increased flexibility of the core. In 2011, Armes and co-workers introduced an efficient and very fast aqueous dispersion polymerization (>99% conversion within 2 h) which allowed access to a number of morphologies (spheres, worms and vesicles) at high solid contents (**figure 1.5 A**).⁷⁸ The authors additionally observed for the first time a number of intermediate morphologies (e.g., octopus, jellyfish, and branched worms), thus enhancing the mechanistic understanding of the PISA process. Since then, the Armes group has been at the forefront of PISA and has expanded the scope to include various core monomers and solvents.⁷⁹ The same group has also studied the order-order morphological transformation of nanomaterials in the presence of external stimuli such as temperature and pH (**figure 1.5 B**) and expanded the applications of PISA particles.^{80,81} Despite these significant developments, an inherent limitation of PISA is the limited cores available for specific solvents (e.g. water) in order to access the synthesis of nanomaterials with various shapes. It should be noted that in particular for RAFT dispersion PISA, one of the blocks needs to gradually become solvophobic (starting from a solvophilic monomer) but not precipitate out (it should stay dispersed in solution) in order to induce self-assembly. Another challenge of PISA is that batch-to-batch variations may sometimes lead to irreproducible morphologies. This can however be improved by developing detailed phase diagrams (from the same macroinitiator) and further one-pot PISA processes. Although different morphologies can

be obtained from the same macroCTA, they typically consist of polymers with different molecular weights (as the second block grows it will first access spheres, then worms and then vesicles; all three with different molecular weights), thus not allowing for a direct comparison between various morphologies with identical molecular weights which is needed for applications. However, by using a thermoresponsive core-forming block, a wide range of morphologies can be formed from a single diblock copolymer composition at different temperatures.⁸¹ Apart from conventional PISA (where temperature is used to mediate the polymerization), different types of PISA have also been reported including photo-PISA,⁸² and polymerization-induced thermal self-assembly (PITSA).^{79,83} It should also be highlighted that initial attempts to utilize ATRP for PISA have been realized, although further research in the area is required. Pleasingly, PISA has already shown great promise in potential applications with the Armes group reporting that nanoparticles can be utilized as lubricants with low viscosity.⁸⁴ Many more examples of applications are expected in the coming decade. The main challenge in the field, which we aimed to address in Chapter 5, is the fact that the majority of current protocols to produce polymeric nanoparticles are limited in polymer scope. These protocols often alter the chemical structure, operate at high temperatures, and can be fairly tedious and time-consuming.

Thus, developing a technique that can easily change the shape of polymeric nanoparticles on-demand under mild conditions is of paramount importance.

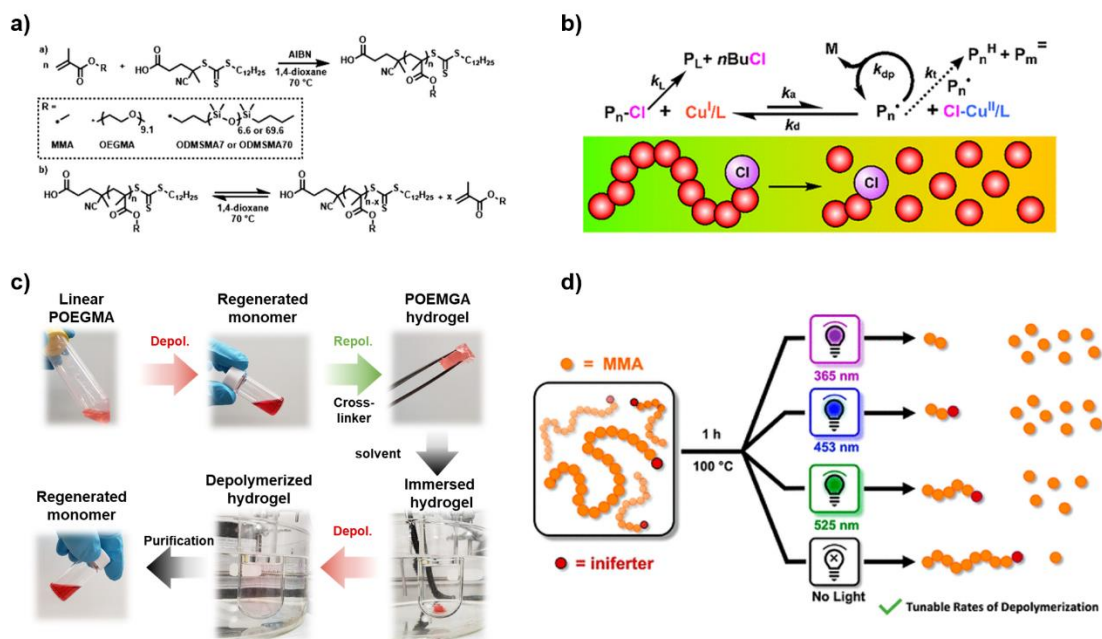


Figure 1. 6: Examples of reversing RDRP through depolymerization. A) RAFT depolymerization of polymers with bulky side chain B) Proposed mechanism of depolymerization of polymers made via ATRP, C) RAFT Depolymerization of poly(oligo(ethylene glycol) methyl ether methacrylate), repolymerization into a hydrogel, and subsequent depolymerization of the hydrogel and D) Light-assisted RAFT depolymerization.

Reversing RDRP

Reversing RDRP is an emerging and intriguing area of research. The depolymerization of polymers back to their initial monomers shows significant potential to push the boundaries of polymer science forward. In the case of polymers that are produced through RDRP and retain functional end-groups, recent demonstrations have shown that these functional end-groups can be activated and under thermodynamically favorable conditions, the polymerization process can be reversed, resulting in the regeneration of virgin monomers from the polymers.⁸⁵⁻⁸⁷

The first examples of depolymerization were demonstrated using polymers with macromonomers as repeated units. First, Gramlich and coworkers, in 2018, demonstrated the *ex-situ* depolymerization (i.e., depolymerization of a purified polymer) of poly(poly(dimethylsiloxane) methacrylate) P(PDMSMA) and poly(oligo(ethylene glycol) methyl ether methacrylate) (POEGMA) bottlebrushes terminated with a trithiocarbonate end-group.⁸⁸ By diluting the polymer in dioxane to a repeat unit concentration of 28 mM and heating the

polymer solution at 70 °C, they were able to regenerate 35% of the monomer after 56 h (**figure 1.6 A**).

The Matyjaszewski group has successfully utilized ATRP-synthesized polymers and an ATRP catalyst to exploit the higher depolymerization propensity of chlorine-capped P(PDMSMA) bottlebrush polymers. By employing a copper(II) chloride/tris(2-pyridylmethyl)amine (CuCl₂/TPMA) catalyst system, the depolymerization process took place at rather high temperatures (170 °C), with a repeat unit concentration of 275 mM.⁸⁹ This method has yielded impressive results, with monomer generation reaching as high as 70-80%. In subsequent examples from our group, RAFT-depolymerization was extended to encompass more challenging non-bulky polymers, resulting in nearly quantitative conversions.⁸⁵ This depolymerization process was carried out in dioxane at 120 °C, using a 5 mM repeat unit concentration. Notably, the RAFT agent employed in the depolymerization process could be reused, enabling the controlled RAFT polymerization of the regenerated monomer. Our lab also demonstrated the first depolymerization of an insoluble hydrogel, as well as thermosensitive polymers that could not have been depolymerized with traditional methods such as pyrolysis due to high temperature requirements (**figure 1.6 C**). The Matyjaszewski group has also reported the depolymerization of non-bulky polymers using copper or iron catalysts, reaching a maximum depolymerization of 70% (**figure 1.6 B**).^{90,91} This was achieved by employing high temperatures (170 °C) and varying repeat unit concentrations. However, it is worth noting that due to the high temperatures involved in ATRP depolymerization, extensive chain-end loss can occur, which limits the system from achieving near-quantitative depolymerization conversions. The current challenge in ATRP depolymerization is to develop milder conditions, including lower temperatures and lower catalyst concentrations, to enable chain end maintenance and maximize depolymerization conversions. This specific challenge will be the focus of Chapter 3. Lastly, the groups of Sumerlin and Anastasaki explored the use of light as a stimulus to assist in the depolymerization reaction. Sumerlin's approach involves radical generation through direct photolysis of the chain-end of the chain transfer agent (CTA), similar to a photoiniferter polymerization process, instead of relying solely on thermal methods as previously utilized.⁹² They investigated depolymerization of PMMA with different end-groups (different RAFT agents) and discovered that approximately 70% depolymerization could be achieved in just 1 hour under optimized conditions (5 mM repeat unit concentration in dioxane) (**figure 1.6 D**). The photoactivation to generate depropagating radicals also appears to lower the temperature at

which depolymerization can occur, with monomer generation observed at temperatures as low as 100 °C. Simultaneously, Anastasaki and colleagues reported the light-accelerated depolymerization of RAFT-synthesized polymethacrylates catalyzed by a photocatalyst, Eosin Y, at 100 °C (5 mM repeat unit concentration in dioxane).⁹³ The synergistic effect of Eosin Y and visible light resulted in a significant acceleration of the depolymerization in the early stages, leading to a final conversion of up to 82% for dithiobenzoate-terminated PMMA. However, neither of these two approaches presented a temporal regulation but only depolymerization rate enhancement.

Challenges Addressed in this Thesis

In this thesis, I will present some of the challenges I addressed in the field of RDRP. The first chapter focuses on a study that challenges a commonly held belief regarding the role of oxygen in polymerization reactions. Our findings reveal that oxygen, contrary to being an undesirable component in the reaction, can actually facilitate polymerization through the *in-situ* formation of a superoxido copper complex. This complex was demonstrated to be a highly active catalyst for ATRP. This research not only enhances the fundamental understanding of ATRP but also provides a straightforward experimental procedure that utilizes an air-insensitive catalyst.

The second chapter focuses on reversing RDRP via light. In particular, I developed a photocatalytic depolymerization procedure, which effectively reverses ATRP and converts pre-synthesized polymers back into monomer. The main challenge in this study was to overcome the harsh depolymerization conditions that often resulted in chain-end loss and inefficient depolymerization. By utilizing photocatalytic depolymerization, I was able to significantly decrease the reaction temperature and minimize the amount of catalyst required. This decrease in temperature and catalyst concentration allowed for temporal regulation of the system, providing a new tool for depolymerization reactions.

Chapter three describes an investigation regarding the polymerization of monomers derived from renewable resources. The objective of this work was twofold: firstly, to investigate and promote the use of monomers obtained from renewable sources, and secondly and most importantly, to explore the optimal polymerization procedure. Surprisingly, despite RAFT polymerization being generally considered more versatile than ATRP, and the majority of renewable monomers being polymerized via RAFT polymerization, I demonstrated that ATRP

can offer superior control in the polymerization of lignocellulose-derived methacrylates. This resulted in polymers with enhanced control over their molar mass distribution. This rare occurrence showcases ATRP as a more suitable method for greener synthesis of polymers from renewable resources, particularly in the case of methacrylates.

In the final chapter, I present our work on polymer self-assembly and how we successfully addressed the challenge of modifying the morphology of polymeric nanoparticles. While various approaches have been developed to obtain polymeric nanoparticles with different morphologies, these techniques often have limitations in terms of the applicable polymer range or require harsh conditions to alter the nanoparticle morphology. By introducing a small amount of transformer (a core-compatible solvent), I was able to precisely control the shape of the nanoparticles. This was achieved by providing flexibility to the core-forming blocks and manipulating the packing parameter. This novel approach offers a versatile and mild method for altering nanoparticle morphology, surpassing the limitations of existing techniques.

References

- (1) Feldman, D. *Des. Monomers Polym.*, **2008**, *11*, 1.
- (2) Staudinger, H. *Berichte der deutschen chemischen Gesellschaft (A and B Series)* **1920**, *53*, 1073.
- (3) Corrigan, N.; Jung, K.; Moad, G.; Hawker, C. J.; Matyjaszewski, K.; Boyer, C. *Prog. Polym. Sci.* **2020**, *111*, 101311.
- (4) Odian, G. *Principles of polymerization*; John Wiley & Sons, 2004.
- (5) Szwarc, M. *Nature* **1956**, *178*, 1168.
- (6) Solomon, D. H.; Rizzardo, E.; Cacioli, P.; U.S. Pat., 4581429, **1986**.
- (7) Wang, J.-S.; Matyjaszewski, K. *J. Am. Chem. Soc.* **1995**, *117*, 5614.
- (8) Kato, M.; Kamigaito, M.; Sawamoto, M.; Higashimura, T. *Macromolecules* **1995**, *28*, 1721.
- (9) Chiefari, J.; Chong, Y.; Ercole, F.; Krstina, J.; Jeffery, J.; Le, T. P.; Mayadunne, R. T.; Meijs, G. F.; Moad, C. L.; Moad, G. *Macromolecules* **1998**, *31*, 5559.
- (10) Georges, M. K.; Veregin, R. P.; Kazmaier, P. M.; Hamer, G. K. *Macromolecules* **1993**, *26*, 2987.
- (11) Hawker, C. J.; Bosman, A. W.; Harth, E. *Chem. Rev.* **2001**, *101*, 3661.
- (12) Benoit, D.; Chaplinski, V.; Braslau, R.; Hawker, C. J. *J. Am. Chem. Soc.* **1999**, *121*, 3904.
- (13) Hawker, C. J. *J. Am. Chem. Soc.* **1994**, *116*, 11185.
- (14) Lorandi, F.; Fantin, M.; Matyjaszewski, K. *J. Am. Chem. Soc.* **2022**, *144*, 15413.
- (15) Perrier, S. b. *Macromolecules* **2017**, *50*, 7433.
- (16) Parkatzidis, K.; Wang, H. S.; Truong, N. P.; Anastasaki, A. *Chem* **2020**, *6*, 1575.
- (17) Junkers, T. *Macromol. Chem. Phys.*, **2017**, *218*, 1600421.
- (18) Guan, Z.; Smart, B. *Macromolecules* **2000**, *33*, 6904.

- (19) Tasdelen, M. A.; Uygun, M.; Yagci, Y. *Macromol. Rapid Commun.* **2011**, *32*, 58.
- (20) Mosnáček, J.; Ilčíková, M. t. *Macromolecules* **2012**, *45*, 5859.
- (21) Konkolewicz, D.; Schröder, K.; Buback, J.; Bernhard, S.; Matyjaszewski, K. *ACS Macro Lett.* **2012**, *1*, 1219.
- (22) Anastasaki, A.; Nikolaou, V.; Zhang, Q.; Burns, J.; Samanta, S. R.; Waldron, C.; Haddleton, A. J.; McHale, R.; Fox, D.; Percec, V. *J. Am. Chem. Soc.* **2014**, *136*, 1141.
- (23) Fors, B. P.; Hawker, C. J. *Angew. Chem. Int. Ed.* **2012**, *51*, 8850.
- (24) Martinez, M. R.; Sobieski, J.; Lorandi, F.; Fantin, M.; Dadashi-Silab, S.; Xie, G.; Olszewski, M.; Pan, X.; Ribelli, T. G.; Matyjaszewski, K. *Macromolecules* **2019**.
- (25) Wenn, B.; Martens, A.; Chuang, Y.-M.; Gruber, J.; Junkers, T. *Polym. Chem.* **2016**, *7*, 2720.
- (26) Fu, L.; Wang, Z.; Lathwal, S.; Enciso, A. E.; Simakova, A.; Das, S. R.; Russell, A. J.; Matyjaszewski, K. *ACS Macro Lett.* **2018**, *7*, 1248.
- (27) Messina, M. S.; Messina, K. M.; Bhattacharya, A.; Montgomery, H. R.; Maynard, H. D. *Prog. Polym. Sci.* **2020**, *100*, 101186.
- (28) Dolinski, N. D.; Page, Z. A.; Discekici, E. H.; Meis, D.; Lee, I. H.; Jones, G. R.; Whitfield, R.; Pan, X.; McCarthy, B. G.; Shanmugam, S. *J. Polym. Sci., Part A: Polym. Chem.* **2019**, *57*, 268.
- (29) Treat, N. J.; Sprafke, H.; Kramer, J. W.; Clark, P. G.; Barton, B. E.; Read de Alaniz, J.; Fors, B. P.; Hawker, C. J. *J. Am. Chem. Soc.* **2014**, *136*, 16096.
- (30) Miyake, G. M.; Theriot, J. C. *Macromolecules* **2014**, *47*, 8255.
- (31) Theriot, J. C.; Lim, C.-H.; Yang, H.; Ryan, M. D.; Musgrave, C. B.; Miyake, G. M. *Science* **2016**, *352*, 1082.
- (32) Buss, B. L.; Lim, C. H.; Miyake, G. M. *Angew. Chem. Int. Ed.* **2020**, *59*, 3209.
- (33) Xu, J.; Jung, K.; Atme, A.; Shanmugam, S.; Boyer, C. *J. Am. Chem. Soc.* **2014**, *136*, 5508.
- (34) Shanmugam, S.; Xu, J.; Boyer, C. *J. Am. Chem. Soc.* **2015**, *137*, 9174.
- (35) Xu, J.; Shanmugam, S.; Duong, H. T.; Boyer, C. *Polym. Chem.* **2015**, *6*, 5615.
- (36) Shanmugam, S.; Xu, J.; Boyer, C. *Angew. Chem. Int. Ed.* **2016**, *55*, 1036.
- (37) Lueckerath, T.; Strauch, T.; Koynov, K.; Barner-Kowollik, C.; Ng, D. Y.; Weil, T. *Biomacromolecules* **2018**, *20*, 212.
- (38) Niu, J.; Lunn, D. J.; Pusuluri, A.; Yoo, J. I.; O'Malley, M. A.; Mitragotri, S.; Soh, H. T.; Hawker, C. J. *Nat. Chem.* **2017**, *9*, 537.
- (39) Zhang, Z.; Corrigan, N.; Bagheri, A.; Jin, J.; Boyer, C. *Angew. Chem.* **2019**, *131*, 18122.
- (40) Wu, C.; Chen, H.; Corrigan, N.; Jung, K.; Kan, X.; Li, Z.; Liu, W.; Xu, J.; Boyer, C. *J. Am. Chem. Soc.* **2019**, *141*, 8207.
- (41) Magenau, A. J.; Strandwitz, N. C.; Gennaro, A.; Matyjaszewski, K. *Science* **2011**, *332*, 81.
- (42) Park, S.; Chmielarz, P.; Gennaro, A.; Matyjaszewski, K. *Angew. Chem. Int. Ed.* **2015**, *54*, 2388.
- (43) Fantin, M.; Isse, A. A.; Venzo, A.; Gennaro, A.; Matyjaszewski, K. *J. Am. Chem. Soc.* **2016**, *138*, 7216.
- (44) Bonometti, V.; Labbé, E.; Buriez, O.; Mussini, P.; Amatore, C. *J. Electroanal. Chem.*, **2009**, *633*, 99.
- (45) Mohapatra, H.; Kleiman, M.; Esser-Kahn, A. P. *Nat. Chem.* **2017**, *9*, 135.
- (46) Wang, Z.; Pan, X.; Yan, J.; Dadashi-Silab, S.; Xie, G.; Zhang, J.; Wang, Z.; Xia, H.; Matyjaszewski, K. *ACS Macro Lett.* **2017**, *6*, 546.

- (47) Wang, Z.; Wang, Z.; Pan, X.; Fu, L.; Lathwal, S.; Olszewski, M.; Yan, J.; Enciso, A. E.; Wang, Z.; Xia, H. *ACS Macro Lett.* **2018**, *7*, 275.
- (48) Collins, J.; McKenzie, T. G.; Nothling, M. D.; Ashokkumar, M.; Qiao, G. G. *Polym. Chem.* **2018**, *9*, 2562.
- (49) McKenzie, T. G.; Colombo, E.; Fu, Q.; Ashokkumar, M.; Qiao, G. G. *Angew. Chem. Int. Ed.* **2017**, *56*, 12302.
- (50) Collins, J.; McKenzie, T. G.; Nothling, M. D.; Allison-Logan, S.; Ashokkumar, M.; Qiao, G. G. *Macromolecules* **2018**, *52*, 185.
- (51) Percec, V.; Guliashvili, T.; Ladislaw, J. S.; Wistrand, A.; Stjerndahl, A.; Sienkowska, M. J.; Monteiro, M. J.; Sahoo, S. J. *Am. Chem. Soc.* **2006**, *128*, 14156.
- (52) Carmean, R. N.; Becker, T. E.; Sims, M. B.; Sumerlin, B. S. *Chem* **2017**, *2*, 93.
- (53) Allison-Logan, S.; Karimi, F.; Sun, Y.; McKenzie, T. G.; Nothling, M. D.; Bryant, G.; Qiao, G. G. *ACS Macro Lett.* **2019**, *8*, 1291.
- (54) An, Z. *ACS Macro Lett.* **2020**, *9*, 350.
- (55) Carmean, R. N.; Sims, M. B.; Figg, C. A.; Hurst, P. J.; Patterson, J. P.; Sumerlin, B. S. *ACS Macro Lett.* **2020**, *9*, 613.
- (56) De Neve, J.; Haven, J. J.; Maes, L.; Junkers, T. *Polym. Chem.* **2018**, *9*, 4692.
- (57) Badi, N.; Lutz, J.-F. *Chem. Soc. Rev.* **2009**, *38*, 3383.
- (58) Soeriyadi, A. H.; Boyer, C.; Nyström, F.; Zetterlund, P. B.; Whittaker, M. R. *J. Am. Chem. Soc.* **2011**, *133*, 11128.
- (59) Anastasaki, A.; Nikolaou, V.; Pappas, G. S.; Zhang, Q.; Wan, C.; Wilson, P.; Davis, T. P.; Whittaker, M. R.; Haddleton, D. M. *Chem. Sci.* **2014**, *5*, 3536.
- (60) Alsubaie, F.; Anastasaki, A.; Wilson, P.; Haddleton, D. M. *Polym. Chem.* **2014**, *6*, 406.
- (61) Gody, G.; Maschmeyer, T.; Zetterlund, P. B.; Perrier, S. *Nat. Commun.* **2013**, *4*, 1.
- (62) Engelis, N. G.; Anastasaki, A.; Nurumbetov, G.; Truong, N. P.; Nikolaou, V.; Shegiwal, A.; Whittaker, M. R.; Davis, T. P.; Haddleton, D. M. *Nat. Chem.* **2017**, *9*, 171.
- (63) Clothier, G. K.; Guimarães, T. R.; Khan, M.; Moad, G.; Perrier, S. b.; Zetterlund, P. B. *ACS Macro Lett.* **2019**, *8*, 989.
- (64) Gody, G.; Zetterlund, P. B.; Perrier, S.; Harrison, S. *Nat. Commun.* **2016**, *7*, 1.
- (65) Lawrence, J.; Lee, S.-H.; Abdilla, A.; Nothling, M. D.; Ren, J. M.; Knight, A. S.; Fleischmann, C.; Li, Y.; Abrams, A. S.; Schmidt, B. V. *J. Am. Chem. Soc.* **2016**, *138*, 6306.
- (66) Gentekos, D. T.; Dupuis, L. N.; Fors, B. P. *J. Am. Chem. Soc.* **2016**, *138*, 1848.
- (67) Whitfield, R.; Truong, N. P.; Messmer, D.; Parkatzidis, K.; Rolland, M.; Anastasaki, A. *Chem. Sci.* **2019**, *10*, 8724.
- (68) Whitfield, R.; Parkatzidis, K.; Truong, N. P.; Junkers, T.; Anastasaki, A. *Chem* **2020**.
- (69) Matyjaszewski, K.; Coca, S.; Gaynor, S. G.; Wei, M.; Woodworth, B. E. *Macromolecules* **1998**, *31*, 5967.
- (70) Yeow, J.; Chapman, R.; Gormley, A. J.; Boyer, C. *Chem. Soc. Rev.* **2018**, *47*, 4357.
- (71) Gody, G.; Barbey, R.; Danial, M.; Perrier, S. *Polym. Chem.* **2015**, *6*, 1502.
- (72) Chapman, R.; Gormley, A. J.; Stenzel, M. H.; Stevens, M. M. *Angew. Chem. Int. Ed.* **2016**, *55*, 4500.
- (73) Theodorou, A.; Liarou, E.; Haddleton, D. M.; Stavrakaki, I. G.; Skordalidis, P.; Whitfield, R.; Anastasaki, A.; Velonia, K. *Nat. Commun.* **2020**, *11*, 1.
- (74) Layadi, A.; Kessel, B.; Yan, W.; Romio, M.; Spencer, N. D.; Zenobi-Wong, M.; Matyjaszewski, K.; Benetti, E. M. *J. Am. Chem. Soc.* **2020**, *142*, 3158.

- (75) Khor, S. Y.; Quinn, J. F.; Whittaker, M. R.; Truong, N. P.; Davis, T. P. *Macromol. Rapid Commun.* **2019**, *40*, 1800438.
- (76) Delaittre, G.; Dire, C.; Rieger, J.; Putaux, J.-L.; Charleux, B. *Chem. Commun.* **2009**, 2887.
- (77) Wan, W.-M.; Hong, C.-Y.; Pan, C.-Y. *Chem. Commun.* **2009**, 5883.
- (78) Blanazs, A.; Madsen, J.; Battaglia, G.; Ryan, A. J.; Armes, S. P. *J. Am. Chem. Soc.* **2011**, *133*, 16581.
- (79) Penfold, N. J.; Yeow, J.; Boyer, C.; Armes, S. P.; *ACS Macro Lett.* **2019**, *8*, 8, 1029.
- (80) Lovett, J. R.; Warren, N. J.; Ratcliffe, L. P.; Kocik, M. K.; Armes, S. P. *Angew. Chem. Int. Ed.* **2015**, *54*, 1279.
- (81) Ratcliffe, L. P.; Derry, M. J.; Ianiro, A.; Tuinier, R.; Armes, S. P. *Angew. Chem. Int. Ed.* **2019**, *58*, 18964.
- (82) Tan, J.; Sun, H.; Yu, M.; Sumerlin, B. S.; Zhang, L. *ACS Macro Lett.* **2015**, *4*, 1249.
- (83) Figg, C. A.; Simula, A.; Gebre, K. A.; Tucker, B. S.; Haddleton, D. M.; Sumerlin, B. S. *Chem. Sci.* **2015**, *6*, 1230.
- (84) Derry, M. J.; Smith, T.; O'hora, P. S.; Armes, S. P. *ACS Appl. Mater. Inter.*, **2019**, *11*, 33364.
- (85) Jones, G. R.; Wang, H. S.; Parkatzidis, K.; Whitfield, R.; Truong, N. P.; Anastasaki, A. *J. Am. Chem. Soc.* **2023**.
- (86) Martinez, M. R.; Matyjaszewski, K. *CCS Chemistry* **2022**, *4*, 2176.
- (87) Tang, H.; Luan, Y.; Yang, L.; Sun, H. *Molecules* **2018**, *23*, 2870.
- (88) Flanders, M. J.; Gramlich, W. M. *Polym. Chem.* **2018**, *9*, 2328.
- (89) Martinez, M. R.; Dadashi-Silab, S.; Lorandi, F.; Zhao, Y.; Matyjaszewski, K. *Macromolecules* **2021**, *54*, 5526.
- (90) Martinez, M. R.; De Luca Bossa, F.; Olszewski, M.; Matyjaszewski, K. *Macromolecules* **2021**, *55*, 78.
- (91) Martinez, M. R.; Schild, D.; De Luca Bossa, F.; Matyjaszewski, K. *Macromolecules* **2022**, *55*, 10590.
- (92) Young, J. B.; Bowman, J. I.; Eades, C. B.; Wong, A. J.; Sumerlin, B. S. *ACS Macro Lett.* **2022**, *11*, 1390.
- (93) Bellotti, V.; Parkatzidis, K.; Wang, H. S.; Watuthanthrige, N. D. A.; Orfano, M.; Monguzzi, A.; Truong, N. P.; Simonutti, R.; Anastasaki, A. *Polym. Chem.* **2023**, *14*, 253.

Chapter 2: Oxygen-Enhanced Atom Transfer Radical Polymerization through the Formation of a Superoxido Copper Complex

This chapter has been published in Journal of American Chemical Society and I am the lead/first author (K. Parkatzidis, N. P. Truong, R. Whitfield, C. E. Campi, B. Grimm-Lebsanft, S. Buchenau, M. A. Rübhausen, S. Harrisson, D. Konkolewicz, S. Schindler, and A. Anastasaki, Oxygen-Enhanced Atom Transfer Radical Polymerization through the Formation of a Copper Superoxido Complex, J. Am. Chem. Soc., 2023, 145, 3, 1906). Permission was obtained from the publisher (American Chemical Society). All the experiments included in this chapter have been performed by myself unless otherwise stated.

Summary

In controlled radical polymerization, oxygen is typically regarded as an undesirable component resulting in terminated polymer chains, deactivated catalysts, and subsequent cessation of the polymerization. In this chapter, I present an unusual atom transfer radical polymerization whereby oxygen favors the polymerization by triggering the *in-situ* transformation of CuBr/L to reactive superoxido species at room temperature. Through a superoxido ARGET-ATRP mechanism, an order of magnitude faster polymerization rate and a rapid and complete initiator consumption can be achieved as opposed to when un-oxidized CuBr/L was instead employed. Very high end-group fidelity has been demonstrated by mass-spectrometry and one-pot synthesis of block and multiblock copolymers while pushing the reactions to reach near-quantitative conversions in all steps. A high molecular weight polymer could also be targeted ($DP = 6400$) without compromising the control over the molar mass distributions ($\mathcal{D} < 1.20$), even at an extremely low copper concentration (4.5 ppm). The versatility of the technique was demonstrated by the polymerization of various monomers in a controlled fashion. Notably, the efficiency of the developed methodology is unaffected by the purity of the starting CuBr, and even a brown highly-oxidized 15-year-old CuBr reagent enabled a rapid and controlled polymerization with a final dispersity of 1.07, thus not only reducing associated costs but also omitting the need for rigorous catalyst purification prior to polymerization.

Introduction

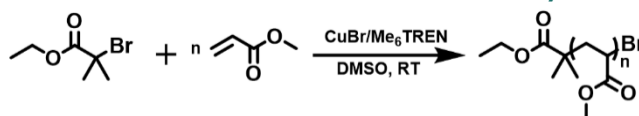
During the past 100 years, there have been extraordinary developments in the field of polymer science. Among these, RDRP has received considerable attention and has been recognized by IUPAC as a potentially world-changing technology in chemistry.¹⁻³ These methods have enabled access to an enormous scope of polymeric and hybrid materials.⁴⁻¹⁷ As it was discussed in Chapter 1, all RDRP methodologies are based on a radical mechanism. This makes them more tolerant to functional groups, solvents and reaction conditions, in contrast to ionic polymerization, but it is this radical nature that requires the vast majority of radical polymerizations to be conducted under anaerobic conditions.¹⁸ Oxygen is a known radical scavenger which can irreversibly react with active carbon-centred radicals in the polymerization, producing peroxy radicals that have poor ability in propagating the polymer chain.^{19,20} Additionally, when a sensitive catalyst, for example copper or any other metal in low oxidation state, is used oxygen can oxidize them affecting their catalytic ability. As a result, the presence of oxygen can lead to terminated polymer chains, deactivated catalyst and subsequent cessation of the polymerization.¹⁸ To avoid this, the reaction mixtures must be either rigorously deoxygenated (i.e. by freeze-pump-thaw cycles, nitrogen sparging, etc.) or the polymerization must be performed in a glovebox. These processes may be time-and-money consuming and limit the practicability of polymerization from both biological and industrial perspectives. To bypass these deoxygenation procedures, lately, a number of so-called "oxygen-tolerant" RDRP approaches have been developed. These make use of a sacrificial reagent (e.g. enzyme, reducing agent, catalyst, etc.) often combined with various stimuli such as light²¹⁻²³ to effectively consume the oxygen prior to the start of the polymerization.²⁴⁻²⁶ For example, the enzyme glucose oxidase (GOx)²⁷ effectively deoxygenates RAFT polymerizations by converting glucose and oxygen to gluconolactone and hydrogen peroxide.^{28,29} In an alternative approach, PET-RAFT polymerizations could be conducted in an open vessel by either adding a reducing agent or by increasing the amount of photocatalyst.³⁰ In ATRP, GOx was utilized as a catalyst to consume oxygen in the presence of glucose and sodium pyruvate, and headspace elimination in conjunction with copper catalysis has also been proved suitable to self-deoxygenate ATRP solutions.³¹⁻³⁴ Other examples in ATRP use reducing agents or light to consume limited amount of oxygen *in-situ*. For example, in photo-ATRP, it was found that the choice of reaction components significantly impacts the rate of oxygen consumption and can subsequently affect both the polymerization time and the dispersity of the resulting

polymer.²⁹ Apart from the *in-situ* generated catalyst, ATRP initiator, in the radical form, could also react with oxygen affecting the control of the polymerization. However, if the head space of the reaction vessel is reduced, thus the amount of dissolved oxygen is limited, the control of the polymerization can still be successful with some percentage of the reaction components getting consumed/sacrificed via the reaction with oxygen.³¹ It can thus be concluded that oxygen is thoroughly removed either prior to the polymerization or as the reaction proceeds by introducing enzymes or reducing agents. As such, oxygen is considered an undesirable component and is associated with extensive termination events and side reactions. On the contrary, oxygen is rarely employed as a reagent in order to benefit a controlled radical polymerization.³⁵ As an exception to this rule, there have been a few reports about the positive role of oxygen in RAFT polymerization. First Boyer and co-workers utilized oxygen as a co-catalyst (in the presence of trimethylamine and zinc photocatalyst) to activate a RAFT agent, demonstrating a new PET-RAFT polymerization under far-red light irradiation.³⁶ The same group also reported an oxygen-mediated reductive quenching pathway whereby the majority of oxygen was sufficiently eliminated while the remaining catalytic amount of oxygen served as a co-catalyst and triggered a controlled polymerization.³⁷ Very recently, Kwon and co-workers reported a novel organic photocatalyst for additive-free oxygen-accelerated polymerization in ambient and aqueous environments. The proposed mechanism included the generation of singlet oxygen by the excited state photocatalyst and activation of the raft agent by the superoxide radical anion. Other examples in RAFT polymerization have employed triethylborane complexes that react with oxygen to produce ethyl radicals that can act as an initiating species instead of free radical initiator, usually employed in RAFT polymerization. In the field of ATRP, Matyjaszewski and co-workers employed GOx and horseradish peroxidase alongside copper complexes to report the first example of "oxygen-fueled" ATRP whereby oxygen was continuously fed into the reaction mixture to generate radicals and allow the polymer chains to grow.³³ In all these examples, a range of additional components is required in conjunction with oxygen to trigger a successful polymerization. Notably, the presence of oxygen is less tolerated in ATRP than in RAFT polymerization, as CuBr/L is an oxygen-sensitive catalyst. As such, when conducting a traditional ATRP, CuBr has to be rigorously purified from oxidized contaminants and kept under an inert atmosphere prior to usage, thus significantly adding to the complexity of the process. Developing more oxygen-tolerant ATRP catalysts would be highly beneficial for a range of practical applications.³⁸ In this chapter, I present the *in-situ* transformation of Cu^IBr/L to

superoxido species $\text{Cu}^{\text{II}}\text{O}_2/\text{L}$ in the presence of Me_6TREN (L) and DMSO. In comparison to the CuBr/L catalyst, the formation of the copper superoxido complex resulted in very fast ATRP, full consumption of the initiator (within seconds) and elimination of the induction period. Upon initiation, a much higher rate of polymerization was achieved (i.e. an order of magnitude higher) and the reactions reached quantitative monomer conversions without compromising the control over the molar mass distributions ($\mathcal{D} = 1.07$). In addition, very high end-group fidelity was confirmed by mass spectrometry allowing for the synthesis of high molecular weight polymers (up to $\text{DP} = 6,400$) as well as the one-pot formation of diblock and multiblock copolymers. The technique was found to be applicable to various monomers while the purity of the initial CuBr did not affect the integrity of the final materials, thus omitting the catalyst purification step that is often required for traditional ATRP reactions.

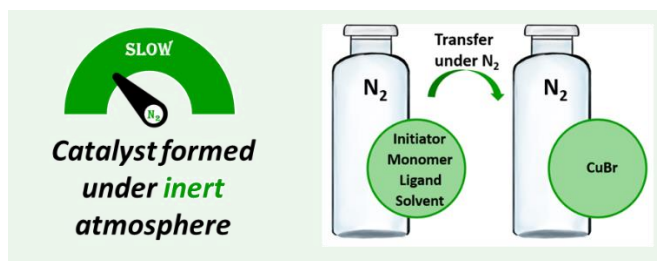
Results and Discussion

Discovery of Oxygen-Enhanced Atom Transfer Radical Polymerization



Scheme 2. 1: General reaction scheme illustrating the polymerization of MA via ATRP.

Our investigation was conducted using MA as a model monomer, CuBr as a copper source, Me_6TREN as a ligand, and DMSO as a solvent (**scheme 2.1**). In traditional ATRP, a common practice is to protect the oxygen-sensitive CuBr catalyst from oxidation by keeping it under an inert atmosphere followed by the addition of a thoroughly deoxygenated solution containing the remainder of the reaction components (e.g. ligand, solvent, initiator, and monomer) (**scheme 2.2**).



Scheme 2. 2: Schematic representation of conventional ATRP in which the formation of the catalyst occurs under inert atmosphere.

Interestingly, when this procedure was applied to low catalyst concentrations (i.e. 0.02 equiv. with respect to the ATRP initiator), a very long induction period was observed with only 4% conversion reached within the first 10 h (**figure and table 2.1**).

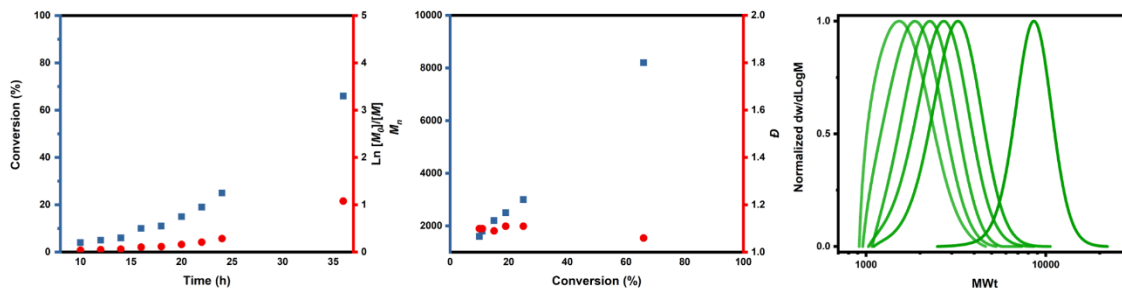


Figure 2. 1: Polymerization kinetic data for conventional ATRP approach of MA under the conditions: $[MA]/[EBiB]/[CuBr]/[Me_6TREN] = 100:1:0.02:0.12$.

$[MA]:[EBib]:[CuBr]:[Me_6TREN]$	Time (h)	Conversion (%)	M_n (Theo.) (Da)	M_n (SEC) (Da)	\bar{D}
100:1:0.02:0.12	10	4	540	-	
	12	5	620	-	
	14	6	710	-	
	16	10	1060	1600	1.10
	18	11	1140	1800	1.10
	20	15	1500	2200	1.09
	22	19	1800	2500	1.11
	24	25	2300	3000	1.10
	36	66	5900	8200	1.06

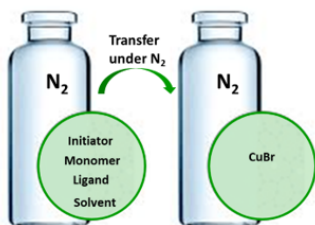


Table 2. 1: 1H NMR and SEC analysis of polymerization kinetic of MA under the conditions: $[MA]/[EBiB]/[CuBr]/[Me_6TREN] = 100:1:0.02:0.12$. The catalyst was formed under conventional ATRP approach.

Following the induction period, a well-controlled polymerization took place, albeit at a very slow rate reaching 66% conversion in 36 h. The prolonged induction period was attributed to slow initiation, as confirmed by the typical kinetic profile and by 1H NMR whereby slow initiator consumption was observed (**figure 2.2**).

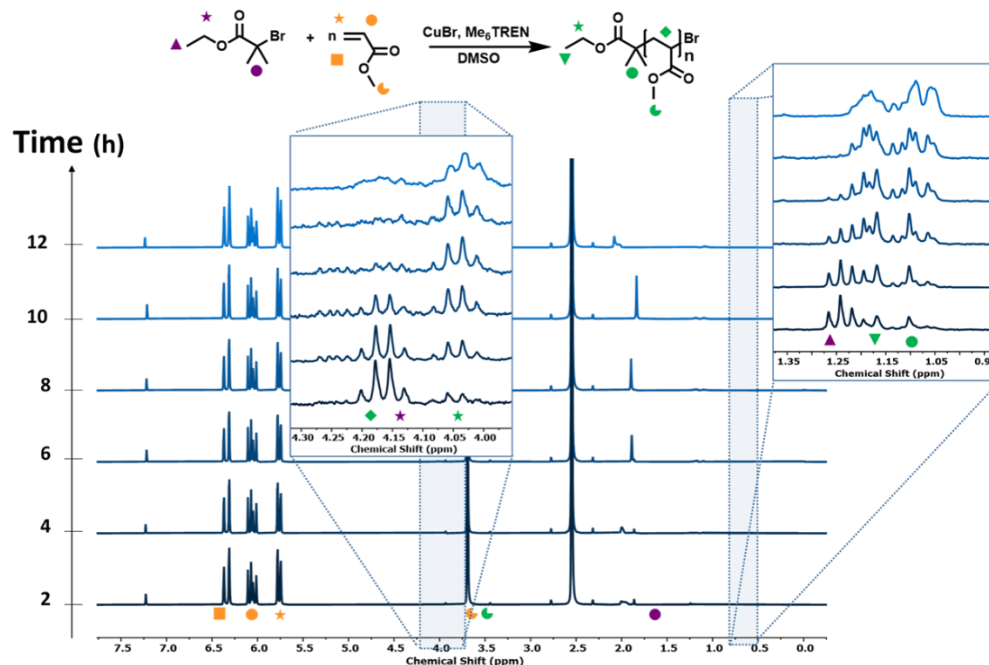


Figure 2. 2: ^1H NMR analysis of the polymerization kinetic of MA for conventional ATRP. Data points are acquired during the induction period of the polymerization.

These results indicate that CuBr/L is oxidized to CuBr_2/L through the persistent radical effect.³⁹ The excess of ligand subsequently acts as a reducing agent and a slow ARGET ATRP takes place at room temperature.⁴⁰ To explore this scenario, we conducted an additional experiment whereby CuBr was replaced by CuBr_2 under otherwise identical conditions. A very comparable kinetic profile was obtained (**figure 2.3, table 2.2**), thus validating our initial hypothesis that most CuBr/L is rapidly converted to CuBr_2/L at the beginning of the reaction.

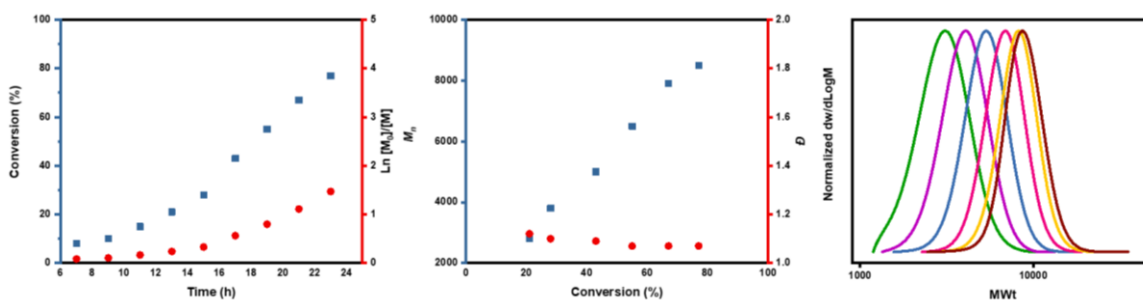


Figure 2. 3: Polymerization kinetics of MA under the conditions: $[\text{MA}]/[\text{EBiB}]/[\text{CuBr}_2]/[\text{Me}_6\text{TREN}] = 100:1:0.02:0.12$.

[MA]:[EBiB]:[CuBr ₂]: [Me ₆ TREN]	Time (h)	Conversion (%)	$M_{n(Theory)}$ (Da)	$M_{n(SEC)}$ (Da)	\bar{D}
100:1:0.02:0.12	7	8	8800	-	
	9	10	1100	-	
	11	15	1500	-	
	13	21	2000	2800	1.12
	15	28	2600	3800	1.10
	17	43	3900	5000	1.09
	19	55	4900	6500	1.07
	21	67	6000	7900	1.07
	23	77	6800	8500	1.07

Table 2. 2: ¹H NMR and SEC analysis of polymerization kinetics of MA under the conditions: [MA]/[EBiB]/[CuBr₂]/[Me₆TREN] = 100:1:0.02:0.12.

However, when the catalyst was formed under ambient atmosphere (i.e. in the presence of air) by simply mixing ppm concentration of CuBr with DMSO and Me₆TREN followed by a conventional deoxygenation of the resulting mixture (**scheme 2.3**), a completely different kinetic profile was observed (**figure 2.4** and **table 2.3**).



Scheme 2. 3: Schematic representation of oxygen-enhanced ATRP in which the formation of the catalyst occurs under ambient atmosphere.

In particular, the long induction period was eliminated and a very fast initiation took place whereby all the ATRP initiator was completely consumed within a few seconds. Notably, the polymerization rate was much faster and detailed kinetic analysis revealed a short induction period of 3.43 min before the polymerization starts with an initial apparent rate constant of 0.0252 min⁻¹. First order kinetics were then observed for 14.5 min (rate constant of 0.069 min⁻¹). Following this period, a steady state radical concentration was reached and the polymerization continued with an apparent rate constant of 0.00491 min⁻¹. M_n increased linearly with time and good agreement between theoretical and experimental molecular weights was observed. \bar{D} values slightly decreased throughout the polymerization, as expected from a controlled process

with the final \bar{D} being as low as 1.09.^{41,42} Importantly, near-quantitative monomer conversions (>99%) could be achieved without compromising the \bar{D} value.

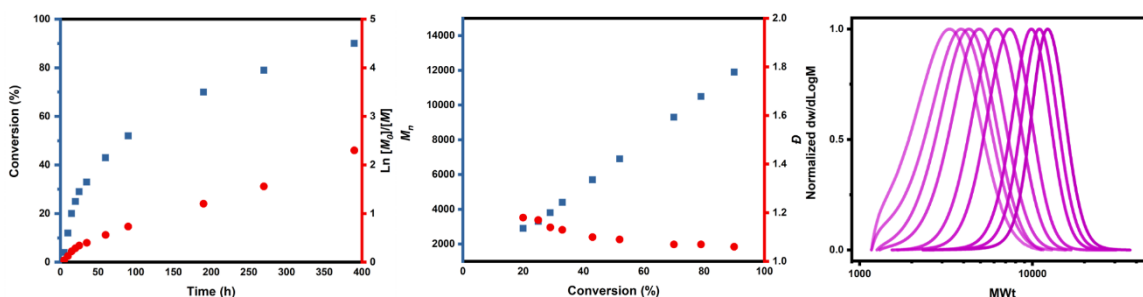


Figure 2. 4: Polymerization kinetic data for oxygen-enhanced ATRP approach of MA under the conditions: $[MA]/[EBiB]/[CuBr]/[Me_6TREN] = 100:1:0.02:0.12$.

$[MA]:[EBiB]:[CuBr]:[Me_6TREN]$	Time (min)	Conversion (%)	$M_n (Theo.)$ (Da)	$M_n (SEC)$ (Da)	\bar{D}
100:1:0.02:0.12	5	4	540	-	-
	10	12	1200	-	-
	15	20	1900	2900	1.18
	20	25	2300	3300	1.17
	25	29	2700	3800	1.14
	35	33	3000	4400	1.13
	60	43	3900	5700	1.10
	90	52	4600	6900	1.09
	190	70	6200	9300	1.07
	270	79	7000	10500	1.07
	390	90	7900	11900	1.06

Table 2. 3: 1H NMR and SEC analysis of polymerization kinetic of MA under the conditions: $[MA]/[EBiB]/[CuBr]/[Me_6TREN] = 100:1:0.02:0.12$. The catalyst was formed under oxygen-enhanced ATRP approach.

Additionally, matrix-assisted laser desorption/ionization time-of flight mass (MALDI-ToF-MS) was conducted to further investigate the living characteristics of the polymerization with both techniques clearly confirming excellent end-group fidelity (**figure 2.5a**). In addition, the high-end group fidelity was further demonstrated by the *in-situ* chain-extension of PMA with another aliquot of MA yielding a clear shift in the SEC traces as shown in **figure 2.5b**.

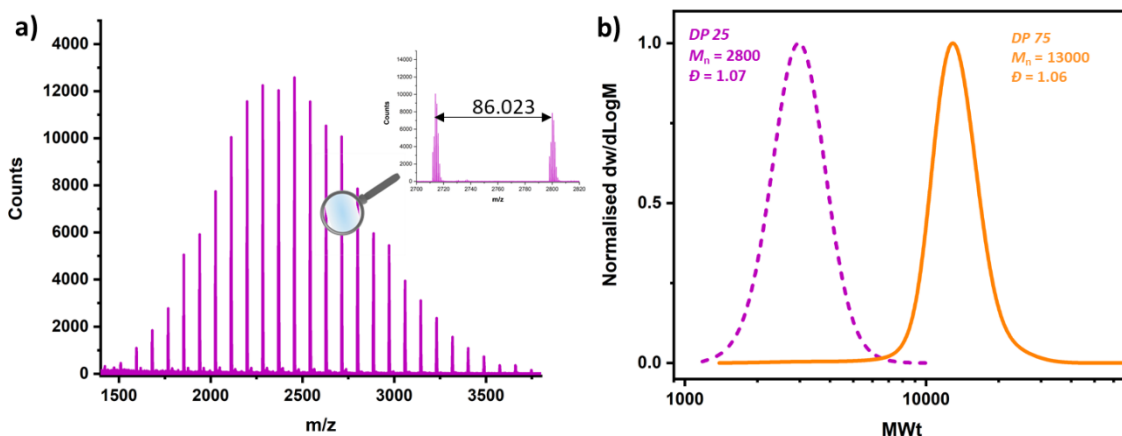


Figure 2. 5: (a) MALDI-ToF-MS analysis of PMA₂₅ synthesized by oxygen-enhanced ATRP and (b) *In-situ* chain-extension experiment. The MALDI-ToF-MS spectrum was acquired by Dr. Richard Whitfield.

To summarize, by simply forming the catalyst under ambient atmosphere and temperature (rather than under inert atmosphere) we were able to trigger a more favorable ATRP reaction with rapid initiator consumption, negligible, if any, induction period, significantly faster polymerization rates and quantitative monomer conversions (**figure 2.6**). It is noted that in our previous work in low ppm ATRP in DMSO,⁴⁰ although we also observed a relatively fast polymerization rate we attributed this to the small extent of reduction of CuBr₂ species (i.e. 1%). However, our current experiments suggest that the presence of oxygen is certainly responsible for the observed acceleration in rate. This is a very intriguing discovery considering that the literature recommends the thorough deoxygenation of the oxygen-sensitive CuBr/L catalyst prior to commencing the polymerization. Since the two experiments were conducted utilizing identical chemical components and ratios, their remarkable difference indicates fundamentally different mechanistic pathways.

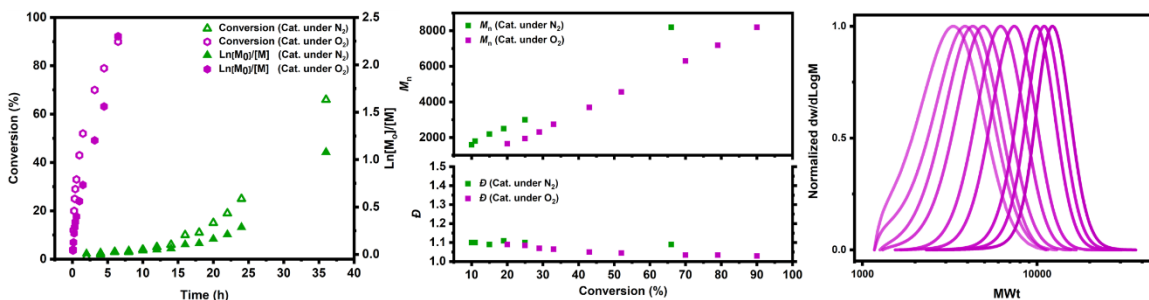


Figure 2. 6: Merged kinetic data comparing oxygen-enhanced ATRP (in purple) and conventional ATRP (in green) and SEC traces of PMA synthesized via oxygen-enhanced ATRP.

Mechanistic Investigation

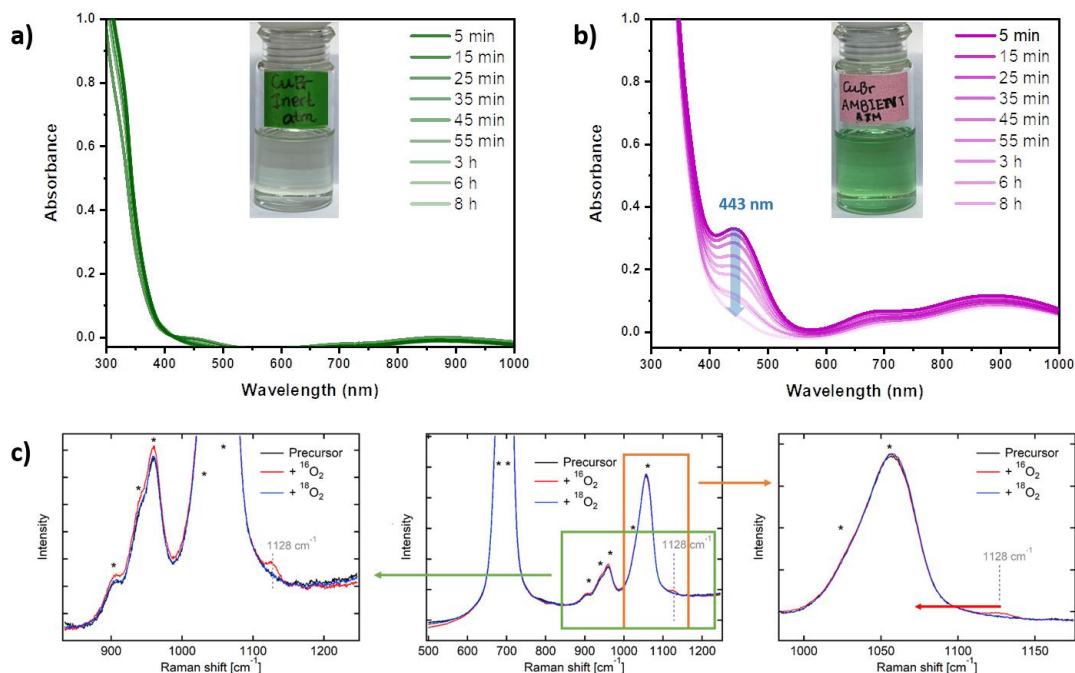
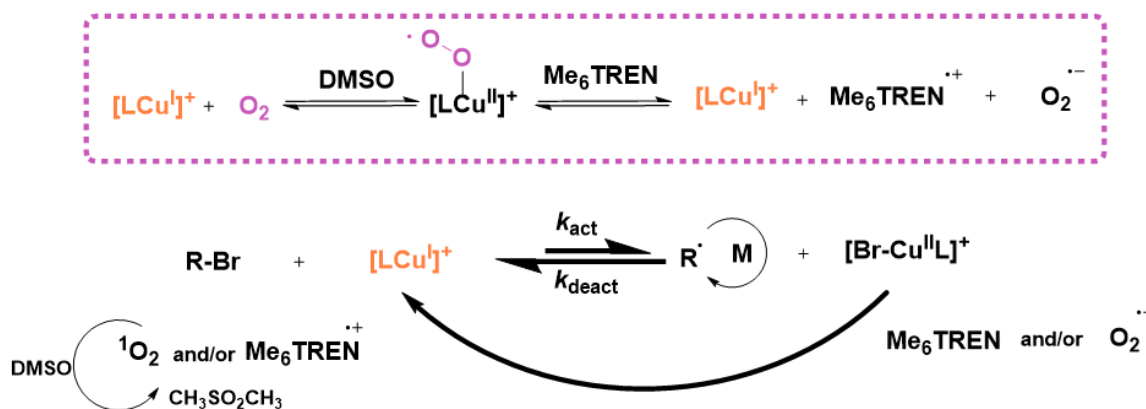


Figure 2. 7: (a) Monitoring of Cu^{II} formation by UV-Vis spectroscopy as formed in traditional ATRP (i.e. by mixing CuBr with deoxygenated Me₆TREN/DMSO under inert atmosphere) (b) Monitoring of Cu^{II} superoxido complex decay over time by UV-Vis spectroscopy as formed in oxygen-enhanced ATRP (i.e. by mixing CuBr with Me₆TREN/DMSO under ambient atmosphere prior to deoxygenation) (c) Raman analysis of the catalyst formed under ambient atmosphere. **The Raman spectrum was acquired and analyzed by the inorganic chemistry groups of professor Rübhausen and professor Schindler.**

Considering that the only difference between the experiments lies in the formation of the catalyst in the presence of air, we hypothesized that the oxygen may trigger the formation of copper superoxido species under our reaction conditions, thus yielding an enhanced ATRP pre-catalyst.^{43,44} To examine this possibility, a solution of DMSO/Me₆TREN/CuBr (in the absence of ATRP initiator and monomer) was prepared in two different ways in order to resemble the two polymerization protocols and visualize potential color differences. In the first case, a previously deoxygenated solution of DMSO/Me₆TREN was added to a vessel already containing deoxygenated CuBr (**figure 2.7a insert**). Upon mixing, the solution remained colorless, as expected, thus confirming that our thorough deoxygenation procedure prevents CuBr from oxidizing. Instead, in the second case where all the components (i.e. DMSO/ Me₆TREN /CuBr) were pre-mixed under ambient atmosphere prior to deoxygenation (**figure 2.7b insert**), a very intense green color could be observed suggesting the oxidation of Cu^I to Cu^{II}. This intense green color has been previously attributed to the formation of copper superoxido complexes.⁴⁵⁻⁴⁹ It is

important to note that this is a much more intense green color when compared to mixing CuBr₂/Me₆TREN/DMSO under ambient temperature which results in a pale green solution. The aforementioned solutions were subsequently measured by ultraviolet visible (UV-Vis) spectroscopy. In the first case (i.e. formation of CuBr/L catalyst under inert atmosphere), minimal absorption occurred in the range of $\lambda = 400-1000$ nm, which is typical of Cu^I(Me₆TREN)Br complexes in DMSO (**figure 2.7a**).⁵⁰ Instead, when the catalyst was formed under ambient atmosphere, an unusual UV-Vis spectrum was obtained which did not correspond to typical absorptions for either Cu^I(Me₆TREN)Br or Cu^{II}(Me₆TREN)Br₂ species (**figure 2.7b**). Specifically, an intense peak at $\lambda = 443$ nm was observed which decayed over a period of 30-60 minutes. This was accompanied by a broad bimodal absorption at $\lambda = 600 - 900$ nm. Notably, the initially observed UV-Vis profile matches very well with the spectra of superoxido copper complexes previously reported in the inorganic chemistry literature,^{45,48,49,51} which suggests that the superoxido complexes can be formed with a reasonable lifetime at room temperature in the presence of a commercially available ligand and DMSO. This contrasts with most current reports in which sophisticated ligands and low temperatures (-20 to -180°C) are required to stabilize the formed superoxido complexes.⁵²⁻⁵⁵ Further evidence of the formation of a superoxido complex is provided through reversibility experiments. It is known that superoxido complexes can undergo reversible reaction with oxygen several times prior to observing an unavoidable irreversible decay.^{45-47,56}

Unfortunately, our attempts to isolate the formed complex were unsuccessful, however a mononuclear end-on superoxido copper complex with a TREN related ligand has previously been structurally characterized, so far the only example that could be crystallized.⁵⁶ To further support the formation of the postulated superoxido copper complex Raman spectroscopy was applied. **Figure 2.7c** shows the characteristic band at 1128 cm⁻¹ of an end-on superoxido copper complex, in perfect agreement with previous measurements^{45,47,49,53} Replacing ¹⁶O₂ by ¹⁸O₂ led to the disappearance of this band, although the expected band of the Cu ¹⁸O₂ species was not observed, presumably due to its overlap with the solvent, DMSO. Taken altogether, the characterization methods employed have provided strong evidence for the formation of a copper superoxido complex at room temperature.



Scheme 2. 4: Proposed oxygen-enhanced ATRP mechanism.

Scheme 2.4 depicts the proposed ATRP mechanism. In the first part of the polymerization (first 20-25 min), an efficient ARGET-ATRP mechanism dominates whereby the combination of CuBr and Me₆TREN DMSO can efficiently activate dioxygen and produce the superoxido complex which is relatively stable at room temperature. The formed superoxido complex is then proposed to undergo a rapid reduction yielding Cu^I, a Me₆TREN radical cation, and O₂ superoxido anion. Cu^I then follows a traditional ATRP pathway whereby it abstracts the halogen resulting in a propagating radical and Cu^{II} deactivator. The excess of ligand as well as the produced superoxido anion can then accelerate the reduction of CuBr₂ accumulated through the ATRP equilibrium. After the first 20-25 min, the superoxido complex irreversibly decays and the mechanism switches to conventional ARGET ATRP. Overall, the acceleration of the polymerization rate is attributed to the fast reduction of Cu^{II} superoxido species to CuBr and the very high end-group fidelity observed can be explained by the gradual generation of CuBr which suppresses its high activity, thus preventing extensive termination events. To further clarify the mechanism, we confirmed the potential of the ligand to act as a reducing agent by a series of polymerization kinetic experiments whereby the more ligand is added, the faster the polymerization rate is while when stoichiometric amounts of ligand and copper are employed, no monomer conversion is observed (**figure 2.8**).

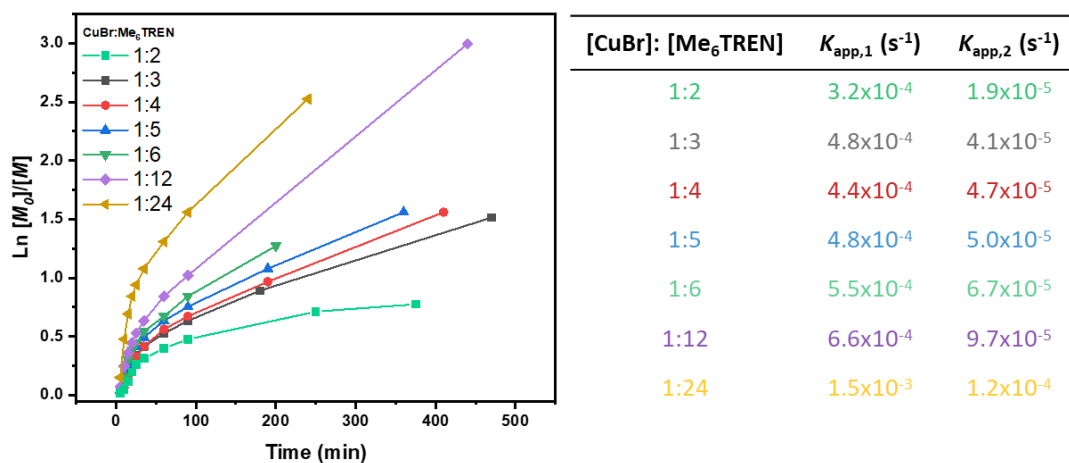


Figure 2. 8: Oxygen-enhanced polymerization kinetics of MA employing different amount of ligands.

Investigation into the Scope of Oxygen-Enhanced ATRP

Synthesis of a Multiblock Copolymer

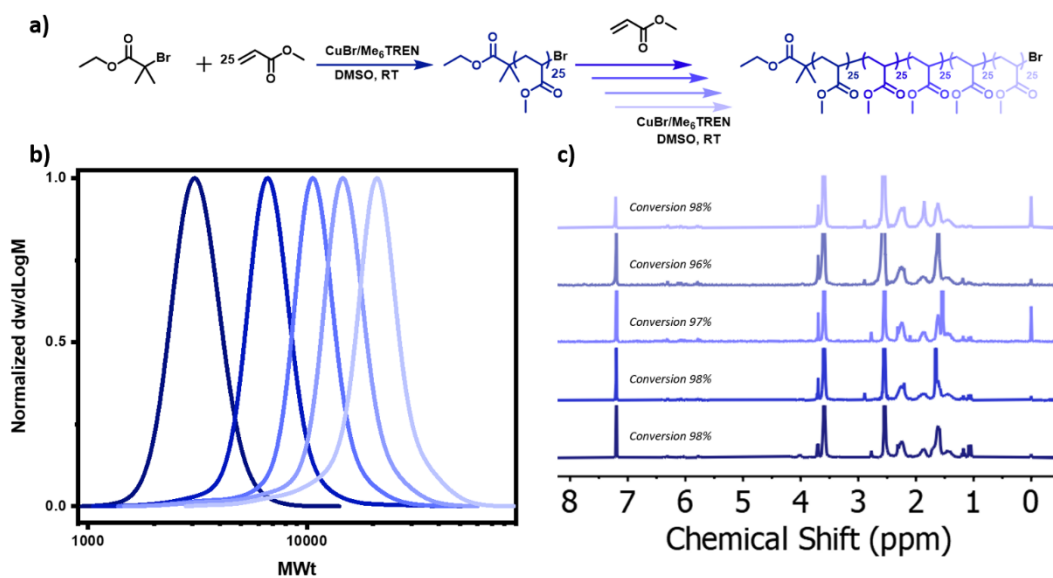


Figure 2. 9: Synthesis and characterization of a pseudo multiblock copolymer by oxygen-enhanced ATRP, (a) SEC traces of the molar mass distributions for consecutive cycles during the synthesis of a PMA pentablock copolymer and (b) ¹H NMR spectra for consecutive cycles whereby very high monomer conversions are reached for each iterative monomer addition step (>97 %).

[MA]:[Ebib]:[CuBr ₂]: [Me ₆ TREN]	Block	Time (h)	Conversion (%)	M_n (Theo.) (Da)	M_n (SEC) (Da)	\mathcal{D}
25:1:0.02:0.12	1 st	12	98	2300	3000	1.07
25:-:0.02:0.12	2 nd	10	98	4600	6400	1.09
25:-:0.02:0.12	3 rd	10	97	6700	10000	1.10
25:-:0.02:0.12	4 th	8	96	8800	13400	1.14
25:-:0.02:0.12	5 th	8	98	10800	17800	1.20

Table 2. 4: ¹H NMR and SEC analysis of the synthesis of a pseudo pentablock copolymer via oxygen-enhanced ATRP.

To explore the potential of oxygen-enhanced ATRP, we first investigated the possibility of synthesizing well-defined block copolymers. Our previously acquired MALDI-ToF-MS spectra indicated very high end-group fidelity without any sign of side reactions or termination events. To further investigate the livingness of the system, we subsequently chain-extended PMA (Block 1, $\mathcal{D} = 1.07$, 98% conversion) by the *in-situ* injection of a second aliquot of monomer into the polymerization mixture, alongside a fresh solution of CuBr/Me₆TREN/DMSO (catalyst formed under ambient atmosphere). It is noted that the additional catalyst was required to enhance the polymerization rate of the second block yielding a pseudo diblock copolymer with a \mathcal{D} of 1.09. The process was then repeated three more times resulting in the one-pot synthesis of a pseudo-pentablock copolymer. By looking at the chromatogram of the final pentablock, negligible, if any, coupling is observed despite the very high monomer conversions targeted for each iterative block addition (**figure 2.9, table 2.4**). This is in contrast to the synthesis of an identical pseudo-pentablock copolymer previously obtained by photo-ATRP in which a high molecular weight shoulder was evident by size exclusion chromatography (SEC) thus suggesting significant termination events.⁵⁷ In addition, our synthesis appears to have very minor low molecular weight tailing in comparison to previously reported Cu(o)-RDRP approaches.⁵⁸ Collectively, our data suggest that oxygen-enhanced ATRP can be utilized as a versatile platform for the one pot synthesis of multiblock copolymers with minimal termination events.

Synthesis of Block Copolymers

To further demonstrate the capabilities of the approach, a series of diblock copolymers consisting of hydrophobic, hydrophilic and semi-fluorinated segments were also synthesized as shown in **figure 2.10**. In all cases, the first block reached near-quantitative monomer conversions and the addition of the second monomer led to well-defined diblock copolymers with the molar mass distribution clearly shifting to higher molecular weights and a final \mathcal{D} of 1.10 or below.

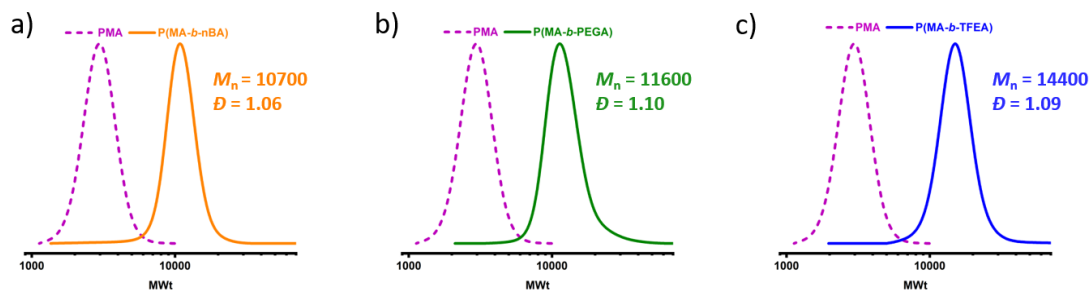


Figure 2. 10: SEC traces of (a) P(MA-*b*-nBA), (b) P(MA-*b*-PEGA) and (c) P(MA-*b*-TFEA) diblock copolymers prepared by oxygen-enhanced ATRP.

Synthesis of High Molecular Weight Polymers

Another testament of excellent end-group fidelity, is the possibility to synthesize polymers with high molecular weight and such materials can exhibit enhanced properties for various applications.⁵⁹ To date, the vast majority of methods available for the synthesis of high molecular weight polymers rely on RAFT polymerization.⁶⁰⁻⁶³ Specifically, for polyacrylates, the vast majority of ATRP reports target DPs lower than 800. We envisioned that our system may afford the synthesis of higher molecular weight polymers due to their high livingness.

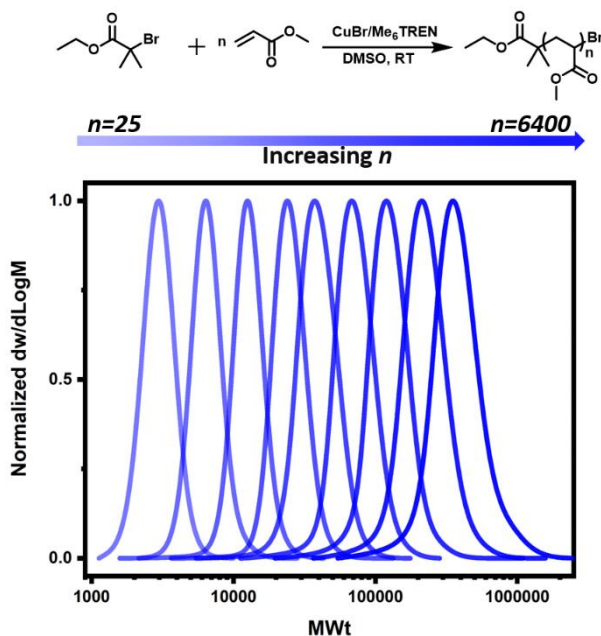


Figure 2. 11: SEC traces of PMA with a range of targeted DPs (25-6400) synthesized via oxygen-enhanced ATRP.

[MA]:[EBiB]:[CuBr]: [Me ₆ TREN]	Cu (ppm)	Time (h)	Conversion (%)	M_n (Theo.) (Da)	M_n (SEC) (Da)	\mathcal{D}
25:1:0.02:0.12	350	12	97	1900	2700	1.08
50:1:0.02:0.12	140	12	97	4400	6300	1.07
100:1:0.02:0.12	70	12	97	8500	12300	1.07
200:1:0.02:0.12	35	12	97	16900	23700	1.08
400:1:0.02:0.12	17.5	24	96	33200	36800	1.11
800:1:0.02:0.12	9	24	96	66200	66800	1.11
1600:1:0.02:0.12	4.5	36	90	124000	115700	1.13
3200:1:0.04:0.22	4.5	37	85	234100	203100	1.16
6400:1:0.04:0.22	4.5	36	85	468000	339300	1.19

Table 2. 5: ¹H NMR and SEC analysis of the PMA with a range of targeted DPs (25-6400) synthesized via oxygen-enhanced ATRP.

A range of different DPs were targeted from 25 to 6,400 (**figure 2.11, table 2.5**). For instance, using only 9 ppm of Cu, PMA with DP = 800 and a \mathcal{D} of 1.11 could be easily obtained at 96% of conversion and with very good agreement between theoretical and experimental molecular weights. Notably, we were able to reach an M_n as high as 340,000 ($\mathcal{D} = 1.19$, targeted DP = 6400) while using only 4.5 ppm of Cu. The possibility to conduct polymerizations with such low copper content significantly minimizes the issues of polymer discoloration, facilitates purification and expands the compatibility of ATRP materials with various applications. Previous ATRP approaches for higher molecular weight polymers relied on either high pressure or heterogeneous catalysts.^{64,65} To the best of our knowledge, this is the highest molecular weight polyacrylates synthesized in organic media and by a homogeneous catalytic system.

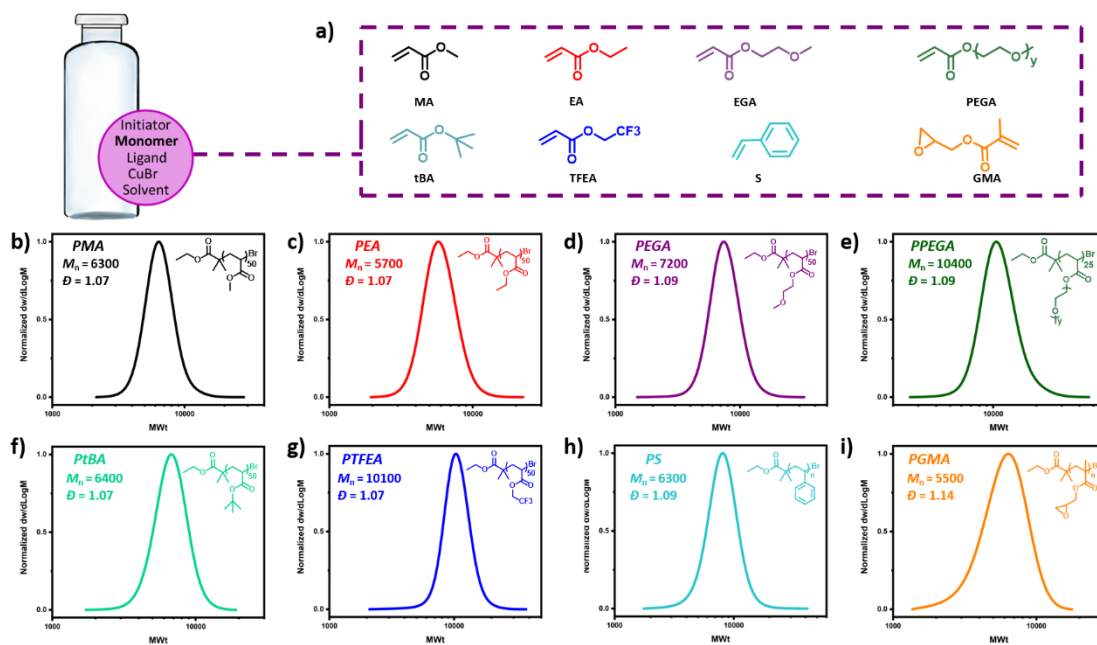


Figure 2. 12: Monomer scope of oxygen-enhanced ATRP showing the SEC traces of the corresponding polymers.

Polymerization of Different Monomers

The scope of the reaction was extended to include a variety of hydrophobic, hydrophilic, semi-fluorinated and functional monomers as depicted in **figure 2.12**. In all cases, near-quantitative conversions could be achieved and well-defined homopolymers with narrow molar mass distributions ($\bar{D} < 1.09$) could be obtained.

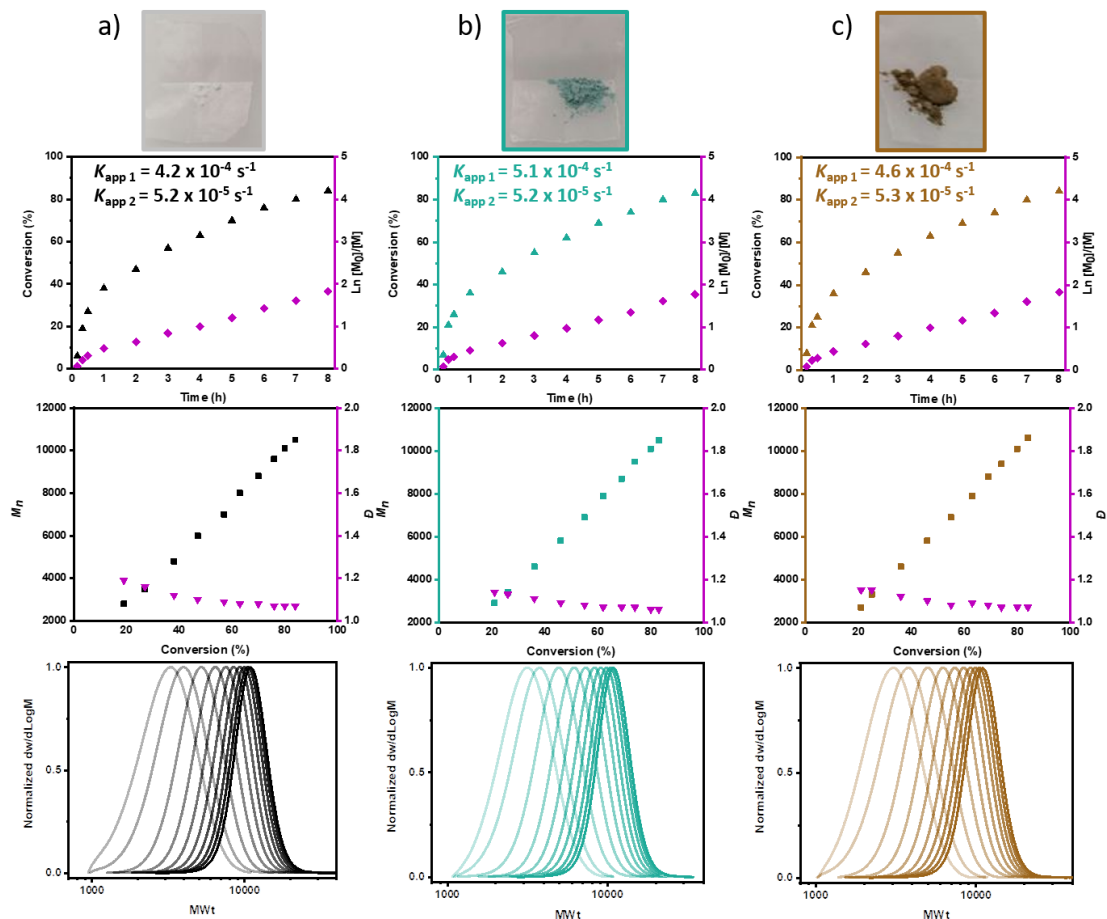


Figure 2. 13: Polymerization kinetics of MA via oxygen-enhanced ATRP utilizing: (a) Highly pure CuBr (>99.999%), (b) Less pure CuBr (98% initial purity followed by storage under ambient atmosphere) and (c) Highly oxidized CuBr (90% initial purity followed by storage at ambient atmosphere for 15 years).

Polymerization with Copper of Different Levels of Purity

Finally, we were interested in exploring the possibility to conduct our experiments without using ultra-pure CuBr. Typically, CuBr can be purchased at different levels of purity and even the purest grade (>99.999%) rarely appears to be a white solid, thus suggesting that some oxidation has already occurred. In addition, CuBr has to be stored under an inert atmosphere to prevent oxidation and even so, it still requires rigorous purification (e.g. by several washings followed by extensive drying under vacuum) prior to usage in traditional ATRP. Since our methodology requires oxygen to form the superoxido complex, we thought that our system may be less affected by oxidation. To investigate this, we conducted three parallel polymerization kinetics using three different grades of CuBr. The first set of kinetics was performed by utilizing CuBr of the highest purity (>99.999%) which visually appears to be a white powder as shown in **figure**

2.13a. The second set of kinetics was designed with a lower purity of CuBr (<98%) that was available in our laboratory (**figure 2.13b**) while in the third set of kinetics we employed a 15-year old CuBr with an intense brown color (as it was not kept under inert atmosphere) (**figure 2.13c**). Despite the clear difference in the initial purity, all polymerizations followed essentially identical profiles with very similar reaction rates for both polymerization regimes. These experiments highlight the robustness of oxygen-enhanced ATRP as it can efficiently operate regardless of the initial CuBr purity thus not only reducing associated costs but also omitting the need for rigorous purification of CuBr prior to the polymerizations.

Conclusions

In summary, I have developed an efficient oxygen-enhanced ATRP methodology which relies on the formation of a superoxido complex at room temperature. UV-Vis, and Raman spectroscopy provided unambiguous evidence for the obtained superoxido complex which was subsequently employed for polymerization reactions proceeding through a new ARGET-ATRP mechanism. The versatility of the methodology was demonstrated by the one-pot synthesis of block and multiblock copolymers, the synthesis of high molecular weight polymers and the extension of the approach to include the polymerization of various monomers. Notably, the polymerization data (e.g. in terms of control over molecular weight, dispersity and polymerization rate) were indistinguishable regardless the purity of the employed CuBr, thus providing for a robust platform for the synthesis of advanced materials without requiring the purchase of costly catalyst or extensive purification methods.

References

- (1) Corrigan, N.; Jung, K.; Moad, G.; Hawker, C. J.; Matyjaszewski, K.; Boyer, C. *Prog. Polym. Sci.* **2020**, *111*, 101311.
- (2) Parkatzidis, K.; Wang, H. S.; Truong, N. P.; Anastasaki, A. *Chem* **2020**, *6*, 1575.
- (3) Gomollón-Bel, F. *Chem. Int.*, **2019**, *41*, 12.
- (4) Whitfield, R.; Truong, N. P.; Messmer, D.; Parkatzidis, K.; Rolland, M.; Anastasaki, A. *Chem. Sci.* **2019**, *10*, 8724.
- (5) Gentekos, D. T.; Sifri, R. J.; Fors, B. P. *Nat. Rev. Mat.* **2019**, *4*, 761.
- (6) Yin, R.; Wang, Z.; Bockstaller, M. R.; Matyjaszewski, K. *Polym. Chem.* **2021**, *12*, 6071.
- (7) De Neve, J.; Haven, J. J.; Maes, L.; Junkers, T. *Polym. Chem.* **2018**, *9*, 4692.
- (8) Discekici, E. H.; Anastasaki, A.; Kaminker, R.; Willenbacher, J.; Truong, N. P.; Fleischmann, C.; Oschmann, B.; Lunn, D. J.; Read de Alaniz, J.; Davis, T. P. *J. Am. Chem. Soc.* **2017**, *139*, 5939.
- (9) Anastasaki, A.; Oschmann, B.; Willenbacher, J.; Melker, A.; Van Son, M. H.; Truong, N. P.; Schulze, M. W.; Discekici, E. H.; McGrath, A. J.; Davis, T. P. *Angew. Chem. Int. Ed.* **2017**, *56*, 14483.
- (10) Soeriyadi, A. H.; Boyer, C.; Nyström, F.; Zetterlund, P. B.; Whittaker, M. R. *J. Am. Chem. Soc.* **2011**, *133*, 11128.
- (11) Boyer, C.; Bulmus, V.; Liu, J.; Davis, T. P.; Stenzel, M. H.; Barner-Kowollik, C. *J. Am. Chem. Soc.* **2007**, *129*, 7145.
- (12) Barner-Kowollik, C.; Davis, T. P.; Heuts, J. P.; Stenzel, M. H.; Vana, P.; Whittaker, M. *J. Polym. Sci., Part A: Polym. Chem.* **2003**, *41*, 365.
- (13) Rosen, B. M.; Percec, V. *Chem. Rev.* **2009**, *109*, 5069.
- (14) Sumerlin, B. S.; *ACS Macro Lett.*, **2012**, *1*, 141.
- (15) Whitfield, R.; Parkatzidis, K.; Truong, N. P.; Junkers, T.; Anastasaki, A. *Chem* **2020**.
- (16) Parkatzidis, K.; Boner, S.; Wang, H. S.; Anastasaki, A. *ACS Macro Lett.* **2022**, *11*, 841.
- (17) Whitfield, R.; Parkatzidis, K.; Rolland, M.; Truong, N. P.; Anastasaki, A. *Angew. Chem. Int. Ed.* **2019**, *58*, 13323.
- (18) Bhanu, V.; Kishore, K. *Chem. Rev.* **1991**, *91*, 99.
- (19) Rolland, M.; Whitfield, R.; Messmer, D.; Parkatzidis, K.; Truong, N. P.; Anastasaki, A. *ACS Macro Lett.* **2019**, *8*, 1546.
- (20) Szczepaniak, G.; Jeong, J.; Kapil, K.; Dadashi-Silab, S.; Yerneni, S. S.; Ratajczyk, P.; Lathwal, S.; Schild, D.; Das, S. R.; Matyjaszewski, K. *Chem. Sci.* **2022**.
- (21) Kütahya, C.; Schmitz, C.; Strehmel, V.; Yagci, Y.; Strehmel, B. *Angew. Chem. Int. Ed.* **2018**, *57*, 7898.
- (22) Aydogan, C.; Yilmaz, G.; Shegiwal, A.; Haddleton, D. M.; Yagci, Y. *Angew. Chem. Int. Ed.* **2022**, e202117377.
- (23) Corrigan, N.; Shanmugam, S.; Xu, J.; Boyer, C. *Chem. Soc. Rev.* **2016**, *45*, 6165.
- (24) Szczepaniak, G.; Fu, L.; Jafari, H.; Kapil, K.; Matyjaszewski, K. *Acc. Chem. Res.* **2021**, *54*, 1779.
- (25) Yeow, J.; Chapman, R.; Gormley, A. J.; Boyer, C. *Chem. Soc. Rev.* **2018**, *47*, 4357.
- (26) Burrige, K. M.; De Alwis Watuthanthrige, N.; Payne, C.; Page, R. C.; Konkolewicz, D. *J. Polym. Sci.* **2021**, *59*, 2530.
- (27) Iwata, H.; Hata, Y.; Matsuda, T.; Ikada, Y. *J. Polym. Sci.*, **1991**, *29*, 1217.

- (28) Chapman, R.; Gormley, A. J.; Stenzel, M. H.; Stevens, M. M. *Angew. Chem. Int. Ed.* **2016**, *55*, 4500.
- (29) Chapman, R.; Gormley, A. J.; Herpoldt, K.-L.; Stevens, M. M. *Macromolecules* **2014**, *47*, 8541.
- (30) Xu, J.; Jung, K.; Atme, A.; Shanmugam, S.; Boyer, C. J. *Am. Chem. Soc.* **2014**, *136*, 5508.
- (31) Jones, G. R.; Anastasaki, A.; Whitfield, R.; Engelis, N.; Liarou, E.; Haddleton, D. M. *Angew. Chem. Int. Ed.* **2018**, *57*, 10468.
- (32) Theodorou, A.; Liarou, E.; Haddleton, D. M.; Stavrakaki, I. G.; Skordalidis, P.; Whitfield, R.; Anastasaki, A.; Velonia, K. *Nat. Commun.* **2020**, *11*, 1486.
- (33) Enciso, A. E.; Fu, L.; Lathwal, S.; Olszewski, M.; Wang, Z.; Das, S. R.; Russell, A. J.; Matyjaszewski, K. *Angew. Chem. Int. Ed.* **2018**, *57*, 16157.
- (34) Marathianos, A.; Liarou, E.; Anastasaki, A.; Whitfield, R.; Laurel, M.; Wemyss, A. M.; Haddleton, D. M. *Polym. Chem.* **2019**, *10*, 4402.
- (35) Nanda, A. K.; Hong, S. C.; Matyjaszewski, K. *Macromol. Chem. Phys.*, **2003**, *204*, 1151.
- (36) Zhang, L.; Wu, C.; Jung, K.; Ng, Y. H.; Boyer, C. *Angew. Chem.* **2019**, *131*, 16967.
- (37) Wu, C.; Jung, K.; Ma, Y.; Liu, W.; Boyer, C. *Nat. Commun.* **2021**, *12*, 478.
- (38) Dworakowska, S.; Lorandi, F.; Gorczyński, A.; Matyjaszewski, K. *Adv. Sci.* **2022**, 2106076.
- (39) Fischer, H. *Chem. Rev.* **2001**, *101*, 3581.
- (40) Whitfield, R.; Parkatzidis, K.; Bradford, K. G.; Truong, N. P.; Konkolewicz, D.; Anastasaki, A. *Macromolecules* **2021**, *54*, 3075.
- (41) Krysz, P.; Matyjaszewski, K. *Eur. Polym. J.* **2017**, *89*, 482.
- (42) Parkatzidis, K.; Rolland, M.; Truong, N. P.; Anastasaki, A. *Polym. Chem.* **2021**, *12*, 5583.
- (43) Mirica, L. M.; Ottenwaelder, X.; Stack, T. D. P. *Chem. Rev.* **2004**, *104*, 1013.
- (44) Elwell, C. E.; Gagnon, N. L.; Neisen, B. D.; Dhar, D.; Spaeth, A. D.; Yee, G. M.; Tolman, W. B. *Chem. Rev.* **2017**, *117*, 2059.
- (45) Schatz, M.; Raab, V.; Foxon, S. P.; Brehm, G.; Schneider, S.; Reiher, M.; Holthausen, M. C.; Sundermeyer, J.; Schindler, S. *Angew. Chem. Int. Ed.* **2004**, *43*, 4360.
- (46) Brückmann, T.; Becker, J.; Turke, K.; Smarsly, B.; Weiß, M.; Marschall, R.; Schindler, S. Z. *Anorg. Allg. Chem.* **2021**, *647*, 560.
- (47) Becker, M.; Heinemann, F. W.; Schindler, S. *Chem. Eur. J.* **1999**, *5*, 3124.
- (48) Will, J.; Wuertele, C.; Becker, J.; Walter, O.; Schindler, S. *Polyhedron* **2019**, *171*, 448.
- (49) Komiyama, K.; Furutachi, H.; Nagatomo, S.; Hashimoto, A.; Hayashi, H.; Fujinami, S.; Suzuki, M.; Kitagawa, T. *Bull. Chem. Soc. Jpn.* **2004**, *77*, 59.
- (50) Alsubaie, F.; Anastasaki, A.; Nikolaou, V.; Simula, A.; Nurumbetov, G.; Wilson, P.; Kempe, K.; Haddleton, D. M. *Macromolecules* **2015**, *48*, 5517.
- (51) Schindler, S. *Eur. J. Inorg. Chem.* **2000**, *2000*, 2311.
- (52) Brinkmeier, A.; Schulz, R. A.; Buchhorn, M.; Spyra, C.-J.; Dechert, S.; Demeshko, S.; Krewald, V.; Meyer, F. J. *Am. Chem. Soc.* **2021**, *143*, 10361.
- (53) Bhadra, M.; Transue, W. J.; Lim, H.; Cowley, R. E.; Lee, J. Y. C.; Siegler, M. A.; Josephs, P.; Henkel, G.; Lerch, M.; Schindler, S. *J. Am. Chem. Soc.* **2021**, *143*, 3707.
- (54) Hoppe, T.; Josephs, P.; Kempf, N.; Wölper, C.; Schindler, S.; Neuba, A.; Henkel, G. Z. *Anorg. Allg. Chem.* **2013**, *639*, 1504.
- (55) Kim, B.; Jeong, D.; Ohta, T.; Cho, J. *Commun. Chem.*, **2019**, *2*, 1.

- (56) Würtele, C.; Gaoutchenova, E.; Harms, K.; Holthausen, M. C.; Sundermeyer, J.; Schindler, S. *Angew. Chem. Int. Ed.* **2006**, *45*, 3867.
- (57) Anastasaki, A.; Nikolaou, V.; Pappas, G. S.; Zhang, Q.; Wan, C.; Wilson, P.; Davis, T. P.; Whittaker, M. R.; Haddleton, D. M. *Chem. Sci.* **2014**, *5*, 3536.
- (58) Boyer, C.; Soeriyadi, A. H.; Zetterlund, P. B.; Whittaker, M. R. *Macromolecules* **2011**, *44*, 8028.
- (59) An, Z. *ACS Macro Lett.* **2020**, *9*, 350.
- (60) Carmean, R. N.; Becker, T. E.; Sims, M. B.; Sumerlin, B. S. *Chem* **2017**, *2*, 93.
- (61) Allison-Logan, S.; Karimi, F.; Sun, Y.; McKenzie, T. G.; Nothling, M. D.; Bryant, G.; Qiao, G. G. *ACS Macro Lett.* **2019**, *8*, 1291.
- (62) Olson, R. A.; Lott, M. E.; Garrison, J. B.; Davidson IV, C. L.; Trachsel, L.; Pedro, D. I.; Sawyer, W. G.; Sumerlin, B. S. *Macromolecules* **2022**.
- (63) Truong, N. P.; Dussert, M. V.; Whittaker, M. R.; Quinn, J. F.; Davis, T. P. *Polym. Chem.* **2015**, *6*, 3865.
- (64) Wang, Y.; Schroeder, H.; Morick, J.; Buback, M.; Matyjaszewski, K. *Macromol. Rapid Commun.* **2013**, *34*, 604.
- (65) Percec, V.; Guliashvili, T.; Ladislaw, J. S.; Wistrand, A.; Stjerndahl, A.; Sienkowska, M. J.; Monteiro, M. J.; Sahoo, S. *J. Am. Chem. Soc.* **2006**, *128*, 14156.

Chapter 3: Photocatalytic ATRP Depolymerization: Temporal Control at Low ppm Catalyst Concentration

This chapter has been published in Journal of American Chemical Society and I am the lead/first author (K. Parkatzidis, N. P. Truong, K. Matyjaszewski, A. Anastasaki, Photocatalytic ATRP Depolymerization: Temporal Control at Low ppm Catalyst Concentration, J. Am. Chem. Soc., 2023, doi.org/10.1021/jacs.3c05632). Permission was obtained from the publisher (American Chemical Society). All the experiments included in this chapter have been performed by myself.

Summary

A photocatalytic ATRP depolymerization is introduced which significantly suppresses the reaction temperature from 170 to 100 °C while enabling temporal regulation. In the presence of low-toxicity iron-based catalysts and under visible light irradiation, near-quantitative monomer recovery could be achieved (up to 90%), albeit with minimal temporal control. By employing ppm concentrations of either FeCl₂ or FeCl₃, the depolymerization during the dark periods could be completely eliminated, thus enabling perfect temporal control and the possibility to modulate the rate by simply turning the light “on” and “off”. Notably, the developed approach allowed to preserve the end-group fidelity throughout the reaction, could be carried out at high polymer loadings (up to 2M) and was compatible with various polymers and light sources. This methodology provides a facile, environmentally friendly and temporally regulated route to chemically recycle ATRP-synthesized polymers, thus opening the door for further opportunities.

Introduction

The enhancement of polymer sustainability is a prominent focus within the field of polymer science and engineering. It encompasses a broad range of approaches including the development of biodegradable and biorenewable polymers,¹ advancements in mechanical recycling,² as well as degradation,³⁻⁶ chemical recycling and upcycling.⁷⁻¹⁰ Depolymerization,

which involves reversing polymerization to regenerate monomers, can be considered as one of the most comprehensive and ideal forms of recycling. By overcoming the drawbacks associated with mechanical recycling, depolymerization offers an appealing opportunity to establish a "circular economy" for plastics.^{11,12} Recognizing its significance, depolymerization processes were listed among the top ten emerging technologies in chemistry by IUPAC in 2019 and 2020.

The concept of reversing polymerization has been understood since the early stages of polymer science. However, it was in 1948 that Dainton and Ivin provided a comprehensive description of this process in thermodynamic terms.^{13,14} Eq. 1 presents the Gibbs free energy associated with polymerization. A negative ΔG signifies the preference for propagation (polymerization), while a positive ΔG suggests the dominance of depropagation (depolymerization).^{15,16} The temperature at which $\Delta G = 0$ is referred to as the ceiling temperature, T_c .¹⁷ At this point, the rates of polymerization and depolymerization are equal. Addition polymerization reactions have negative enthalpic contributions (ΔH), indicating that the monomer possesses a higher energy state compared to the polymer. For polymerization of a vinyl monomer, whereby a σ -bond is formed from a less stable π -bond, ΔH is typically around -20 kcal/mol. The change in entropy (ΔS) of almost all polymerization processes is negative as the number of molecules and the degrees of freedom both decrease as monomer is converted to polymer. The relationship between the Gibbs energy under standard conditions, ΔG° (usually pure monomer or a 1 M solution), and the equilibrium constant, K_{eq} , is shown in eq 2, where K_{eq} is defined as the ratio of the rate constant of propagation, k_p , to the rate constant of depropagation, k_{dp} , which is in turn related to the monomer concentration at equilibrium, $[M]_{eq}$ (eq 3).

$$\Delta G = \Delta H - T\Delta S \quad (1)$$

$$\Delta G^\circ = -RT \ln K_{eq} \quad (2)$$

$$K_{eq} = \frac{k_p}{k_{dp}} = \frac{1}{[M]_{eq}} \quad (3)$$

Based on these equations, when a polymerization is heated above its ceiling temperature (T_c), the rate of depropagation surpasses the rate of polymerization. As a result, monomer is generated until a new equilibrium concentration ($[M]_{eq}$) is attained. It may seem plausible to conclude that depolymerization can be induced by simply heating a polymer above its T_c , given the general trend of negative ΔH and $-T\Delta S$ in most polymerizations. The monomer could be "removed" from the equilibrium, for example, through evaporation, until no polymer remains.

However, this oversimplified perspective does not provide an accurate understanding of how depolymerization can be practically achieved. The ceiling temperature often reveals only a fraction of the whole depolymerization process. Since the equilibrium between monomer and polymer involves only active polymer chains, for a pre-synthesized polymer to be depolymerized we must first transform chains to an active state so that depropagation can occur (if temperature and concentration are amenable to the thermodynamics of this). This would normally mean having to supply enough energy for random scission of chains to occur. However, many “controlled” polymerizations (particularly RDRP techniques) rely on the presence of reactive/capped chain-ends, in contrast to the terminated chains found in polymers made via FRP.¹⁸ High end-group fidelity is crucial to the formation of well-defined macromolecular architectures such as block copolymers in RDRP. The ω chain-ends which make controlled polymerization possible (e.g., halogens or RAFT agent Z groups, etc.) can in many cases also be leveraged to overcome the energetic barrier to depolymerization at lower temperatures and initiate depropagation reactions.

In the existing literature, there are numerous examples where polymers synthesized using controlled polymerization methods can undergo depolymerization under specific conditions, whereas analogous polymers prepared using conventional methods remain thermally stable.^{19,20} These examples predominantly involve depolymerization solely triggered by heat. Although the advantages of light have been fully exploited to efficiently catalyze controlled radical polymerizations, they have been rarely employed for the polar opposite: reversing controlled radical polymerization through depolymerization.²¹⁻²³ Aside from the undeniable sustainability benefits, intriguing mechanistic aspects present themselves.

Currently, the vast majority of depolymerizations operate exclusively by using heat as an external stimulus.^{19,24} For example, Gramlich and co-workers explored the propensity of RAFT-synthesized macromonomer-based polymers to undergo depolymerization using trithiocarbonate as the RAFT agent.²⁵ In 2022, our group expanded the scope of thermal RAFT depolymerization to include non-bulky polymers such as poly(methyl methacrylate) (PMMA) regenerating the monomer at a high yield under thermodynamically favorable conditions.²⁶ A year later, Sumerlin’s group and our group independently demonstrated the possibility to accelerate depolymerizations in the presence of either visible or UV irradiation.^{27,28} However, in both instances the contribution of thermal depolymerization was very prominent (i.e. high

depolymerization conversions could be achieved even in the absence of light), and as such temporal regulation was not possible. For ATRP, Raus first showed that during the polymerization of macromonomers, significant depolymerization could be detected even at relatively low temperatures, thus prohibiting high polymerization conversions.²⁹ Matyjaszewski's group also demonstrated the depolymerization of bulky polymers at 170 °C using copper catalysis.³⁰ Ouchi and co-workers were the first to enable the thermal depolymerization of PMMA by utilizing a ruthenium catalyst, recovering up to 24% of monomer.³¹ Matyjaszewski and co-workers also reported successful thermal depolymerization of non-bulky polymers using either copper or iron catalysis at 170 °C.^{32,33} Nevertheless, high monomer conversions could not be reached due to the significant loss of end-group observed at high depolymerization temperatures. Preliminary efforts to use light for depolymerization were recently conducted by Yagci's group using dimanganese decacarbonyl, albeit leading to low conversions (<20%) and detrimental side reactions.³⁴ As such, an efficient photocatalytic ATRP depolymerization enabling temporal control and high monomer conversions remains elusive.

Although the fundamental principle of reversing controlled polymerization has been recognized for quite some time, the research focused on depolymerization for monomer regeneration is a relatively recent development. As a result, the field of reversed controlled polymerization is considered to be an emerging area with significant potential. It offers exciting opportunities for advancing chemical recycling, introducing novel techniques for polymer characterization, and uncovering previously unknown mechanistic pathways.

Results and Discussion

In this work, I developed a photocatalytic ATRP depolymerization method using iron catalysis. The highlights of this approach are presented in **figure 3.1**.

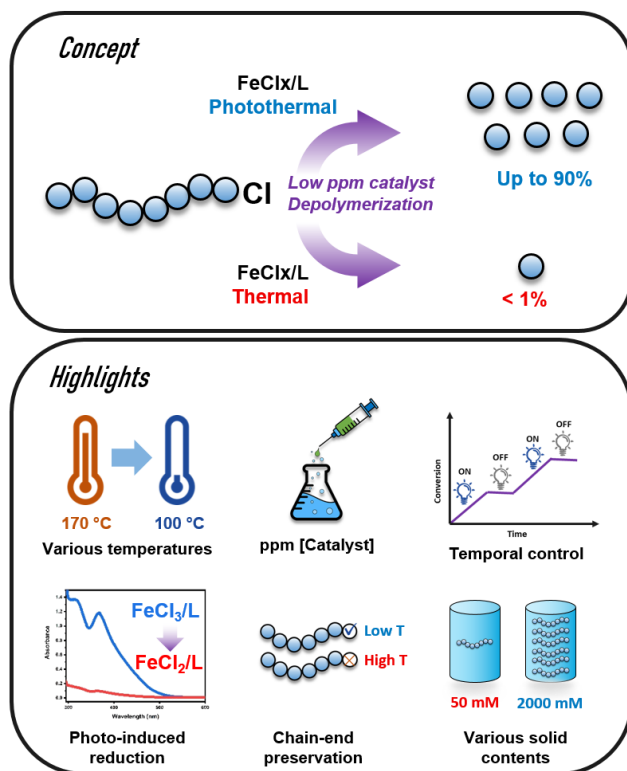


Figure 3. 1: Schematic illustration and highlights of photocatalytic depolymerization.

Poly(benzyl methacrylate) (PBzMA) macroinitiator was synthesized by an optimized activator regenerated by electron transfer (ARGET) ATRP approach³² in acetonitrile using ethyl chlorophenyl acetate as the initiator, N,N,N',N'',N'''-pentamethyldiethylenetriamine (PMDETA) as the ligand and tin(II) 2-ethylhexanoate as the reducing agent (**figure 3.2a**). The synthesis resulted in a well-defined PBzMA with narrow molar mass distributions ($\mathcal{D} \approx 1.15$), as recorded by SEC (**figure 3.2b**). Upon careful purification (**figure 3.2c**), via 3 cycles of precipitation in cold methanol, the polymer was isolated, dried and subsequently used for the depolymerization experiments.

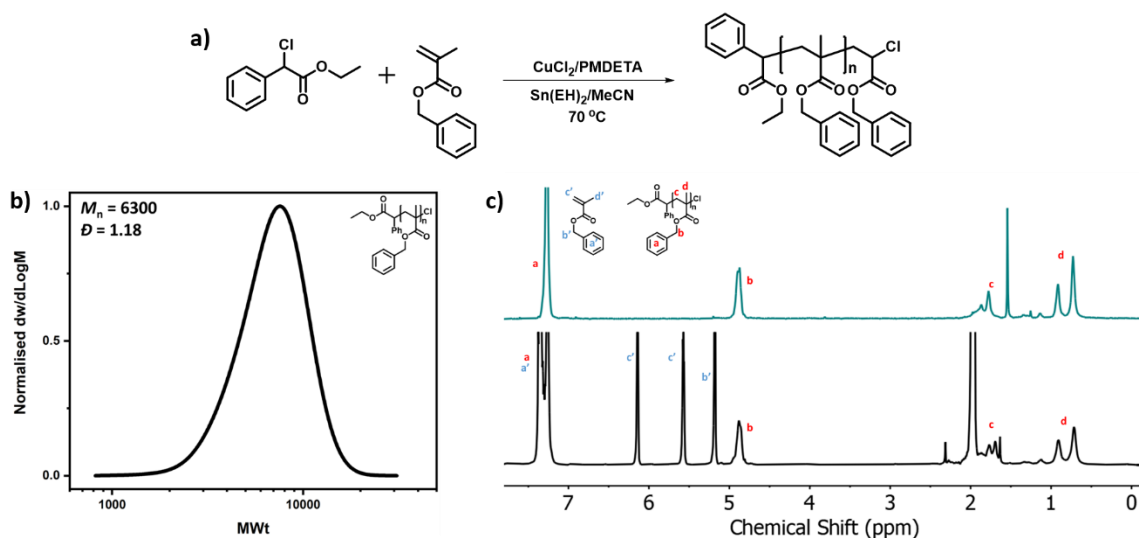


Figure 3. 2: a) Chemical illustration of polymerization of benzyl methacrylate via ARGET ATRP under the following conditions: [ECPA]:[BzMA]:[CuCl₂]:[PMDETA]:[Sn(EH)₂] = [1]:[100]:[0.2]:[0.2]:[0.08] in MeCN (1:1.25 solvent to monomer volume ratio) at 70 °C. b) SEC trace of purified PBzMA c) ¹H NMR spectra of PBzMA before (bottom) and after (top) purification.

In search for a suitable photocatalytic ATRP depolymerization system, our efforts were directed to iron catalysis using FeCl₂, due to the low catalyst toxicity and cost. First we conducted control experiments where PBzMA was diluted to solvent and subsequently heated up at 170 °C under blue light irradiation. As it can be seen in **figure 3.3** there is no monomer conversion after 1h of reaction. Further control experiments revealed that in order for the depolymerization to occur, the full catalytic system (iron/ligand) is required with minimal effect of the excess of ligand, as opposed to copper catalyzed depolymerization (**figure 3.3**).³²

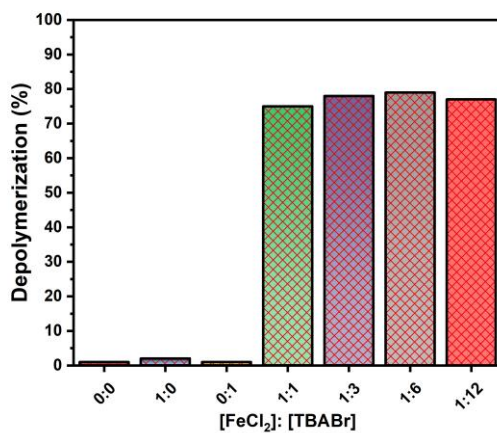


Figure 3. 3: Control experiments in photocatalytic depolymerization of PBzMA. The repeat unit concentration was 50 mM and the samples were taken after 1 h of reaction at 170 °C and under blue light irradiation using 0.05 equivalent of FeCl₂.

Employing stoichiometric amounts of catalyst (i.e. 1 equiv. of FeCl₂ with respect to the halogen end-group) under blue light irradiation at 170 °C, within 5 min of reaction, almost 90% of monomer was successfully regenerated as confirmed by ¹H NMR spectroscopic analysis (figure 3.4).

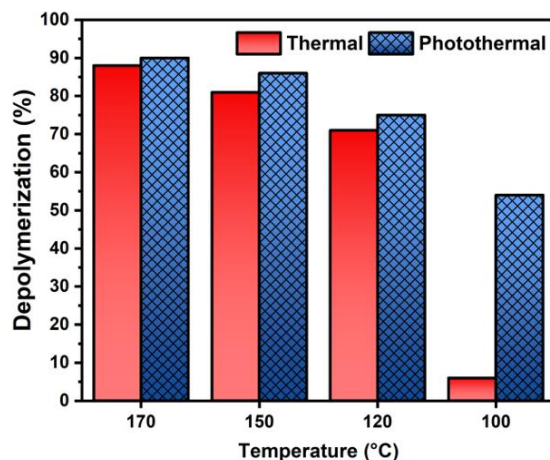


Figure 3. 4: Comparison of thermal (red) and photothermal (blue) depolymerization of PBzMA at different temperatures using 1 equivalent of catalyst. The repeat unit concentration was 50 mM and the samples were taken after 1 h of reaction.

To date, this is the highest depolymerization conversion reported for ATRP-synthesized polymers. However, the control experiment in the absence of light irradiation (i.e. using only heat) revealed only slightly lower (88%) conversions (figure 3.4), thus suggesting that temporal control under these conditions would not be feasible due to noticeable contribution of thermal depolymerization. To address this, we gradually decreased the depolymerization temperature from 170 °C to 150 °C and 120 °C (figure 3.4). Although photothermal depolymerization again reproducibly yielded slightly higher conversions as opposed to the exclusively thermal system, the significant extent of depolymerization observed under heat still prohibited the possibility of temporal control. However, the fact that 120 °C still resulted in appreciable depolymerization conversion (i.e. 71%) was very encouraging as previous reports reached comparable yields at much higher temperatures (e.g. 170 °C). Notably, at 100 °C the thermal depolymerization was significantly suppressed with only 6% of conversion achieved within comparable timeframes (figure 3.4 and table 3.1).

Temperature °C	Thermal Depolymerization (%)	Photothermal Depolymerization (%)
170	88	90
150	81	86
120	71	75
100	6	54

Table 3. 1: Depolymerization of PBzMA at different temperatures using 1 equiv. of catalyst. [Polymer]:[FeCl₂]:[TBABr] = [1]:[1]:[1] in DCB at 50 mM repeat unit concentration. The reactions were stopped after 1 h except the reaction at 100 °C, which was left for 2 h.

Intrigued by this data, we subsequently investigated the possibility of “on/off” temporal control during depolymerization using intermittent light and dark exposure. During the first period of light irradiation (i.e. 20 min), 18% of depolymerization conversion was attained (**figure 3.5**). However, upon switching the light “off”, the depolymerization continued at a comparable rate reaching 31% of conversion within another 20 min.

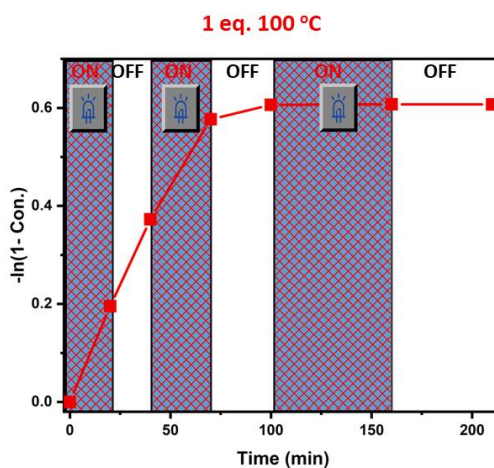


Figure 3. 5: Temporal control of depolymerization of PBzMA at 100 °C using 1 equivalent of catalyst.

Initially, we were perplexed by the lack of temporal control in this system as the control thermal experiment revealed only minimal conversion in the absence of light irradiation. The lack of temporal control was attributed to the high concentration of polymer radicals generated by the FeCl₂ activator which, upon switching the light “off”, may act as reducing agents of the *in-situ* formed FeCl₃ thereby resulting in the continuation of the depolymerization.^{35,36}

Inspired by previous works in photomediated RDRPs, we envisioned that lowering the catalyst concentration may lead to enhanced temporal control.³⁷⁻³⁹ Our hypothesis was that by

significantly reducing the catalyst concentration, we will not only lower the amount of active chains at a given time, but we will also completely eliminate the thermal depolymerization.

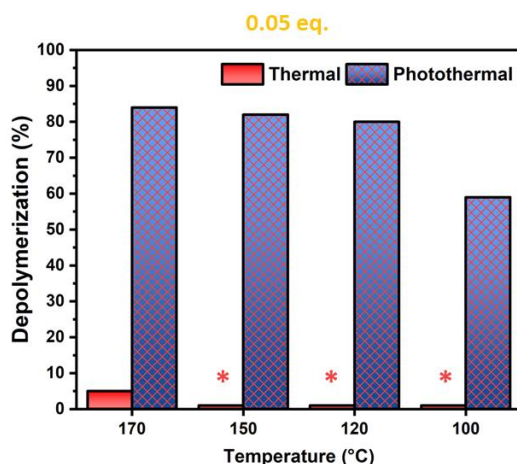
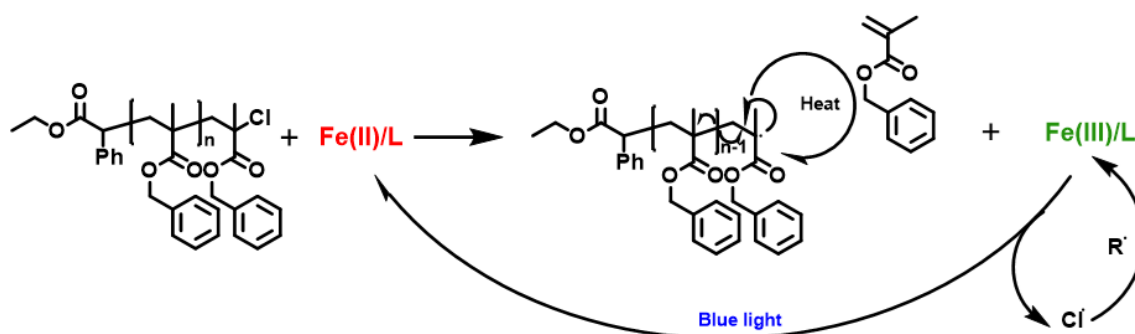


Figure 3. 6: Comparison of thermal (red) and photothermal (blue) depolymerization of PBzMA at different temperatures using 0.05 equivalent of catalyst. The repeat unit concentration was 50 mM and the samples were taken after 1 h of reaction.

Indeed, when 0.05 equiv. of FeCl_2 were employed, a pronounced contribution of light was already evident even at 170 °C whereby only 5% of conversion was observed in the absence of irradiation (**figure 3.6**). Instead, photothermal depolymerization at 170 °C yielded 84% of BzMA. To the best of our knowledge, this is the highest depolymerization conversion achieved in the presence of ppm catalyst concentration as previous strategies, of ATRP-synthesized polymers, reported lower yields while employing up to 200 times higher catalyst loadings. The high depolymerization conversions achieved are attributed to the use of light as an external stimulus, with the proposed mechanism depicted in **scheme 3.1**. FeCl_2 activates the chain-end forming FeCl_3 and enables the unzipping of the polymer chain. Blue light irradiation then enables the continuous reduction of FeCl_3 back to FeCl_2 , thus facilitating an efficient depolymerization equilibrium.⁴⁰



Scheme 3. 1: Proposed mechanism of photocatalytic ATRP depolymerization.

Notably, by further lowering the temperature to 150, 120 and 100 °C, the thermal depolymerization could be completely eliminated, thus indicating that temporal control should now be feasible. Indeed, an improved temporal control was observed as shown in **figure 3.7**. For instance, by switching the reaction “off” at 70 min, a complete discontinuation of the depolymerization was observed. On re-exposing the mixture to light irradiation, the original depolymerization rate was restored. The slightly imperfect temporal control observed at the very early depolymerization stages (< 5% of total conversion) was attributed to a small amount of radicals generated by the activator. Collectively, our data show that by utilizing ppm concentrations of FeCl₂ at low temperatures (i.e. 100 °C), enhanced temporal control can be attained.

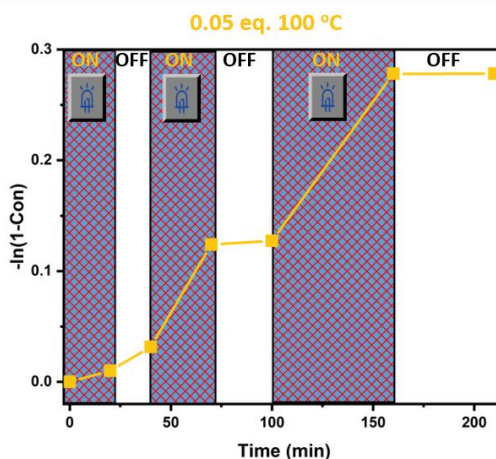


Figure 3. 7: Temporal control of depolymerization of PBzMA at 100 °C using 0.05 equivalent of catalyst.

Figure 3.8 further highlights the superiority of photocatalytic depolymerization as very high conversions can be achieved regardless of the catalyst concentration employed. Instead, thermal

depolymerizations can only achieve high yields at much higher catalyst loadings (at least 16 times higher) (table 3.2).

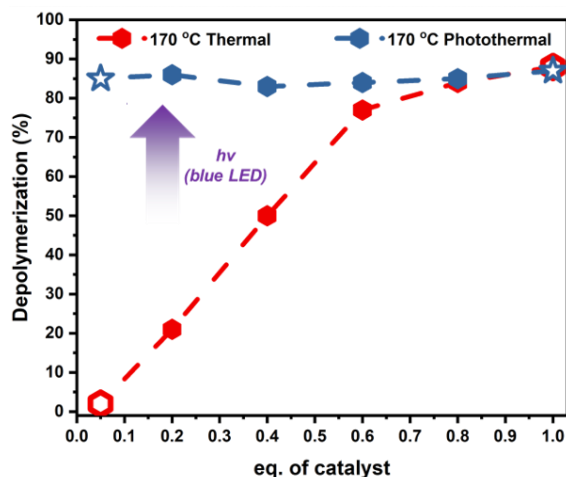


Figure 3. 8: Thermal (red) and photothermal (blue) depolymerization of PBzMA at different catalyst concentrations. The repeat unit concentration was 50 mM and the samples were taken after 1 h of reaction at 170 °C.

Eq. of Catalyst	Thermal Depolymerization (%)	Photothermal Depolymerization (%)
4	83	85
1	88	87
0.8	84	75
0.6	77	84
0.4	50	83
0.2	21	86
0.05	2	85

Table 3. 2: Depolymerization of PBzMA using different catalyst equivalents at 100 and 170 °C in thermal (red) and photothermal (blue) system. The equivalents of catalyst are calculated in regards to chain end-group. For example 1 eq of catalyst means [Polymer]:[FeCl₂]:[TBABr] = [1]:[1]:[1]. The repeat unit concentration was 50 mM and the samples were taken after 1 h of reaction.

To develop a more user-friendly photothermal depolymerization protocol, we were subsequently interested in replacing the FeCl₂ activator with FeCl₃ deactivator. FeCl₃ is a more air-stable pre-catalyst, thus further simplifying our approach.^{36,40} In addition, starting the reaction directly with the deactivator may further suppress depolymerization during the “dark” periods as the amount of active FeCl₂ will be even more limited. Kinetic experiments of FeCl₂ versus FeCl₃ were first conducted under identical concentrations with FeCl₃ exhibiting a slightly

lower depolymerization rate following an initial induction period (**figure 3.9**), as expected from the polymerization literature.⁴⁰

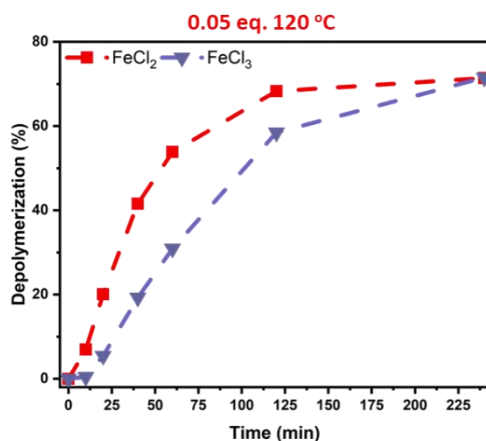


Figure 3. 9: Comparison of depolymerization kinetics utilizing FeCl₂ (red) and FeCl₃ (purple) catalyst.

Photothermal depolymerization of PBzMA at 170 °C using 1 eq. of FeCl₃ led to approximately 85% of depolymerization with the control experiment revealing only 25% of conversion in the absence of irradiation (**figure 3.10a**). When the catalyst concentration was decreased down to 0.05 eq., photothermal depolymerization reached 70% depolymerization while the thermal contribution was less than 5% (**figure 3.10b**).

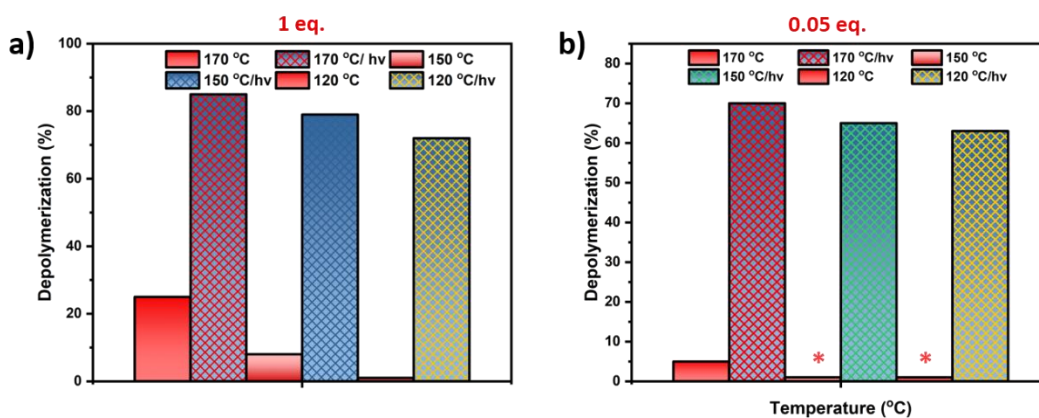


Figure 3. 10: Comparison of thermal and photothermal depolymerization of PBzMA at different temperatures using a) 1 and b) 0.05 equivalent of FeCl₃-catalyst.

Using 0.05 eq. of catalyst, no conversion was observed under exclusively thermal depolymerization at either 150 or 120 °C perhaps suggesting that the better temporal control can

be achieved under these temperatures (figure 3.10b). Although “on/off” experiments via photothermal depolymerization at 170 °C and 150 °C were moderately successful, the recommended temperature for ideal temporal control is 120 °C.

Figure 3.11 shows that a photothermal depolymerization at 170, 150 or 120 °C yields approximately similar conversions in the absence of “off” cycles. However, for each “off” cycle at either 150 or 120 °C, the final depolymerization conversion is significantly lowered. For example, at 170 °C by keeping the light “off” for 20 min, followed by a prolonged light “on” period only 30% of conversion can be reached. Instead, by continuously irradiating the reaction mixture (i.e. without the initial “off” period), much higher conversions were attained (>80%). These results suggest that increasing the depolymerization temperature leads to a significant loss of end-group, which can also be observed by ¹H NMR (figures 3.12), as the higher the temperature of the reaction the lower the final depolymerization conversion. This is in line with previous reports and it is considered as the main problem of depolymerization at higher temperatures.^{30,32,33}

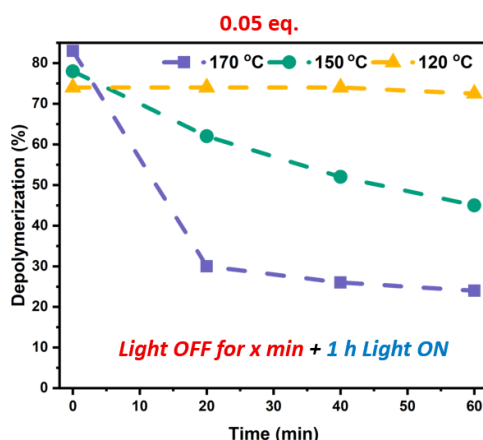


Figure 3. 11: Incubation experiments at different temperatures.

In contrast, photothermal depolymerizations at 120 °C are completely unaffected by the “off” periods and equally high overall conversions can be obtained despite several light/dark cycles.

Figure 3.12 shows our optimal data whereby excellent temporal control can be observed throughout the depolymerization without compromising the final conversion.

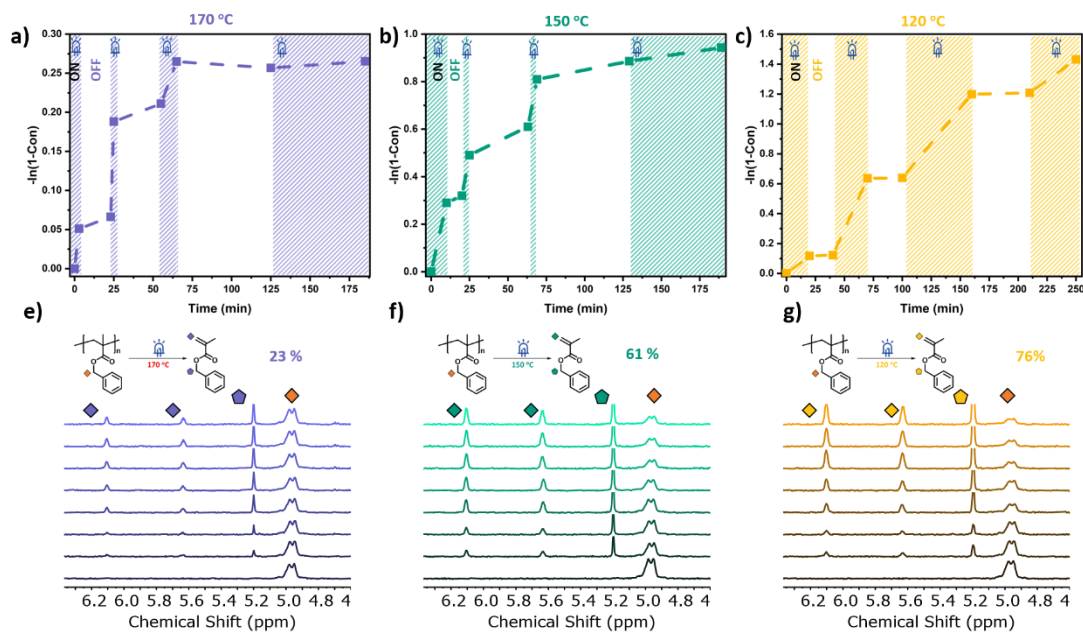


Figure 3. 12: (a-c) Temporal control of depolymerization of PBzMA at 170, 150 and 120 °C using 0.05 equivalent of catalyst, (e-g) ¹H NMR spectra of the temporal control experiments.

Last but not least, we examined the possibility of the developed photothermal depolymerization to operate under higher concentrations (so far the experiments were performed at 50 mM repeating unit). Notably, even at 2 M concentration of repeating unit, 50% of conversion could be obtained, thus highlighting the robustness of the system.

Repeat unit concentration (mM)	Photothermal Depolymerization (%)
50	83
250	71
500	68
750	58
1000	56
1500	54
2000	48

Table 3. 3: Photocatalytic depolymerization of PBzMA at different repeat unit concentration using 1 eq. of FeCl₂. The samples were taken after 1 h of reaction at 170 °C.

Conclusion

To summarize, I have developed an efficient photocatalytic ATRP depolymerization using very low concentrations of the low-toxicity FeCl₂ or FeCl₃. By lowering the reaction temperature from 170 to 120 or 100 °C, thermal depolymerization was successfully eliminated thus allowing to regulate the depolymerization via intermittent “on/off” cycles. Importantly, under judiciously optimized conditions, the end-group fidelity could be preserved throughout the reaction enabling a perfect temporal regulation regardless of the number of “on/off” cycles conducted. This depolymerization methodology offers a facile chemical recycling approach to reach near-quantitative monomer conversions while also enabling temporal regulation.

References

- (1) Miller, S. A.; *ACS Macro Lett.*, **2013**, *2*, 6, 550.
- (2) Vogt, B. D.; Stokes, K. K.; Kumar, S. K. *ACS Appl. Polym. Mater.*, **2021**, *3*, 4325.
- (3) Adili, A.; Korpusik, A. B.; Seidel, D.; Sumerlin, B. S. *Angew. Chem. Int. Ed.* **2022**, *61*, e202209085.
- (4) Garrison, J. B.; Hughes, R. W.; Sumerlin, B. S. *ACS Macro Lett.* **2022**, *11*, 441.
- (5) Korpusik, A. B.; Adili, A.; Bhatt, K.; Anatot, J. E.; Seidel, D.; Sumerlin, B. S. *J. Am. Chem. Soc.* **2023**.
- (6) Pal, D.; Konar, D.; Sumerlin, B. S. *Macromol. Rapid Commun.* **2023**, 2300126.
- (7) Korley, L. T.; Epps III, T. H.; Helms, B. A.; Ryan, A. J. *Science* **2021**, *373*, 66.
- (8) Jehanno, C.; Alty, J. W.; Roosen, M.; De Meester, S.; Dove, A. P.; Chen, E. Y.-X.; Leibfarth, F. A.; Sardon, H. *Nature* **2022**, *603*, 803.
- (9) Zhu, Y.; Romain, C.; Williams, C. K. *Nature* **2016**, *540*, 354.
- (10) Rosenboom, J.-G.; Langer, R.; Traverso, G. *Nat. Rev. Mat.* **2022**, *7*, 117.
- (11) Coates, G. W.; Getzler, Y. D. *Nat. Rev. Mat.* **2020**, *5*, 501.
- (12) Hong, M.; Chen, E. Y.-X. *Green Chem.*, **2017**, *19*, 3692.
- (13) Ivin, K. *Angew. Chem., Int. Ed. Engl.*, **1973**, *12*, 487.
- (14) Dainton, F.; Ivin, K. *Nature* **1948**, *162*, 705.
- (15) Odian, G. *Principles of polymerization*; John Wiley & Sons, **2004**.
- (16) Young, R. J.; Lovell, P. A. *Introduction to polymers*; CRC press, **2011**.
- (17) Snow, R.; Frey, F. J. *Am. Chem. Soc.* **1943**, *65*, 2417.
- (18) Corrigan, N.; Jung, K.; Moad, G.; Hawker, C. J.; Matyjaszewski, K.; Boyer, C. *Prog. Polym. Sci.* **2020**, *111*, 101311.
- (19) Martinez, M. R.; Matyjaszewski, K. *CCS Chemistry* **2022**, *4*, 2176.
- (20) Jones, G. R.; Wang, H. S.; Parkatzidis, K.; Whitfield, R.; Truong, N. P.; Anastasaki, A. J. *Am. Chem. Soc.* **2023**.
- (21) Aydogan, C.; Yilmaz, G.; Shegiwal, A.; Haddleton, D. M.; Yagci, Y. *Angew. Chem. Int. Ed.* **2022**, *61*, e202117377.
- (22) Bobrin, V. A.; Zhang, J.; Corrigan, N.; Boyer, C. *Adv. Mater. Technol.*, **2023**, *8*, 2201054.

- (23) Chen, M.; Zhong, M.; Johnson, J. A. *Chem. Rev.* **2016**, *116*, 10167.
- (24) Tang, H.; Luan, Y.; Yang, L.; Sun, H. *Molecules* **2018**, *23*, 2870.
- (25) Flanders, M. J.; Gramlich, W. M. *Polym. Chem.* **2018**, *9*, 2328.
- (26) Wang, H. S.; Truong, N. P.; Pei, Z.; Coote, M. L.; Anastasaki, A. *J. Am. Chem. Soc.* **2022**, *144*, 4678.
- (27) Young, J. B.; Bowman, J. I.; Eades, C. B.; Wong, A. J.; Sumerlin, B. S. *ACS Macro Lett.* **2022**, *11*, 1390.
- (28) Bellotti, V.; Parkatzidis, K.; Wang, H. S.; Watuthanthrige, N. D. A.; Orfano, M.; Monguzzi, A.; Truong, N. P.; Simonutti, R.; Anastasaki, A. *Polym. Chem.* **2023**, *14*, 253.
- (29) Raus, V.; Cadova, E.; Starovoytova, L.; Janata, M. *Macromolecules* **2014**, *47*, 7311.
- (30) Martinez, M. R.; Dadashi-Silab, S.; Lorandi, F.; Zhao, Y.; Matyjaszewski, K. *Macromolecules* **2021**, *54*, 5526.
- (31) Sano, Y.; Konishi, T.; Sawamoto, M.; Ouchi, M. *Eur. Polym. J.* **2019**, *120*, 109181.
- (32) Martinez, M. R.; De Luca Bossa, F.; Olszewski, M.; Matyjaszewski, K. *Macromolecules* **2021**, *55*, 78.
- (33) Martinez, M. R.; Schild, D.; De Luca Bossa, F.; Matyjaszewski, K. *Macromolecules* **2022**, *55*, 10590.
- (34) Arslan, Z.; Kiliclar, H. C.; Yagci, Y. *Des. Monomers Polym.*, **2022**, *25*, 271.
- (35) Rolland, M.; Truong, N. P.; Whitfield, R.; Anastasaki, A. *ACS Macro Lett.* **2020**, *9*, 459.
- (36) Dadashi-Silab, S.; Pan, X.; Matyjaszewski, K. *Macromolecules* **2017**, *50*, 7967.
- (37) Whitfield, R.; Parkatzidis, K.; Rolland, M.; Truong, N. P.; Anastasaki, A. *Angew. Chem. Int. Ed.* **2019**, *58*, 13323.
- (38) Dolinski, N. D.; Page, Z. A.; Discekici, E. H.; Meis, D.; Lee, I. H.; Jones, G. R.; Whitfield, R.; Pan, X.; McCarthy, B. G.; Shanmugam, S. *J. Polym. Sci., Part A: Polym. Chem.* **2019**, *57*, 268.
- (39) Mosnáček, J.; Ilčíková, M. t. *Macromolecules* **2012**, *45*, 5859.
- (40) Dadashi-Silab, S.; Matyjaszewski, K. *Molecules* **2020**, *25*, 1648.

Chapter 4: Photo-Induced Iron-Catalyzed ATRP of Renewable Monomers in Low-Toxicity Solvents: A Greener Approach

This chapter has been published in ACS Macro Letters and I am the lead/first author (K. Parkatzidis, S. Boner, H.S. Wang, A. Anastasaki, Photoinduced Iron-Catalyzed ATRP of Renewable Monomers in Low-Toxicity Solvents: A Greener Approach, ACS Macro Lett., 2022, 11, 7, 841). Permission was obtained from the publisher (American Chemical Society).

Summary

Producing polymers from renewable resources via more sustainable approaches has become increasingly important. In this Chapter I present the polymerization of monomers obtained from bio-based renewable resources, employing an environmentally friendly photo-induced iron-catalyzed ATRP in low-toxicity solvents. It is demonstrated that renewable monomers can be successfully polymerized into sustainable polymers with controlled molecular weights and narrow molar mass distributions (\mathcal{D} as low as 1.17). This is in contrast to RAFT polymerization, arguably the most commonly employed method to polymerize bio-based monomers, which led to poorer molecular weight control and higher dispersities for these specific monomers (\mathcal{D} s ~1.4). The versatility of our approach was further highlighted by the temporal control demonstrated through intermittent “on/off” cycles, controlled polymerizations of a variety of monomers and chain lengths, oxygen-tolerance, and high end-group fidelity exemplified by the synthesis of block copolymers. This work highlights photo-induced iron-catalyzed ATRP as a powerful tool for the synthesis of renewable polymers.

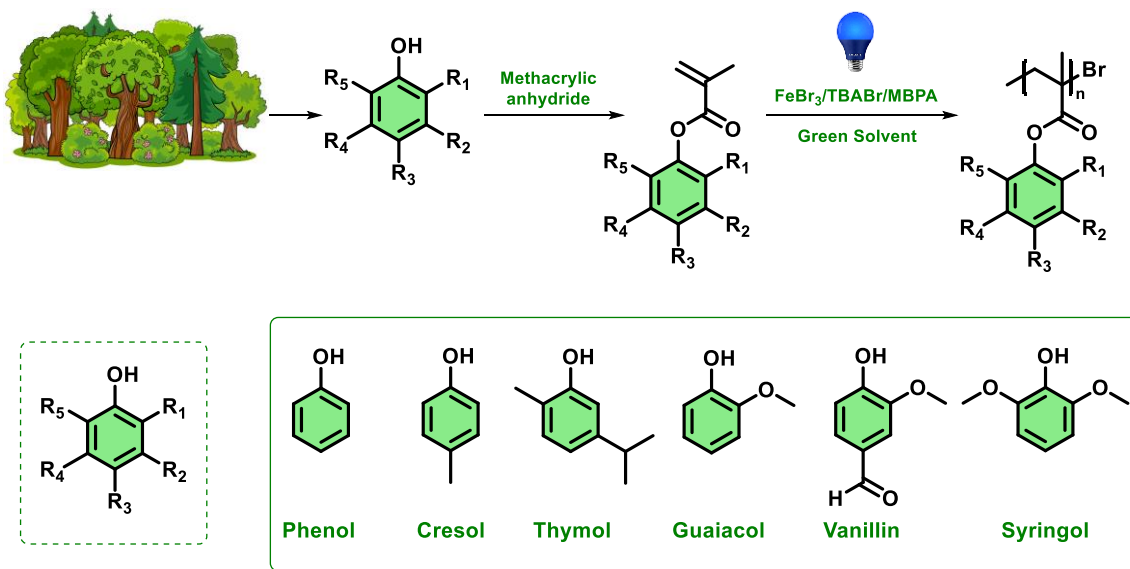
Introduction

Directing polymerization methodologies towards more sustainable pathways is of paramount and ever-increasing importance.^{1,2} However, numerous factors should be considered to improve the feasibility of sustainable polymerization methodologies.³ To begin with, the most important factor is the origin of monomers to be polymerized. Currently, the vast majority of monomers used for the synthesis of polymers are based on fossil fuel feedstocks. Recently, in search for more sustainable alternatives, the synthesis of polymers from renewable resources has attracted significant attention, showing great promise in counterbalancing the use of fossil fuel feedstock.⁴ Indeed, biomass-derived materials have been employed as an alternative and renewable resource for the synthesis of monomers.⁵⁻⁸ For example, lignocellulose is an inexpensive renewable waste product which can be produced in high abundance.^{4,9} In particular, lignin can provide multiple phenol derivatives, the secondary alcohol of which can be easily modified under mild conditions to offer polymerizable building blocks.¹⁰ Another promising family of renewable resources that can be used for monomer production are terpenes, which can be extracted from plants, providing interesting biological properties.^{11,12}

The synthesis of polymers from renewable resources is important not only from a sustainability viewpoint, but also because it leads to the production of novel polymeric materials with unique properties.^{7,13-16} To maximize the range of polymeric materials that can be attained, reversible deactivation radical polymerization (RDRP) has recently been employed to polymerize a range of renewable monomers.^{9,10} For the majority of cases, reversible addition-fragmentation chain-transfer (RAFT) polymerization has been employed for the polymerization of biomass-based monomers as it is one of the most versatile RDRP techniques.^{14,17-22} However, RAFT polymerization of some renewable methacrylate monomers leads to relatively broad molar mass distributions (\bar{D} s ~1.3-1.7).^{9,23} In parallel, copper-mediated atom transfer radical polymerization (ATRP) has also been employed in polymerization of renewable monomers, but to a relatively lesser extent.²⁴⁻³¹ It is noted that both polymerization methods typically employ toxic components/solvents that prevent the development of a more sustainable polymerization procedure.³² Arguably, one of the most environmentally friendly RDRP methodologies is iron (Fe) ATRP.³³⁻³⁵ Iron is one of the most abundant metals on Earth and is inexpensive, non-toxic, and biocompatible.³⁶ The possibility to utilize light (rather than heat) as an external stimulus to mediate Fe ATRP is also advantageous from a sustainability point of view.³ In a similar fashion to

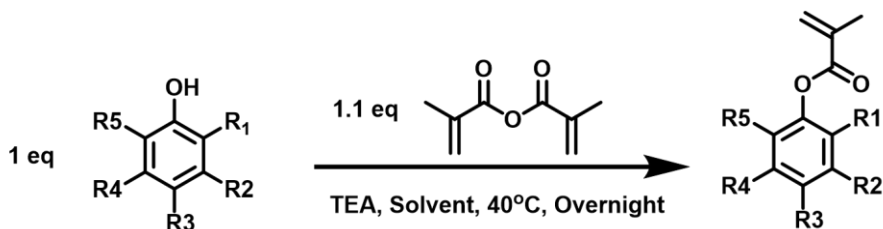
conventional RAFT and copper ATRP, highly toxic solvents such as acetonitrile, anisole or trifluoroethanol are often required to conduct a successful Fe ATRP.^{37,38} In this work, we aim to develop a greener and efficient approach, to polymerize renewable monomers by employing environmentally friendly photo-induced iron-catalyzed ATRP in low-toxicity solvents while maintaining narrow molar mass distributions for all the synthesized sustainable polymers.

Results and Discussion



Scheme 4. 1: Synthesis of sustainable biomass-derived monomers and their corresponding polymers.

We first synthesized six different methacrylic monomers through the esterification of lignin derivatives (phenol, p-cresol, guaiacol, vanillin, syringol) and a thyme-derived terpene compound (thymol) using methacrylic anhydride, which is less toxic than methacryloyl chloride, the more frequently employed compound in this type of reaction (**scheme 4.1**)



Scheme 4. 2: General schematic illustration for the synthesis of renewable monomers.

2-Methyltetrahydrofuran was used as the solvent for the methacrylation (**scheme 4.2**), a “greener” alternative when compared with more toxic and commonly employed organic solvents such as dichloromethane.^{39,42} The monomers were purified thoroughly in order to avoid any contamination with the initial alcohols, which in some cases may be hazardous. After the successful synthesis of the renewable monomers, we sought to perform polymerizations via photo-induced iron-catalyzed ATRP.

Phenyl methacrylate (PheMA) was used as the model monomer, tetraethylene glycol dimethyl ether (TEGDME) as the model low-toxicity solvent, FeBr₃ as the metal source, tetrabutylammonium bromide (TBABr) as the ligand, and methyl α-bromophenylacetate (MBPA) as the initiator.

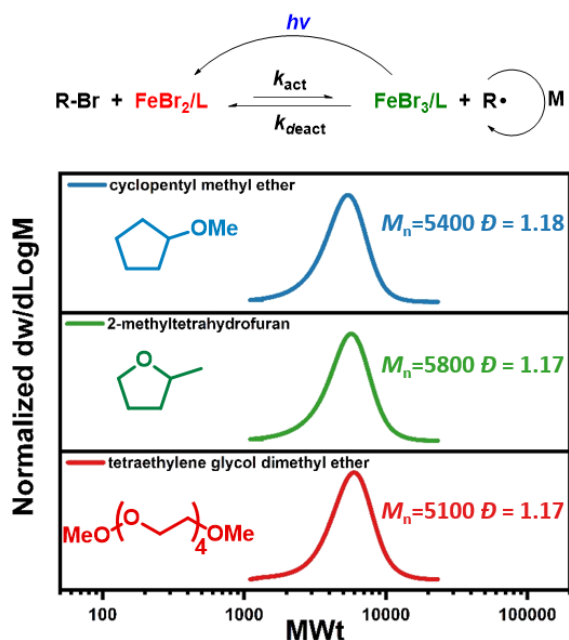


Figure 4. 1: Demonstration of a sustainable polymerization methodology via photo-induced iron-catalyzed ATRP of bio-based monomers. SEC traces of PPhEMA synthesized in three low-toxicity/green solvents.

Initial experiments were conducted with a ratio of [MBPA]:[FeBr₃]:[TBABr] = 1:0.1:0.1 and a targeted degree of polymerization (DP) of 50. All experiments were performed under blue light LED irradiation (48 W, $\lambda = 465$ nm (± 5 nm)) in a homemade box. Under the aforementioned conditions, well-defined PPhEMA could be obtained within 90 min with good control over the molecular weight and low dispersity as determined by SEC ($M_n = 5100$, $\mathcal{D} = 1.17$, **figure 4.1**, **table 4.1**). It can therefore be concluded that TEGDME does not decrease the catalyst’s activity (by

ligation to Fe)^{40,41} and as such is an excellent solvent choice for the photo-induced iron-catalyzed ATRP of renewable monomers. The possibility to utilize alternative low-toxicity and green solvents was also investigated using 2-methyltetrahydrofuran and cyclopentyl methyl ether.³⁹ Under otherwise identical conditions, both solvents fully solubilized the catalyst, resulting in PPheMA with very similar control over the molecular weight and dispersity as in the case of TEGDME. Although the remaining experiments were conducted in TEGDME, the other two solvents were proven equally efficient to mediate a successful photo-induced iron-catalyzed ATRP, thus suggesting no competing solvent-catalyst complexation.

[PheMA]:[MBPA]:[FeBr ₃]:[TBABr]	Solvent	Time (h)	Conversion (%)	<i>M_n</i> (the.)	<i>M_n</i> (SEC)	<i>D</i>
50:1:0.1:0.1	TEGMED	1.5	70	5900	5100	1.17
50:1:0.1:0.1	mTHF	1.5	72	6100	5800	1.17
50:1:0.1:0.1	CPME	1.5	64	5400	5400	1.18

Table 4. 1: ¹H NMR and SEC analysis for the synthesis of PPheMA in three different solvents, under otherwise identical conditions, utilizing photo-induced iron-catalyzed ATRP.

Next, we were interested in whether an “on/off” temporal control is possible during the polymerization of these renewable monomers. To assess this possibility, we monitored the growth of PPheMA chains during alternating periods of light and dark, using ¹H NMR to calculate the monomer conversion. Under the previously established conditions ([PheMA]:[MBPA]:[FeBr₃]:[TBABr] = 50:1:0.1:0.1), negligible polymerization was observed during the dark periods (<3%, **table 4.2**) whereas a clear increase in monomer conversion was observed when the reaction was exposed to visible light irradiation (**figure 4.2**). The small percentage of polymerization noticeable during the dark periods was attributed to the relatively high catalyst loading and is in agreement with previous reports.^{37,42}

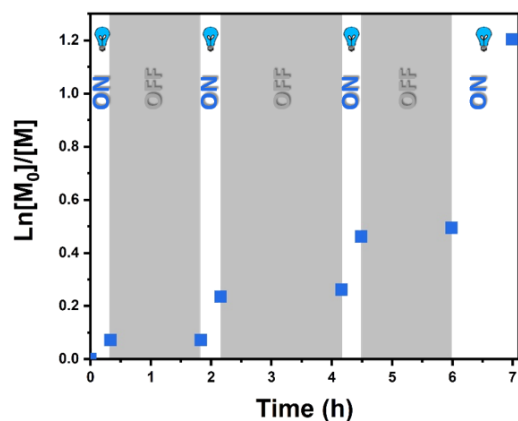


Figure 4. 2: Demonstration of temporal control during the polymerization of PheMA.

To fully eliminate the conversion during the “off” cycles, a further decrease of the catalyst concentration is recommended, albeit at the expense of higher dispersity polymers.⁴³

Entry	ON – OFF	Time (h)	Conversion (%)
1	ON	0-0.33	7
2	OFF	0.33-1.83	7
3	ON	1.83-2.16	21
4	OFF	2.16-4.16	23
5	ON	4.16-4.49	37
6	OFF	4.49-5.99	40
7	ON	5.99-6.99	70

Table 4. 2: ¹H NMR analysis showing the temporal control during the polymerization of PheMA, utilizing photo-induced iron-catalyzed ATRP.

To explore the potential of our technique to control the polymerization of higher molecular weight polymers, a range of DPs were targeted.

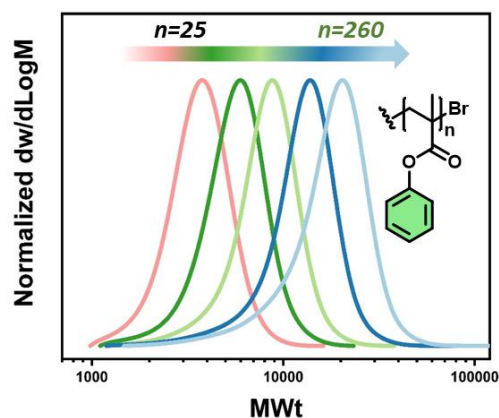


Figure 4. 3: SEC traces of PPheMA with different degrees of polymerization.

Good control and low dispersities were observed regardless of the initial chain length targeted (**figure 4.3, table 4.3**). Considering the recent interest in oxygen-tolerant polymerizations,⁴⁴⁻⁴⁶ we also attempted our polymerizations in the absence of any external deoxygenation by simply minimizing the reaction vessel's headspace to reduce the amount of the initially present oxygen.

[PheMA]:[MBPA]:FeBr ₃ :[TBABr]	Time (h)	Conversion (%)	$M_{n(\text{the.})}$	$M_{n(\text{SEC})}$	\mathcal{D}
25:1:0.1:0.1	1.5	64	2800	3400	1.15
50:1:0.1:0.1	1.5	70	5900	5100	1.17
67:1:0.1:0.1	1.5	62	7000	7400	1.18
133:1:0.1:0.1	1.5	60	13200	11000	1.22
266:1:0.1:0.1	1.5	50	21800	15100	1.27

Table 4. 3: ¹H NMR and SEC analysis for the synthesis of PPheMA in tetraethylene glycol dimethyl ether, with targeted different degrees of polymerization, utilizing photo-induced iron-catalyzed ATRP.

We also wanted to investigate whether our method allows the low-volume synthesis of polymers as this may be of high interest to applications that require the use of low reaction scales (i.e. biological studies, bioconjugations, etc.). For this purpose, we conducted the polymerization of PheMA in reaction volumes of 50 and 100 μL (25 and 50 mg of monomer, respectively) without any deoxygenation procedure and observed good control over the polymerization (**figure 4.4**), thus highlighting the versatility of our method.

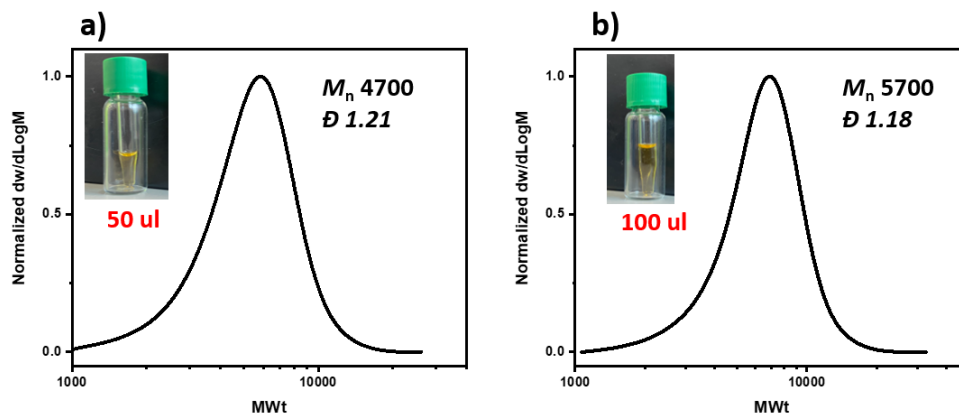


Figure 4. 4: SEC traces of PPheMA synthesized in tetraethylene glycol dimethyl ether, utilizing iron-catalyzed ATRP without any deoxygenation procedure: a) In 50 µl polymerization solution and b) In 100 µl polymerization solution.

Finally, we wanted to investigate the end-group fidelity achieved through our methodology. To assess this, a PPheMA macroinitiator ($M_n = 6500$, $\mathcal{D} = 1.17$) was chain-extended, furnishing higher molecular weight polymers while maintaining low dispersity ($M_n = 12300$, $\mathcal{D} = 1.24$, **figure 4.5**, **table 4.4**).

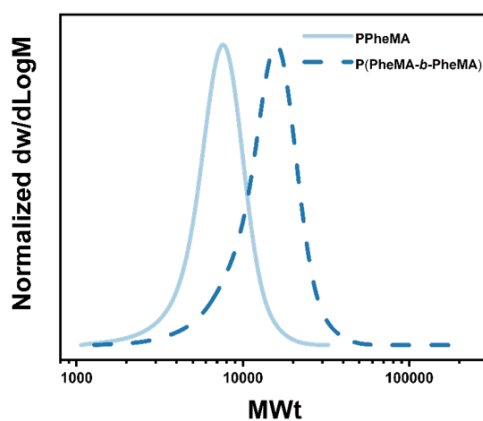


Figure 4. 5: SEC traces showing the chain-extension of PPheMA.

[PheMA]:[MBPA]:FeBr ₃ :[TBABr]	N° of Block	Time (h)	Conversion (%)	M _n (the.)	M _n (SEC)	Đ
50:1:0.1:0.1	Block 1	2	81	6800	6500	1.17
60:1:0.2:0.2	Block 2	1.5	63	12900	12300	1.24

Table 4. 4: ¹H NMR and SEC analysis for the synthesis of PPheMA macro initiator and its chain-extension, after purification, with PheMA in tetraethylen glycol dimethyl ether, utilizing photo-induced iron-catalyzed ATRP.

Upon establishing optimized conditions, we then successfully polymerized a range of renewable monomers, as indicated in **scheme 4.1**. It is noted that for the liquid monomers including cresol methacrylate (CreMA), guaiacol methacrylate (GuMA), and thymol methacrylate (ThyMA), a ratio of monomer to solvent 1:1 was employed. Instead, the polymerization of solid monomers (i.e. vanillin methacrylate (VaMA) and syringol methacrylate(SyrMA)) required an increased solvent loading to fully dissolve the initial monomer (1.5 equivalents with respect to monomer). With these modifications, all monomers were efficiently polymerized yielding controlled molecular weights and low dispersities (**figure 4.6, table 4.5**).

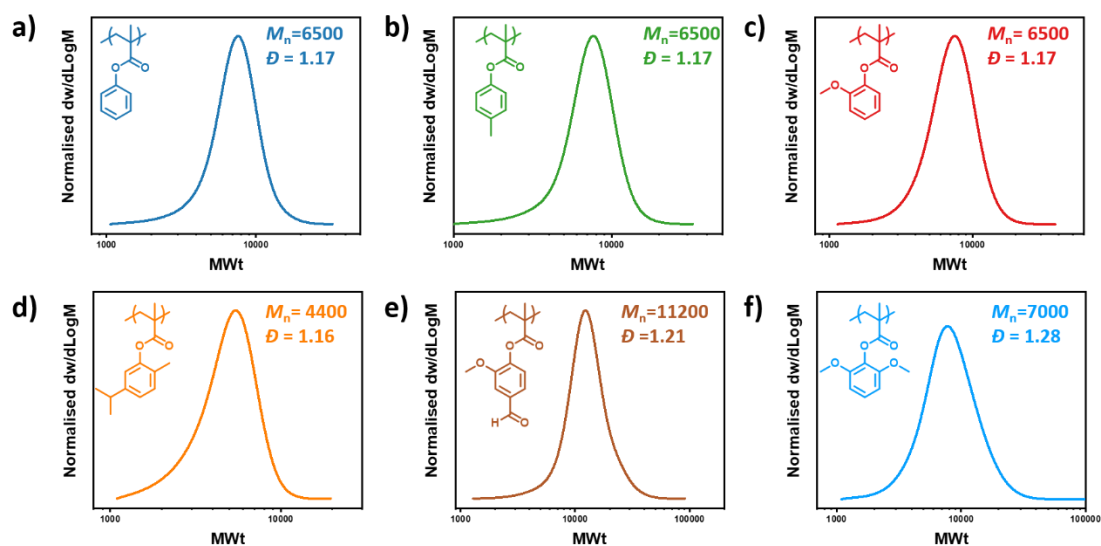


Figure 4. 6: SEC traces of renewable polymers synthesized via photo-induced iron-catalyzed ATRP: a) PPheMA, b) PCreMA, c) PGuMA, d) PThyMA, e) PVaMA, and f) PSyrMA.

[Monomer]:[MBPA]:FeBr ₃ :[TBABr]	Monomer	Time (h)	Conversion (%)	M _n (the.)	M _n (SEC)	Đ
50:1:0.1:0.1	PheMA	2	81	6800	6600	1.17
50:1:0.1:0.1	CreMA	2	95	8600	6500	1.17
50:1:0.1:0.1	GuMA	2	91	9000	6400	1.17
50:1:0.1:0.1	ThyMA	2	58	6500	4400	1.16
50:1:0.1:0.1	VaMA	2	84	9500	11200	1.21
50:1:0.1:0.1	SyrMA	2	90	10200	7000	1.28

Table 4. 5: ¹H NMR and SEC analysis for the polymerization of different renewable monomers, utilizing photo-induced iron-catalyzed ATRP. For the polymerization of solid monomers (VaMA and SyrMA) 1:1.5 monomer-to-solvent (tetraethylen glycol dimethyl ether) ratio was used while for the rest liquid monomer the ratio was 1:1.

An additional block copolymer was also targeted, consisting of PGuMA ($M_n = 6500$, $\bar{D} = 1.17$), as the first block. In the presence of catalyst, PGuMA was chain-extended with PheMA resulting in a diblock with good control (**figure 4.7**).

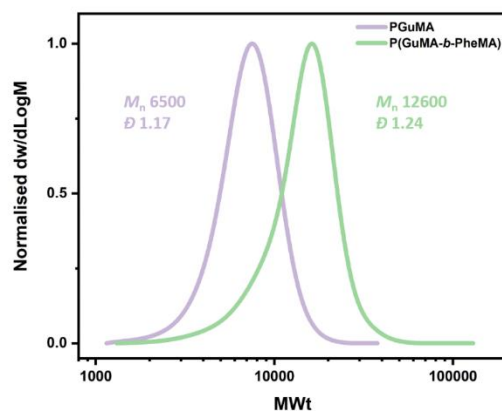


Figure 4. 7: SEC traces of PGuMA macro initiator and its chain-extension, after purification, with PhMA in tetraethylene glycol dimethyl ether, utilizing photo-induced iron-catalyzed ATRP.

Intrigued by the excellent control over the dispersities attained through our photo-induced iron-catalyzed ATRP, we were interested in a direct comparison with conventional thermal RAFT polymerization which is the most commonly employed method to polymerize such renewable monomers.⁹ By replicating the experiments in the presence of 2-cyano-2-propyl benzodithioate and 10% of AIBN, PheMA was effectively polymerized by RAFT polymerization albeit the final dispersity was as high as 1.43.

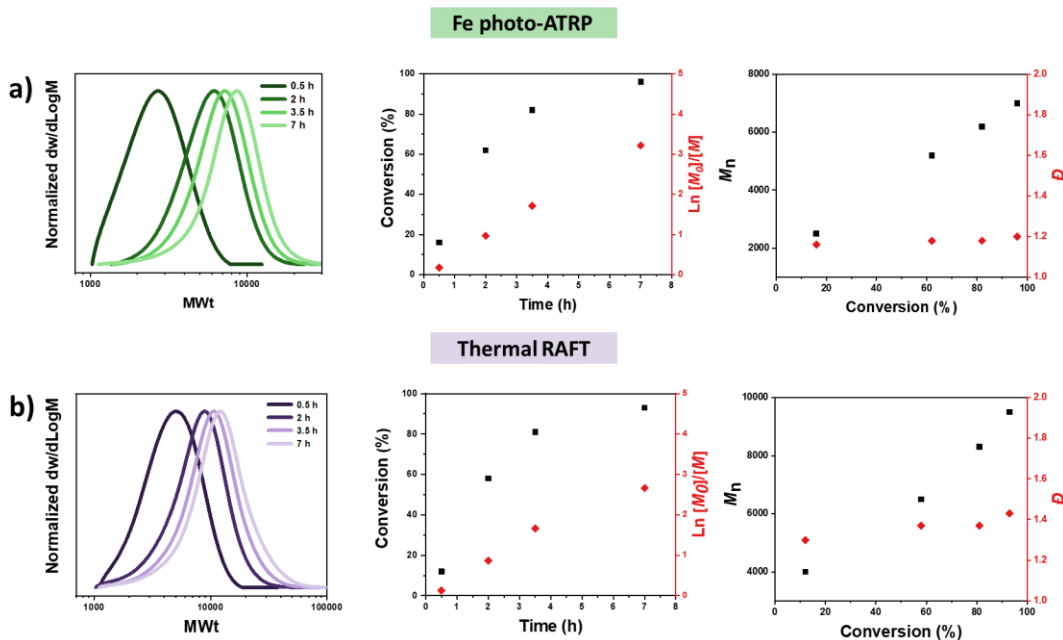


Figure 4. 8: Polymerization kinetics of PheMA utilizing a-c) Photo-induced iron-catalyzed ATRP and d-f) Conventional thermal RAFT polymerization.

Detailed kinetic analysis was conducted to compare photo-induced iron-catalyzed ATRP with thermal RAFT polymerization under otherwise identical conditions (same monomer/targeted DP/ solvent). Although both systems displayed features of a controlled polymerization such as a linear increase of $\ln([M]_0)/[M]$ over time (**figure 4.8**), and comparable reaction rates, some important differences were also observed. The first observation was a clear discrepancy between theoretical and experimental molecular weights. For instance, in the case of photo-induced iron-catalyzed ATRP an M_n of 5,200 was obtained by SEC at 62% of conversion which is in close agreement with the theoretical M_n (5,200). Instead, when RAFT polymerization was employed, a higher experimental M_n ($M_{SEC}=6,500$) was observed at a similar conversion (i.e. 60%). We hypothesized that this discrepancy could be explained by the incomplete consumption of the RAFT agent.² Indeed, the UV-SEC detector confirmed that the RAFT agent was not fully consumed, even at higher monomer conversions which verified our original hypothesis. This discovery may also be associated with our second observation in that polymers synthesized by RAFT polymerization showed significantly higher dispersity values (1.37 and 1.43 at ~60 and 90% conversion, respectively), as opposed to 1.18 and 1.20 for Fe-ATRP (**figure 4.8**). The higher dispersities observed by RAFT polymerization are attributed to the slow consumption of the RAFT agent as a result of less efficient fragmentation and the potential hybrid behavior RAFT

may have.⁴⁷ Instead, the lower \bar{D} s obtained via photo-induced iron-catalyzed ATRP indicate a faster and more complete initiator consumption.⁴⁸ To further understand our data, we conducted two additional control experiments.

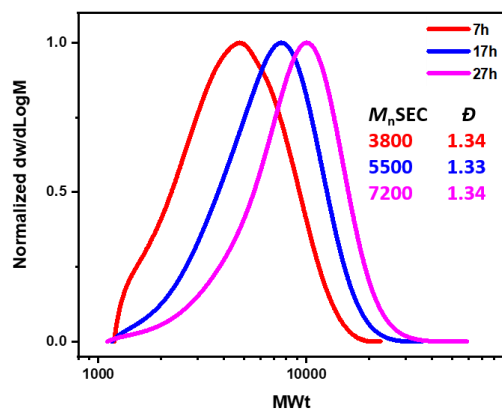


Figure 4. 9: SEC traces of PheMA synthesized in tetraethylen glycol dimethyl ether, utilizing PET-RAFT polymerization.

First, we polymerized PheMA using photo-induced electron-energy transfer (PET) RAFT instead of thermal RAFT. Under otherwise identical conditions, PET RAFT gave rise to a similarly high dispersity ($\bar{D}=1.34$, **figure 4.9**), thus further supporting insufficient fragmentation with the selected RAFT agent. Second, to examine whether the polymerization temperature can affect the polymerization control, we conducted in parallel a polymerization of PheMA with thermal RAFT polymerization at 70 °C, and also iron-catalyzed photo-induced ATRP at the same temperature. The results show the superiority of iron-catalyzed photo-induced ATRP over RAFT in the polymerization of PheMA ($\bar{D}= 1.2$ Vs 1.4, **figure 4.10**), suggesting that temperature is not the main factor behind the relatively lesser control in the RAFT polymerization of these monomers.

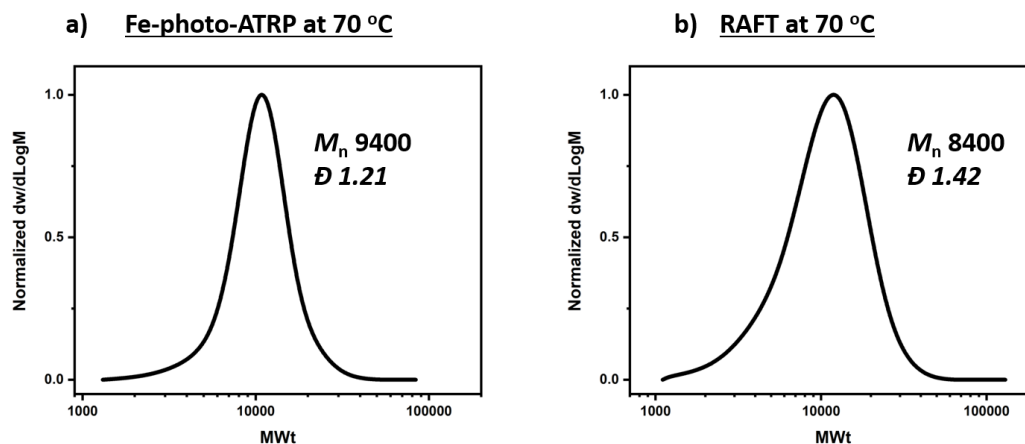


Figure 4. 10: SEC traces of PheMA synthesized in tetraethylen glycol dimethyl ether, utilizing a) Iron-catalyzed photo-induced ATRP at 70 °C and b) Thermal RAFT polymerization at 70 °C.

Conclusion

In summary, I developed a more sustainable RDRP methodology, whereby photo-induced iron-catalyzed ATRP is leveraged to polymerize a variety of renewable monomers in low-toxicity solvents. Low \bar{D} s were obtained for all cases and detailed kinetics confirmed a controlled polymerization. The high end-group fidelity of the polymers was demonstrated via chain-extensions and block copolymers. Additionally, good temporal control over the polymerization could be achieved through light/dark iterations. Importantly, the polymerization reactions can be performed without any deoxygenation, simplifying the polymerization procedure. Finally, I show that photo-induced iron-catalyzed ATRP provides better control over the polymerization of the specific family of renewable methacrylate monomers than conventional RAFT polymerization, thus highlighting the superiority of the developed approach.

References

- (1) Epps III, T. H.; Korley, L. T.; Yan, T.; Beers, K. L.; Burt, T. M. *JACS Au* **2021**, *2*, 3.
- (2) Whitfield, R.; Parkatzidis, K.; Truong, N. P.; Junkers, T.; Anastasaki, A. *Chem* **2020**, *6*, 1340.
- (3) Dworakowska, S.; Lorandi, F.; Gorczyński, A.; Matyjaszewski, K. *Adv. Sci.* **2022**, 2106076.
- (4) O’Dea, R. M.; Willie, J. A.; Epps III, T. H. *ACS Macro Lett.* **2020**, *9*, 476.
- (5) Meier, M. A.; Metzger, J. O.; Schubert, U. S. *Chem. Soc. Rev.* **2007**, *36*, 1788.
- (6) Biermann, U.; Bornscheuer, U.; Meier, M. A.; Metzger, J. O.; Schäfer, H. J. *Angew. Chem. Int. Ed.* **2011**, *50*, 3854.
- (7) Bass, G. F.; Epps III, T. *Polym. Chem.* **2021**.
- (8) Gandini, A. *Macromolecules* **2008**, *41*, 9491.
- (9) Hatton, F. L. *Polym. Chem.* **2020**, *11*, 220.
- (10) Veith, C.; Diot-Néant, F.; Miller, S. A.; Allais, F. *Polym. Chem.* **2020**, *11*, 7452.
- (11) Noppalit, S.; Simula, A.; Ballard, N.; Callies, X.; Asua, J. M.; Billon, L. *Biomacromolecules* **2019**, *20*, 2241.
- (12) Parkatzidis, K.; Chatzinikolaïdou, M.; Koufakis, E.; Kaliva, M.; Farsari, M.; Vamvakaki, M. *Polym. Chem.* **2020**, *11*, 4078.
- (13) Zhan, K.; Ejima, H.; Yoshie, N. *ACS Sustain. Chem. Eng.* **2016**, *4*, 3857.
- (14) Mahajan, J. S.; O’Dea, R. M.; Norris, J. B.; Korley, L. T.; Epps III, T. H. *ACS Sustain. Chem. Eng.* **2020**, *8*, 15072.
- (15) Upton, B. M.; Kasko, A. M. *Chem. Rev.* **2016**, *116*, 2275.
- (16) Wang, Z.; Ganewatta, M. S.; Tang, C. *Prog. Polym. Sci.* **2020**, *101*, 101197.
- (17) Wang, S.; Bassett, A. W.; Wieber, G. V.; Stanzione III, J. F.; Epps III, T. H. *ACS Macro Lett.* **2017**, *6*, 802.
- (18) Liu, S.; Zhang, X.; Li, M.; Ren, X.; Tao, Y. *J. Polym. Sci., Part A: Polym. Chem.* **2017**, *55*, 349.
- (19) Holmberg, A. L.; Stanzione III, J. F.; Wool, R. P.; Epps III, T. H. *ACS Sustain. Chem. Eng.* **2014**, *2*, 569.
- (20) Holmberg, A. L.; Nguyen, N. A.; Karavolias, M. G.; Reno, K. H.; Wool, R. P.; Epps III, T. H. *Macromolecules* **2016**, *49*, 1286.
- (21) Holmberg, A. L.; Karavolias, M. G.; Epps, T. H. *Polym. Chem.* **2015**, *6*, 5728.
- (22) Emerson, J. A.; Garabedian, N. T.; Burris, D. L.; Furst, E. M.; Epps III, T. H. *ACS Sustain. Chem. Eng.* **2018**, *6*, 6856.
- (23) Holmberg, A. L.; Reno, K. H.; Nguyen, N. A.; Wool, R. P.; Epps III, T. H. *ACS Macro Lett.* **2016**, *5*, 574.
- (24) Palà, M.; Woods, S. E.; Hatton, F. L.; Lligadas, G. *Macromol. Chem. Phys.* **2022**, 223, 2200005.
- (25) Bensabeh, N.; Moreno, A.; Roig, A.; Monaghan, O. R.; Ronda, J. C.; Cádiz, V.; Galià, M.; Howdle, S. M.; Lligadas, G.; Percec, V. *Biomacromolecules* **2019**, *20*, 2135.
- (26) Bensabeh, N.; Moreno, A.; Roig, A.; Rahimzadeh, M.; Rahimi, K.; Ronda, J. C.; Cádiz, V.; Galià, M.; Percec, V.; Rodriguez-Emmenegger, C. *ACS Sustain. Chem. Eng.* **2019**, *8*, 1276.
- (27) Bensabeh, N.; Ronda, J. C.; Galià, M.; Cádiz, V.; Lligadas, G.; Percec, V. *Biomacromolecules* **2018**, *19*, 1256.
- (28) Moreno, A.; Bensabeh, N.; Parve, J.; Ronda, J. C.; Cádiz, V.; Galià, M.; Vares, L.; Lligadas, G.; Percec, V. *Biomacromolecules* **2019**, *20*, 1816.
- (29) Mosnáček, J.; Matyjaszewski, K. *Macromolecules* **2008**, *41*, 5509.

- (30) Okada, S.; Matyjaszewski, K. *J. Polym. Sci., Part A: Polym. Chem.* **2015**, *53*, 822.
- (31) Wang, J.; Yuan, L.; Wang, Z.; Rahman, M. A.; Huang, Y.; Zhu, T.; Wang, R.; Cheng, J.; Wang, C.; Chu, F. *Macromolecules* **2016**, *49*, 7709.
- (32) Truong, N. P.; Jones, G. R.; Bradford, K. G.; Konkolewicz, D.; Anastasaki, A. *Nat. Rev. Chem.* **2021**, *5*, 859.
- (33) Layadi, A.; Kessel, B.; Yan, W.; Romio, M.; Spencer, N. D.; Zenobi-Wong, M.; Matyjaszewski, K.; Benetti, E. M. *J. Am. Chem. Soc.* **2020**, *142*, 3158.
- (34) Yin, X.; Wu, D.; Yang, H.; Wang, J.; Huang, R.; Zheng, T.; Sun, Q.; Chen, T.; Wang, L.; Zhang, T. *ACS Macro Lett.* **2022**, *11*, 693.
- (35) Dadashi-Silab, S.; Kim, K.; Lorandi, F.; Schild, D. J.; Fantin, M.; Matyjaszewski, K. *Polym. Chem.* **2022**, *13*, 1059.
- (36) Dadashi-Silab, S.; Matyjaszewski, K. *Molecules* **2020**, *25*, 1648.
- (37) Dadashi-Silab, S.; Matyjaszewski, K. *ACS Macro Lett.* **2019**, *8*, 1110.
- (38) Teodorescu, M.; Gaynor, S. G.; Matyjaszewski, K. *Macromolecules* **2000**, *33*, 2335.
- (39) Jessop, P. G. *Green Chem.*, **2011**, *13*, 1391.
- (40) Rolland, M.; Truong, N. P.; Whitfield, R.; Anastasaki, A. *ACS Macro Lett.* **2020**, *9*, 459.
- (41) Wang, Y.; Matyjaszewski, K. *Macromolecules* **2010**, *9*, 4003.
- (42) Dolinski, N. D.; Page, Z. A.; Discekici, E. H.; Meis, D.; Lee, I. H.; Jones, G. R.; Whitfield, R.; Pan, X.; McCarthy, B. G.; Shanmugam, S. *J. Polym. Sci., Part A: Polym. Chem.* **2019**, *57*, 268.
- (43) Whitfield, R.; Parkatzidis, K.; Rolland, M.; Truong, N. P.; Anastasaki, A. *Angew. Chem. Int. Ed.* **2019**, *58*, 13323.
- (44) Theodorou, A.; Liarou, E.; Haddleton, D. M.; Stavrakaki, I. G.; Skordalidis, P.; Whitfield, R.; Anastasaki, A.; Velonia, K. *Nat. Commun.* **2020**, *11*, 1.
- (45) Szczepaniak, G.; Fu, L.; Jafari, H.; Kapil, K.; Matyjaszewski, K. *Acc. Chem. Res.* **2021**, *54*, 1779.
- (46) Parkatzidis, K.; Truong, N. P.; Antonopoulou, M. N.; Whitfield, R.; Konkolewicz, D.; Anastasaki, A. *Polym. Chem.* **2020**, *11*, 4968.
- (47) Pietsch, C.; Fijten, M. W.; Lambermont-Thijs, H. M.; Hoogenboom, R.; Schubert, U. S. *J. Polym. Sci., Part A: Polym. Chem.* **2009**, *47*, 2811.
- (48) Parkatzidis, K.; Rolland, M.; Truong, N. P.; Anastasaki, A. *Polym. Chem.* **2021**, *12*, 5583.

Chapter 5: Transformer-Induced Metamorphosis of Polymeric Nanoparticle Shape at Room Temperature

*This chapter has been published in *Angewandte Chemie* and I am the first/lead author (K. Parkatzidis, N. P. Truong, M. Rolland, V. Lutz-Bueno, E. H. Pilkington, R. Mezzenga, A. Anastasaki, *Transformer-Induced Metamorphosis of Polymeric Nanoparticle Shape at Room Temperature*, *Angew. Chem.*, 2022,134, e2021134). Permission was obtained from the publisher (John Wiley and Sons).*

Summary

Controlled polymerizations have enabled the production of nanostructured materials with different shapes, each exhibiting distinct properties. Despite the importance of shape, current morphological transformation strategies are limited in polymer scope, alter the chemical structure, require high temperatures, and are fairly tedious. In this Chapter I present a rapid and versatile morphological transformation strategy that operates at room temperature and does not impair the chemical structure of the constituent polymers. By simply adding a molecular transformer to an aqueous dispersion of polymeric nanoparticles, a rapid evolution to the next higher-order morphology was observed, yielding a range of morphologies from a single starting material. Significantly, this approach can be applied to nanoparticles produced by disparate block copolymers obtained by various synthetic techniques including emulsion polymerization, polymerization-induced self-assembly and traditional solution self-assembly.

Introduction

A key feature of RDRP (and of ionic polymerizations) is that the vast majority of the generated polymer chains possess an active end-group which can be further exploited to form block copolymers.¹ In the previous Chapters, several methods to prepare well-defined block copolymers with high end-group fidelity were developed. Among the existing block copolymers, polymeric amphiphiles (i.e. block copolymers consisting of two or more blocks with at least one solvophilic and one solvophobic block) have attracted great attention in the field of soft

nanoscale materials.² Under specific conditions, polymeric amphiphiles can self-assemble into well-defined nanomaterials.³ Recently, polymeric nanomaterials/nanoparticles have been synthesized with different shapes/morphologies, similar to natural nano-objects such as bacteria and viruses.⁴ The most common shapes reported for polymeric nanomaterials are spheres, worms, vesicles and lamellae.

Polymeric materials of different shapes have found a plethora of applications in a wide range of fields in both academic research and industry.⁵ Spherical micelles and vesicles have diverse applications in drug delivery, in which hydrophobic or hydrophilic drugs are encapsulated in the hydrophobic core of spheres or the water pocket of vesicles, respectively.⁶ Encapsulating drugs inside these nanoparticles provides benefits such as minimizing the premature degradation of drugs, decreasing off-target side effects and enhancing drug efficacy.⁷ Polymeric vesicles have also been used in catalysis, in which catalysts are encapsulated inside the vesicles to be protected from degradation.⁸ In addition, using polymeric nanoparticles in catalysis can also improve the solubility of catalysts (by shielding them from precipitation) and increase their local concentration at the reaction site inside the nanoparticles.⁹ Additional applications of polymeric micelles are their use as ultra-low viscosity lubricants, where dispersion of polymeric nanoparticles in mineral oil dramatically decreases the friction coefficient of the lubricant oil.¹⁰ More recently, attention has been drawn into the use of polymeric nanoworms.¹¹ In the field of drug delivery, nanoworms have great potential to become the next generation of highly efficient nanocarriers due to a number of benefits, including longer circulation time, higher accumulation at target tissues, deeper penetration into dense microenvironments and higher loading capacity when compared to traditional spherical analogues.¹² Furthermore, catalysts encapsulated inside nanoworms exhibit high photo-stability and degradation efficiency, confirming the benefits of using these materials as templates for inorganic nanoparticles and photocatalytic applications.¹³ In addition, nanoworms have shown great promise for new applications when used as building blocks for superstructures, synthetic dendritic cells for immunotherapy and thermoresponsive gels for biomedical applications.¹⁴ Owing to these advantageous characteristics, numerous synthetic techniques for these nanoparticles have emerged including so-called traditional self-assembly (TSA),⁴ emulsion and dispersion polymerizations,¹⁵ PISA,¹⁶ and crystallization-driven self-assembly (CDSA).¹⁷

In TSA, a pre-synthesized diblock copolymer is first dissolved in a good solvent that can solvate both blocks, and then a poor solvent for one block is gradually added to the polymer solution. The solvophobic block gradually becomes non-soluble in the mixture of poor and good solvents, inducing self-assembly of the block copolymer. Depending on various parameters such as solvent, polymer molecular weight, poor solvent addition rate, polymer concentration, and salt concentration, nanoparticles can be prepared with different shapes (for example spheres, worms and vesicles).¹⁸ This technique is arguably simple as it requires only a syringe pump to control the addition of the poor solvent. And importantly, it is theoretically applicable to a wide range of polymers including functional polymers. Despite these advantages, this technique has some drawbacks. For example, multiple parameters affect the resulting morphology and hence, to obtain nanoparticles with a specific shape, time-consuming optimization is required. Yet, and despite the optimization, in many cases the desired morphology cannot be obtained easily.¹⁹ This technique is also limited to very small scales and low concentrations of polymers, typically in a range of milligrams, as the rapid self-assembly of concentrated polymer solution often leads to aggregation and uncontrolled particle shapes.

Similar to the TSA technique, CDSA can assemble solubilized block copolymers into nanoparticles. Instead of hydrophobic interaction of the solvophobic block, CDSA is based on the crystallization of the core-forming block while the other block of the copolymer is soluble in the solvent forming the particle's shell.²⁰ In CDSA, the driving force of self-assembly is the slow crystallization process. Thanks to this, CDSA is one of the best procedures to prepare worm-shaped nanomaterials and, until today, remains the only technique that can control the length of nanoworms.²¹ However, a main drawback of this approach is the very narrow polymer scope as the core-forming block must crystallize in a specific solvent. It is also very time-consuming as it takes days to weeks to grow worms. Additionally, a very limited amount of cargoes (drugs and catalysts) can be encapsulated in the particle core as the encapsulation may affect the crystallinity and the ability of the core-forming block to self-assemble. Similar to traditional self-assembly, CDSA requires the time-consuming pre-synthesis of block copolymers. Recently, *in-situ* methods that can make block copolymers which form polymeric nanoparticles in one pot have been developed. Amongst these methods, emulsion polymerization (based on RDRP) and PISA are the most facile and versatile techniques.

Emulsion polymerization is one of the most widely used techniques in production of polymers and polymeric nanoparticles both in academia and in industry.²² In emulsion polymerization, the monomer exhibits poor solubility in the selected solvent and instead forms droplets stabilized by surfactant. Since the concentration of the surfactant is higher than the critical micelle concentration, micelles of surfactants are formed where the majority of the polymerization process occurs. The monomers diffuse from the initial monomer droplets to micelles, converting them into solid nanoparticles. Water is usually used as the continuous phase due to its high heat capacity, and emulsion polymerizations typically produce spherical nanoparticles.²³

PISA is the most recently developed methodology in polymer self-assembly, providing numerous advantages. In PISA, a soluble homopolymer is pre-synthesized and then chain-extended to form a diblock copolymer.²⁴ The self-assembly occurs during the growth of the second block; although the monomer is solvent-soluble, the resulting diblock becomes solvent-insoluble upon reaching a particular molecular weight. The advantages of PISA are the scalability of the synthesis, the versatility of the components (different polymers and solvents can be used) and the production of various shapes of nanomaterials from the same polymerization (at different conversions). However, PISA has several inherent disadvantages. For instance, the obtained morphologies can be affected by multiple parameters including the molecular weight, solid content, polymer type, pH, salt concentration, etc.²⁵ Practically, it is quite difficult to obtain pure morphologies and a mixture of morphologies are often obtained due to the sensitivity of the procedure. Similar to emulsion polymerization, the formation of nanomaterials in PISA typically takes place at high temperatures (above 60-70 °C) that may be an issue in many applications, such as encapsulation of thermo-sensitive molecules or drugs. In addition, since the shape of nanomaterials is determined by the chain length of the second block, accessing nanoparticles of identical shapes and molecular weights remains challenging.²⁶

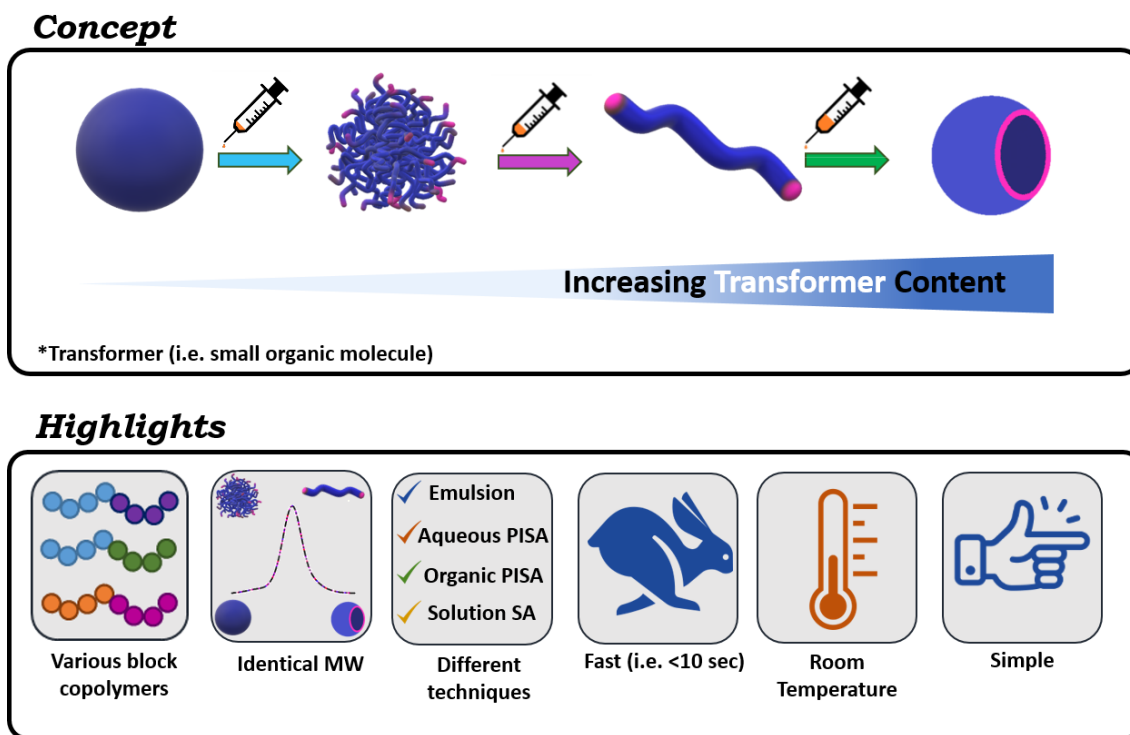
A particular focus of these strategies is to control the nanoparticle morphology from low to high order (e.g. from spheres to worms, and vesicles), as they exhibit distinct properties and performance.¹² These properties are typically acquired by using nanoparticles composed of disparate block copolymers of varied molecular weights, synthesized by different techniques.^{12,27,28} To realize a more direct comparison among various morphologies (e.g. enable structure-property relationship studies or theoretical simulations), alternative strategies that

allow the efficient transformation between different nanoparticle shapes have also been developed.²⁹⁻³³ Additional benefits of these strategies include the use of a single block copolymer to produce polymeric nanoparticles of various shapes (i.e. rather than synthesizing block copolymers consisting of different degrees of polymerization (DPs)) and the facile identification of conditions for morphological transformation (i.e. instead of requiring the optimization of multiple parameters to control the morphology). For instance, the addition of salt (ion interaction) in poly(styrene-*b*-acrylic acid) nanoparticles, obtained through traditional solution self-assembly, triggered transformation into various morphologies.²⁹ This transformation was induced due to decreased repulsion within the hydrophilic segments caused by the binding or bridging of the corona forming block (e.g. poly(acrylic acid)). In another report, poly(lauryl methacrylate-*b*-benzyl methacrylate) nanoparticles produced by PISA were shown to undergo a change in morphology by adjusting the solution temperature.³⁴ Such temperature-induced morphological transformations do not rely on thermo-responsive polymers but on the surface solvation of the nanoparticles.³⁴ In contrast, other strategies exclusively require thermo-responsive materials to trigger such transformations.^{35,36} Further methods include the use of external stimuli such as light, pH and chemical stimuli to aid morphological transformations.³⁷⁻³⁹ Despite these significant advances, current transformation approaches are limited in polymer scope (i.e. transformation is possible through a specific diblock copolymer rather than a range of materials), typically require a significant temperature change which may be incompatible with certain applications (e.g. $T > 50$ °C may prevent drug encapsulation), may alter the chemical structure among different shapes through either demanding chemical modifications or the use of stimuli such as pH and light, and can be fairly tedious and time-consuming (i.e. transformation is completed in hours).^{32,40-42}

Results and Discussion

In this Chapter I present a simple and fast methodology that allows for a rapid and efficient transformer-induced metamorphosis (TIM) of polymeric nanoparticles through the addition of small organic molecules, referred to in this work as transformers. This methodology does not change the molecular weight or chemical structure of the polymers, operates at room

temperature, and is applicable to a range of block copolymers and synthetic techniques (scheme 5.1).



Scheme 5. 1: Schematic illustration and highlights of transformer-induced metamorphosis (TIM).

First, spherical particles were synthesized by aqueous reversible addition–fragmentation chain-transfer polymerization (RAFT) emulsion polymerization of styrene utilizing poly(di(ethylene glycol) ethyl ether methacrylate-co-N-(2-hydroxypropyl) methacrylamide) (P(DEGMA-co-HPMA)) ($M_n = 8600$, **figure 5.1**) as the macromolecular chain transfer agent (macro-CTA). This macro-CTA was synthesized through an adapted RAFT-mediated solution polymerization protocol.¹¹

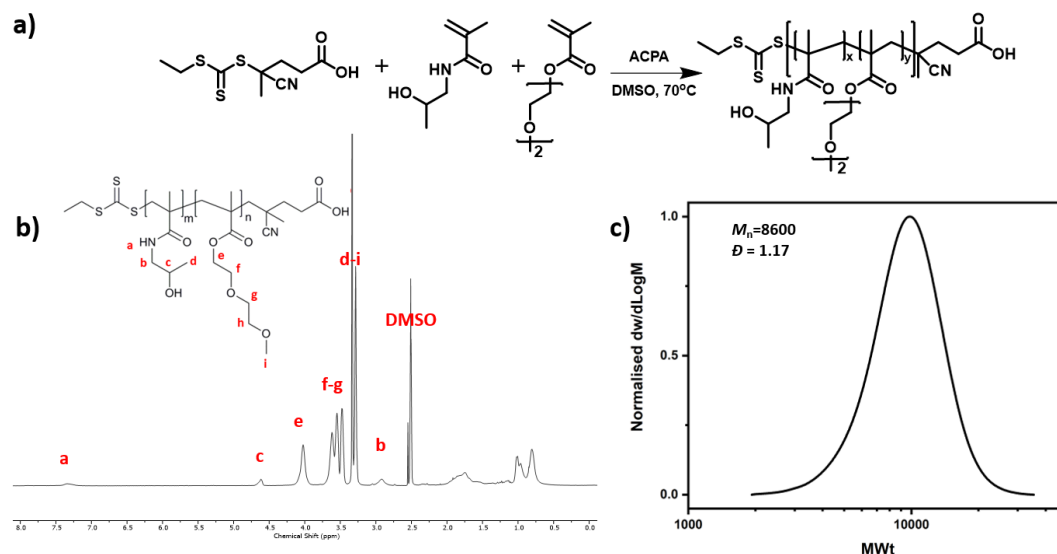


Figure 5. 1: a) Chemical scheme of P(DEGMA-*co*-HPMA) synthesis, b) ¹H NMR spectrum of purified P(DEGMA-*co*-HPMA) measured in DMSO-*d*₆ and c) SEC trace of the P(DEGMA-*co*-HPMA).

It is noted that this macro-CTA is a thermo-responsive polymer that can form aggregates at 70 °C. The emulsion polymerization was commenced at 70 °C yielding a well-defined diblock copolymer P((DEGMA-*co*-HPMA)-*b*-styrene) ($M_n=14300$, **figure 5.2**). The unreacted styrene was then evaporated and the solution was cooled down at room temperature. Using transmission electron microscopy (TEM) analysis, spherical aggregates (~ 1200 nm) were observed and their spherical morphology remained intact for several months (**figure 5.3b**).

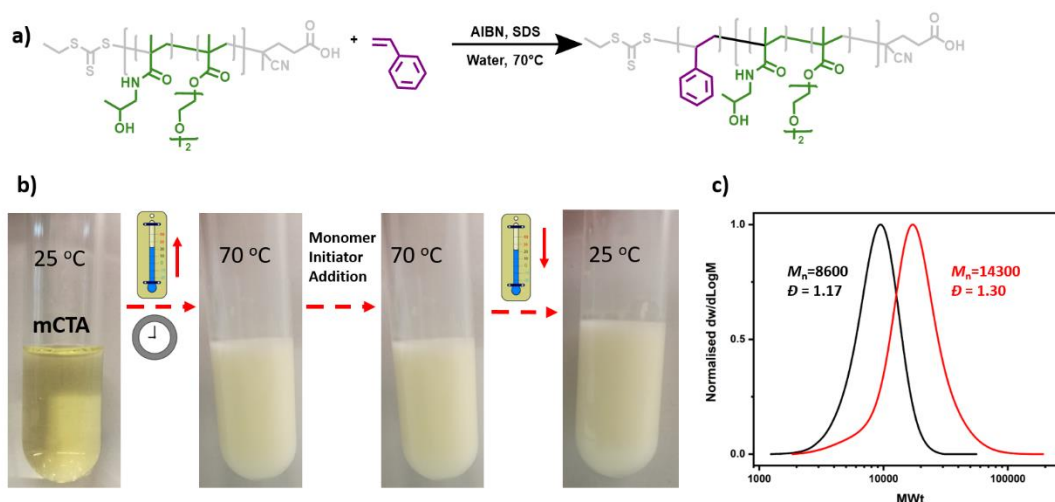


Figure 5. 2: a) Chemical scheme of P((DEGMA-*co*-HPMA)-*b*-styrene) synthesis, b) Optical representation of the emulsion polymerization procedure and c) SEC traces of P(DEGMA-*co*-HPMA) (left trace) and P((DEGMA-*co*-HPMA)-*b*-styrene) (right trace).

Interestingly, when a small amount of a molecular transformer (i.e. toluene, $5 \mu\text{l ml}^{-1}$) was added, at room temperature, a turbidity change was immediately noticed upon mildly shaking the solution for approximately 5 seconds (**figure 5.3d**).

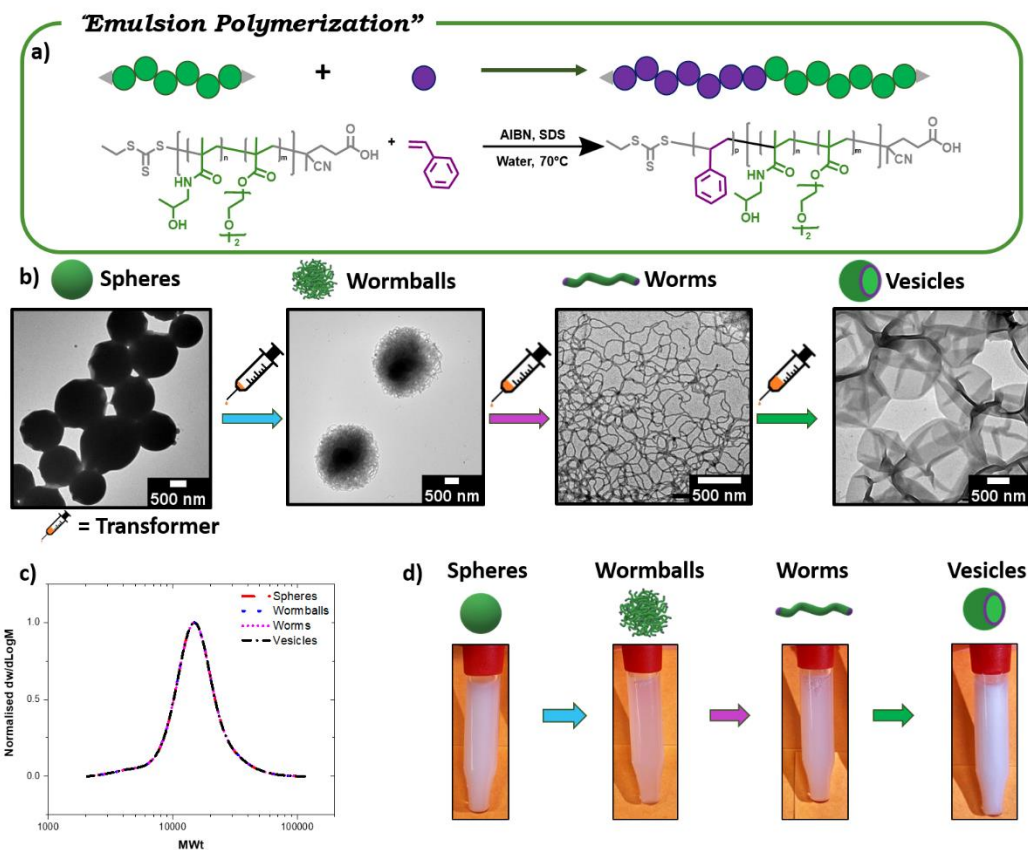


Figure 5.3: TIM of polymeric nanoparticles obtained via emulsion polymerization. a) Schematic representation of RAFT emulsion polymerization, b) TEM images of spheres, wormballs, worms and vesicles, c) SEC traces showing identical molar mass distributions of various morphologies, d) Schematic representation of the morphologies and visualization of change in turbidity of P((DEGMA-co-HPMA)-b-styrene) nanoparticles in water after sequential addition of transformer.

Subsequent TEM analysis revealed a change from the initial spherical aggregates to wormballs (**figure 5.3b**). This interesting morphology suggests that acquiring worm-like nanoparticles may also be possible. Indeed, by further increasing the amount of the injected transformer (additional $10 \mu\text{l ml}^{-1}$), worm-like nanoparticles could be obtained as confirmed by TEM, while accompanied by a further change in turbidity (**figure 5.3b**). It is also noted that at room temperature, and in the presence of added toluene, the original macro-CTA is water-soluble, thus forming the corona while polystyrene (PS) is water-insoluble and therefore becoming the core. Our current hypothesis is that the transformer (i.e. toluene, which has a solubility parameter similar to that

of the core) does not only plasticize the PS core, thus increasing the mobility of the rigid PS chains, but also facilitates the morphological transformation. To confirm this hypothesis, we continued adding the transformer in the worm-like nanoparticles anticipating a switch to an even higher order morphology. As expected, the formation of vesicles was evident by TEM (additional $35 \mu\text{l ml}^{-1}$) and was also supported by a change in turbidity (**figure 5.3d**). This data suggest that toluene plays the role of a morphological transformer. In particular, toluene exhibits a very similar solubility parameter with that of the PS core (i.e. $\delta_{\text{PS}} = 16.6\text{--}20.2$, and $\delta_{\text{toluene}} = 18.2$) and therefore it can enter the core and increase the volume of the core hydrophobic segment (v).⁴³ Such change in v increases the critical packing parameter p ($p=v/al$), leading to the transformation into different morphologies.⁴⁴ Importantly, the ^1H NMR spectra of the polymers before and after the transformation showed identical chemical structures (**figure 5.4**), thus confirming that the shape transformation occurred without altering the polymer composition.

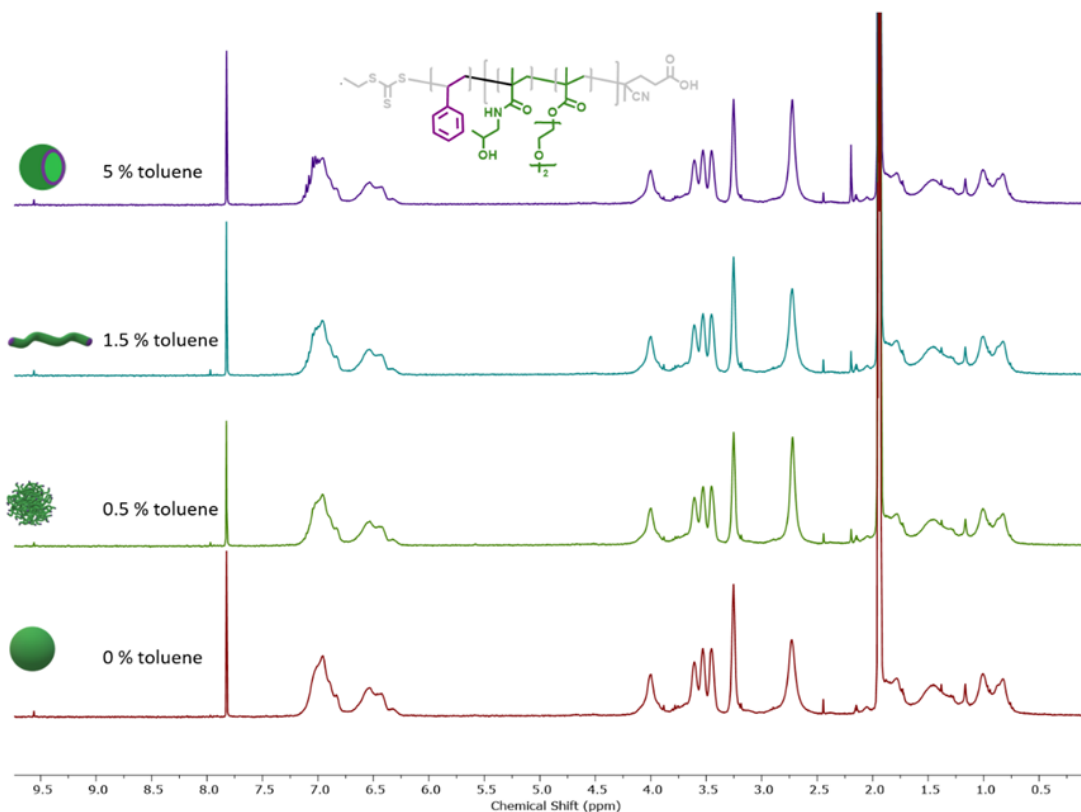


Figure 5. 4: ^1H NMR spectra of P((DEGMA-*co*-HPMA)-*b*-styrene) after addition of different amounts of toluene to obtain different morphologies. The water dispersions of the polymeric nanoparticles were dried via air purging in order to eliminate the amount of water. The spectra were measured in a mixture of acetone- d_6 : chloroform- d in a 5:1 ratio.

In addition, SEC revealed indistinguishable molar mass distributions for all the obtained nanoparticles, which is in contrast to traditional PISA whereby the change in the molecular weight of the second block triggers the morphological transformation. Instead, in our approach, the addition of a small amount of transformer is solely responsible for the rapid evolution to the next higher-order morphology. It is noted that our strategy is different to many other techniques based on controlling either the self-assembly process or the interfacial interaction between the polymeric corona and the surrounding medium.³²

We were then interested in exploring whether the transformer-induced metamorphosis of polymeric nanoparticles could be applied not only to different block copolymers, but also to various self-assembly systems. To investigate this, an aqueous PISA formulation was followed utilizing poly(glycerol monomethacrylate) (PGMA) as the hydrophilic stabilizer block and poly(glycidyl methacrylate) (PGlyMA) as the core-forming block (**figures 5.5**).

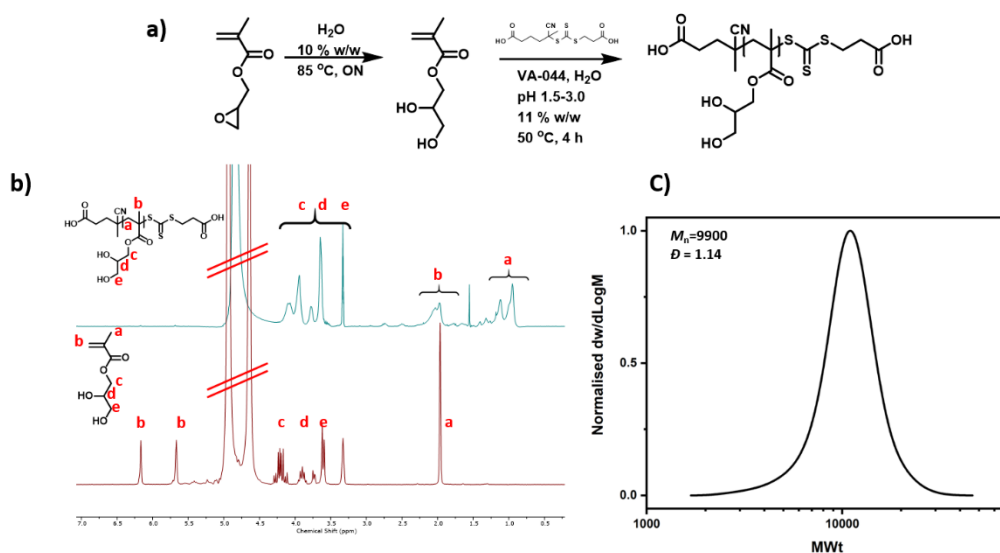


Figure 5. a) Chemical scheme of GMA (first step) and PGMA (second step) synthesis, b) ¹H NMR spectra of GMA (bottom) and PGMA (top) measured in methanol-d₄ and c) SEC traces of PGMA.

It is noted that this is a completely different diblock than in the previous system, in order to highlight the versatility of our method. In particular, in the emulsion approach the diblock was composed of a thermo-responsive corona and a hydrophobic PS core. Instead, in the current PISA example, the diblock consists of a water-soluble corona and PGlyMA as the core. By targeting a degree of polymerization (DP 35) of GlyMA, full monomer conversion was obtained and TEM analysis exclusively showed spherical nanoparticles (~ 15 nm) (**figures 5.6 and 5.7**).

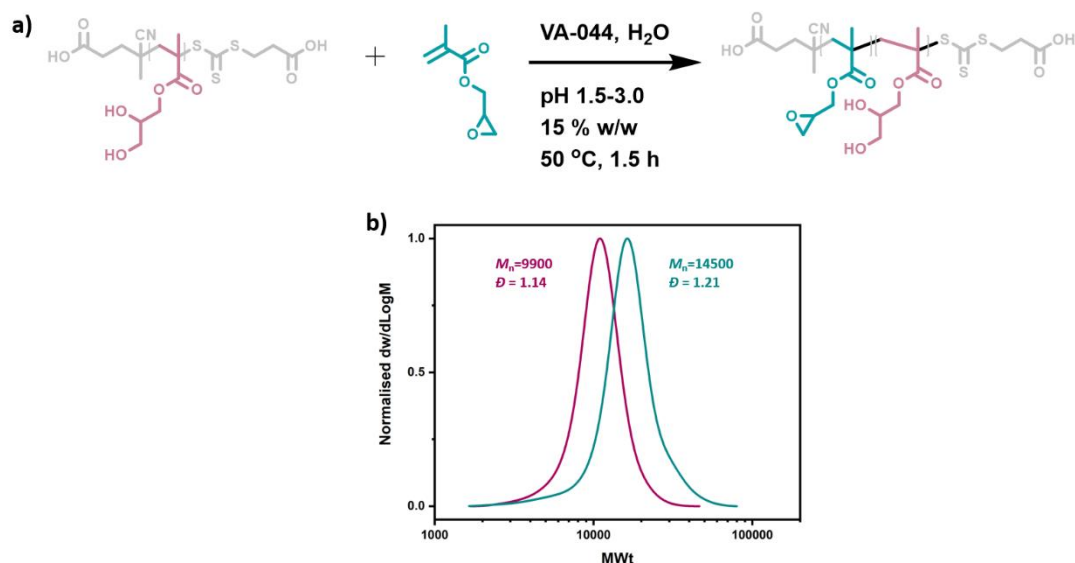


Figure 5. 6: a) Chemical scheme of P(GMA-*b*-GlyMA) synthesis and b) SEC traces of PGlyMA (left trace) and P(GMA-*b*-GlyMA) (right trace).

GlyMA was then added as the molecular transformer as this would resemble the solubility parameter of the core. By injecting GlyMA (60 $\mu\text{l ml}^{-1}$), a rapid and quantitative transformation from spherical to worm-like nanoparticles was observed (**figure 5.7b**). The morphological change was also accompanied by the formation of a gel, as can be seen in **figure 5.7c**, further supporting the formation of worm-like nanoparticles. Although this PISA system produced spherical micelles (which are different to the spherical aggregates formed by the emulsion approach), both systems can undergo a transformation from spheres to worms, thus being consistent with TIM. Upon adding more transformer, a fluid emulsion-like solution was generated and TEM confirmed the formation of vesicles. The morphology assignments were confirmed by small-angle X-ray scattering (SAXS) in solution. The radially integrated SAXS patterns, shown as the intensity I as a function of the scattering vector q , are interpreted based on the slopes of form factors for monodisperse and dilute solutions (**figure 5.7d**).

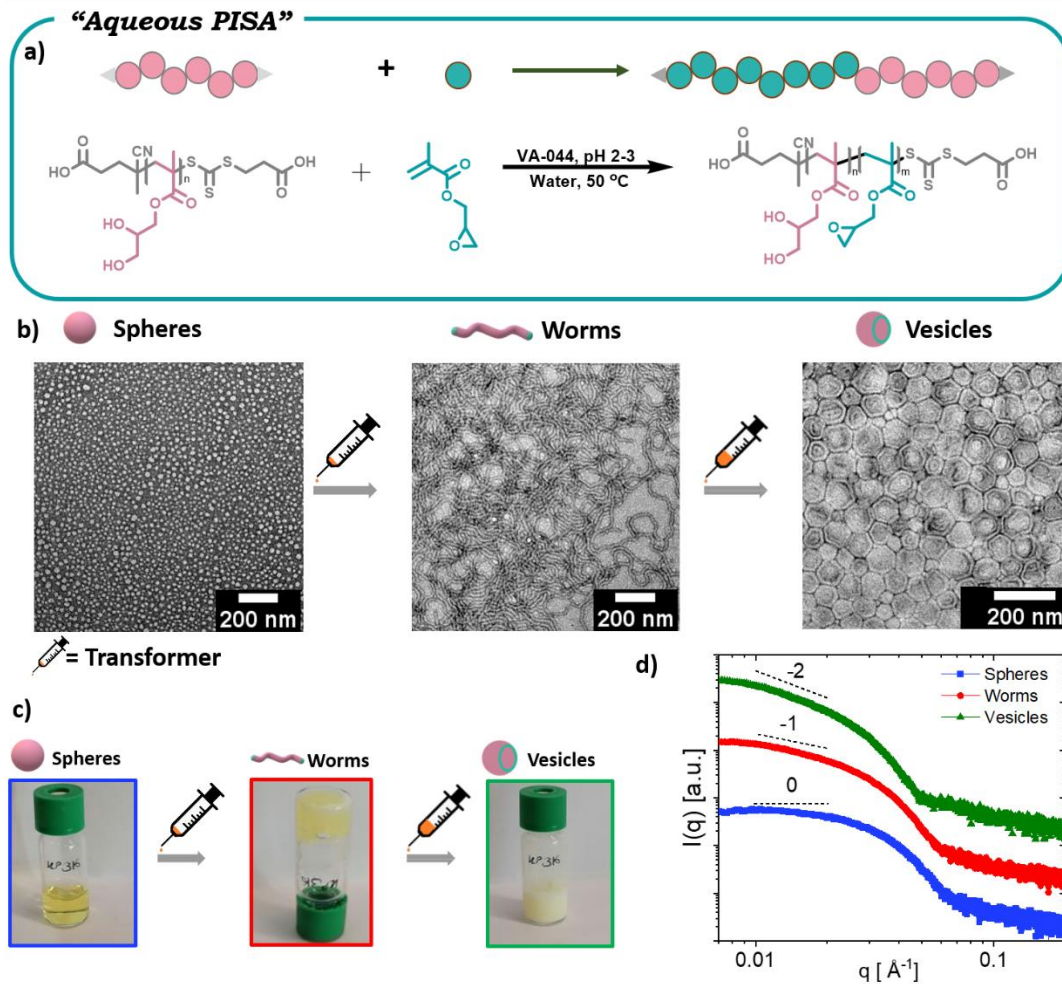


Figure 5. 7: TIM of polymeric nanoparticles obtained via aqueous PISA. a) Schematic representation of RAFT emulsion polymerization, b) TEM images of spheres, worms and vesicles, c) Visual representation of various morphologies d) Small-angle X-ray scattering data confirming the formation of different morphologies in bulk. The SAXS data were acquired and analyzed by Dr. Lutz-Bueno in the group of professor Mezzenga.

A low- q slope of nearly 0 indicates spherical morphologies, while a slope of -1 indicates linear rigid morphologies, such as worms. Slopes of -2 are related to the presence of flat aggregates consistent with vesicles,⁴⁵ confirming that the morphologies assigned by TEM are in line with SAXS characterization. Last but not least, SEC analysis showed identical molecular weights for all the obtained morphologies (figure 5.8).

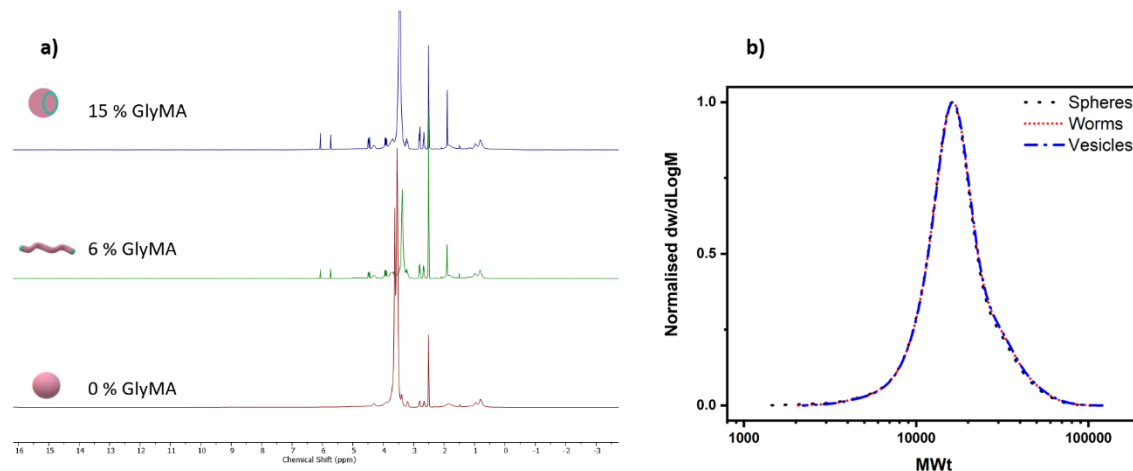


Figure 5. 8: a) ¹H NMR spectra of P(GMA-*b*-GlyMA), measured, after addition of different amounts of GlyMA to obtain different morphologies. The water dispersions of the polymeric nanoparticles were dried via air purging in order to eliminate the amount of water. The spectra were measured in a methanol-*d*₄ and b) SEC traces of P(GMA-*b*-GlyMA) after addition of different amounts of GlyMA to obtain different morphologies. SEC analysis was conducted without water removal.

As such, it is evident that TIM of polymeric nanoparticles can operate efficiently in various systems, without the need to change the temperature or pH, which is distinct from recently reported approaches.³² To further probe the potential of our approach, an organic PISA formulation was subsequently employed. Poly(oligo(ethylene glycol)) methyl ether methacrylate (POEGMA, average M_n 300) was used as the hydrophilic macromolecular chain transfer agent (**figures 5.9**) and the RAFT dispersion polymerization of styrene was conducted in methanol (**figure 5.10**).⁴⁶

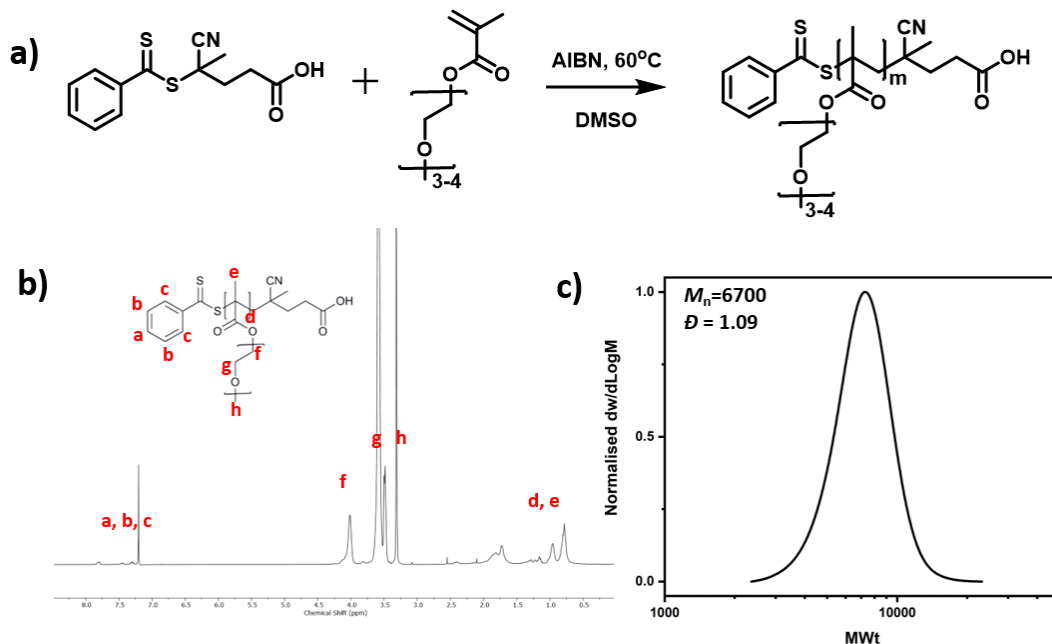


Figure 5.9: a) Chemical scheme of P(POEGMA) synthesis, b) ¹H NMR analysis of purified P(POEGMA) measured in chloroform-d and c) SEC trace of P(POEGMA).

After polymerization, the solution was dialyzed against water to remove methanol and unreacted monomer. The resulting solution was then analyzed by TEM and distinct worm-like nanoparticles were observed.

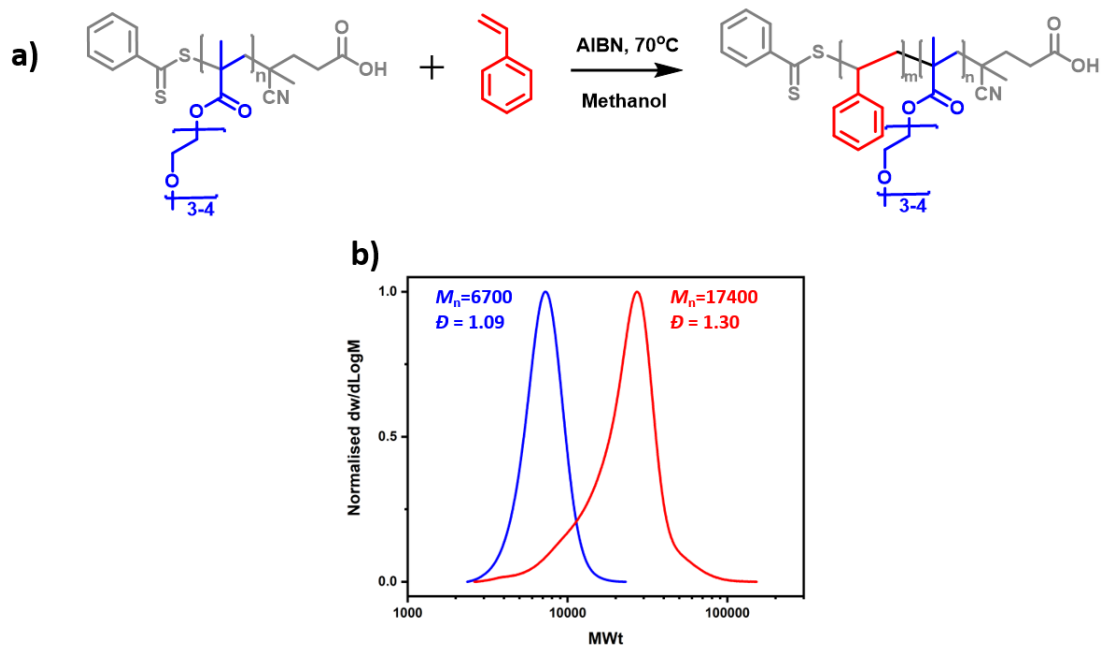


Figure 5.10: a) Chemical scheme of P(POEGMA-*b*-styrene) synthesis and b) SEC traces of P(POEGMA) (left trace) and P(POEGMA-*b*-styrene) (right trace).

A small amount of toluene was then added ($5 \mu\text{l ml}^{-1}$) which induced the transformation from worms to vesicles. Cryogenic EM further confirmed the existence of worms and vesicles in solution, thus supporting the successful morphological transformation (**figure 5.11c**).

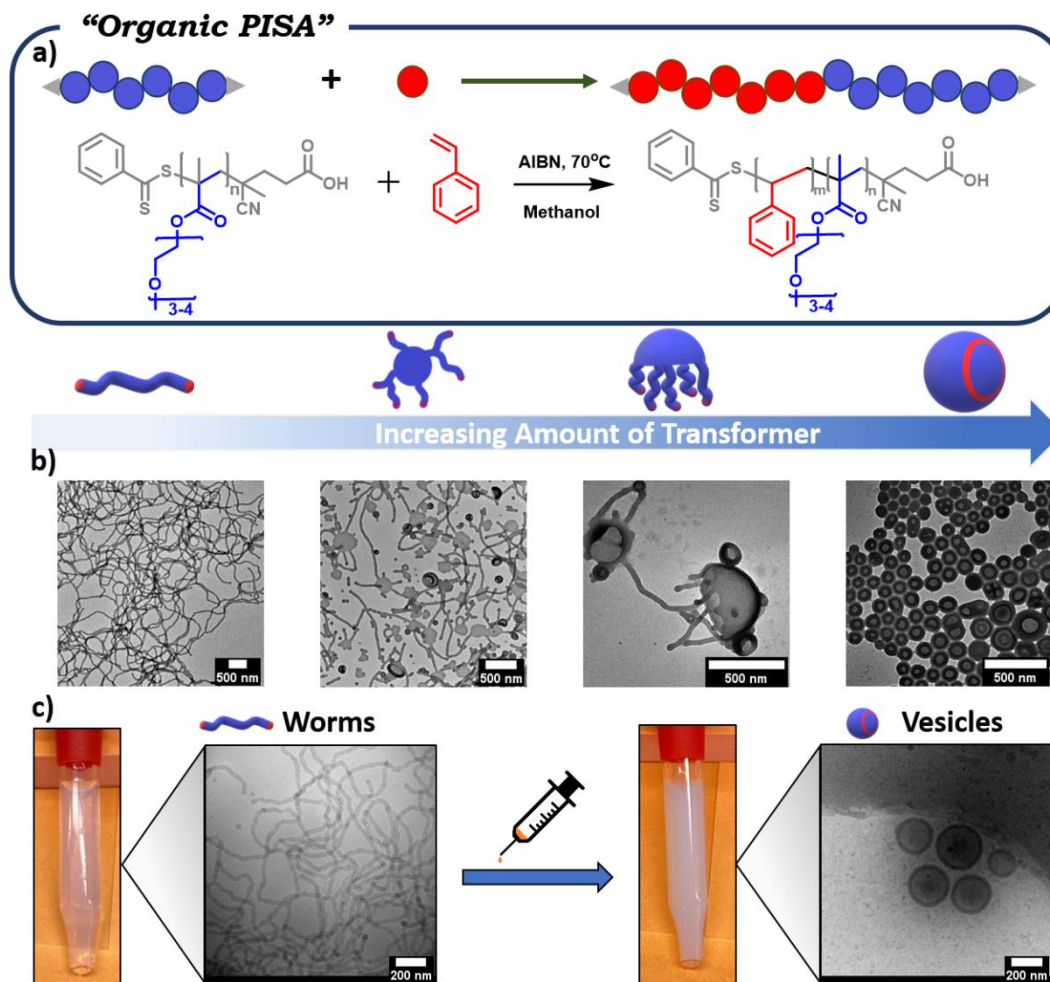


Figure 5. 11: TIM of polymeric nanoparticles obtained via organic PISA. a) Schematic representation of RAFT dispersion polymerization, b) TEM images of worms, octopi-like morphology, jellyfish and vesicles respectively, c) Visual representation and cryo-EM of worms and vesicles. The cryo-EM images were acquired by Dr. Pilkington.

This data also highlighted that the observed morphologies are not an artifact of a “drying” effect as in the solvent evaporation methodologies.⁴⁷ The transformation could also be visualized by a clear change in turbidity. It is noted that SEC traces of both worms and vesicles showed overlapping molar mass distributions (**figure 5.12b**).

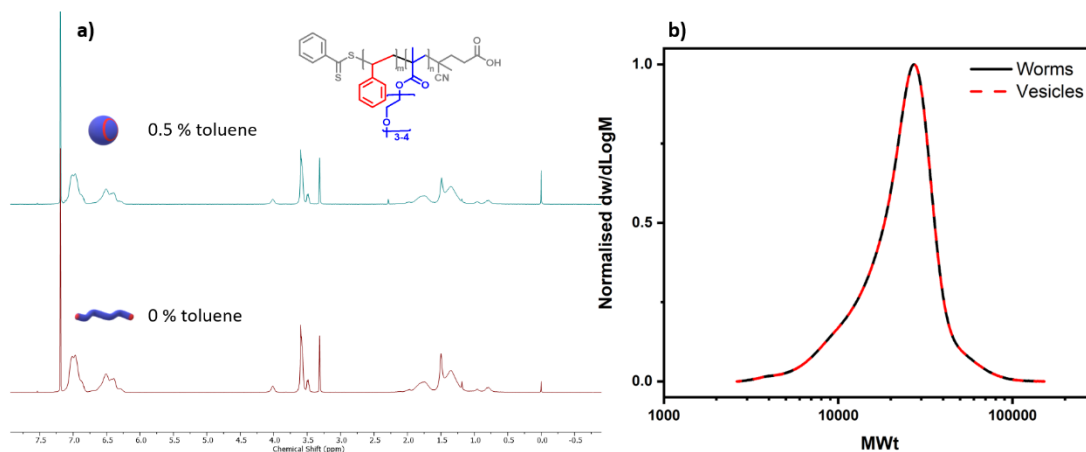


Figure 5. 12: a) ¹H NMR spectra of P(POEGMA-*b*-styrene) with (top spectrum) and without (bottom spectrum) addition of toluene. The water dispersions of the polymeric nanoparticles were dried via air purging in order to eliminate the amount of water. The ¹H NMR spectra were recorded in chloroform-*d*, and b) SEC traces of P(POEGMA-*b*-styrene) before and after addition of toluene. SEC analysis was conducted without water removal.

Interestingly, at even lower transformer concentrations ($2 \mu\text{l ml}^{-1}$ and $3 \mu\text{l ml}^{-1}$), several characteristic intermediate morphologies were observed. In particular, mixed phases consisting of flat lamellar disks interlinked with worms (octopi-like morphology) and jellyfish-like morphologies could be clearly detected by TEM (**figure 5.11b**). These intermediate morphologies not only suggest that we indeed have a transformation from worms to vesicles, but also indicate that the transformer is triggering a similar mechanistic pathway to traditional PISA but without the need to increase the molecular weight of the second block.²⁶ We also conducted additional experiments in which various organic molecules were used as potential morphological transformers. Interestingly, water-miscible organic molecules, such as tetrahydrofuran, could not alter the worm-like shape. In contrast, other water-immiscible molecules including styrene, xylene and mesitylene could act as efficient transformers owing to their resemblance with the hydrophobic core. Instead, cyclohexane and hexane, despite being water-immiscible, did not lead to a successful morphological transformation under the conditions studied. This may be due to their saturated structure which is different to the PS core (**figure 5.13**).

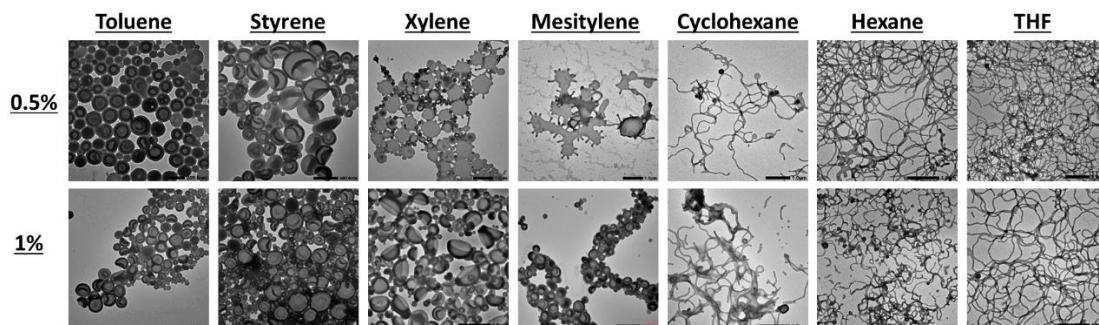


Figure 5.13: Addition of different organic molecules into P(POEGMA-*b*-styrene) worm-like nanoparticles/water dispersion.

As a final experiment, the block copolymer obtained by organic PISA was freeze-dried and re-dissolved in acetone. A traditional self-assembly procedure in water was then followed and upon dialysis TEM showed the formation of worms. TIM was then applied by the addition of toluene and the shape was instantly changed from worms to vesicles (**figure 5.14**). These preliminary data suggest that our method can also be applied in traditional self-assembly strategies.

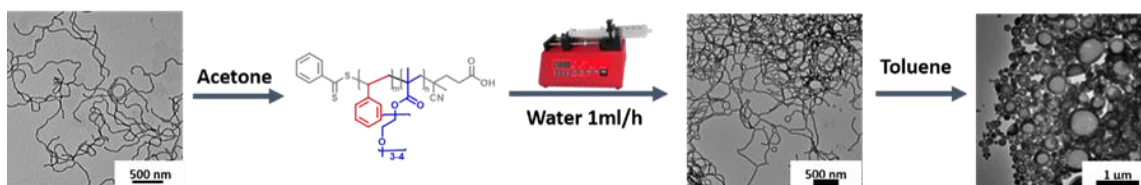


Figure 5.14: Formation of worms via traditional solution self-assembly of P(POEGMA-*b*-styrene) and the morphological transformation of worms to vesicles.

Conclusion

In summary, I have developed a transformer-induced metamorphosis strategy that allows for the rapid transformation between different morphologies by adjusting the amount of an added organic molecule that matches the solubility parameter of the core. The successful transformation was confirmed by TEM, cryo-EM, and SAXS while SEC revealed identical molecular weights for all the obtained morphologies. Importantly, our approach operates at room temperature and without altering the chemical structure of the obtained morphologies. Such strategy can further enable structure-property relationship studies and theoretical simulations.

References

- (1) Dau, H.; Jones, G. R.; Tsogtgerel, E.; Nguyen, D.; Keyes, A.; Liu, Y.-S.; Rauf, H.; Ordonez, E.; Puchelle, V.; Basbug Alhan, H. *Chem. Rev.* **2022**, *122*, 14471.
- (2) Alexandridis, P.; Lindman, B. *Amphiphilic block copolymers: self-assembly and applications*; Elsevier, **2000**.
- (3) Mai, Y.; Eisenberg, A. *Chem. Soc. Rev.* **2012**, *41*, 5969.
- (4) Zhang, L.; Eisenberg, A. *Science* **1995**, *268*, 1728.
- (5) Elsabahy, M.; Wooley, K. L. *Chem. Soc. Rev.* **2012**, *41*, 2545.
- (6) Hubbell, J. A.; Chilkoti, A. *Science* **2012**, *337*, 303.
- (7) Gref, R.; Minamitake, Y.; Peracchia, M. T.; Trubetskoy, V.; Torchilin, V.; Langer, R. *Science* **1994**, *263*, 1600.
- (8) Boucher-Jacobs, C.; Rabnawaz, M.; Katz, J. S.; Even, R.; Guironnet, D. *Nat. Commun.* **2018**, *9*, 1.
- (9) Tanner, P.; Baumann, P.; Enea, R.; Onaca, O.; Palivan, C.; Meier, W. *Acc. Chem. Res.* **2011**, *44*, 1039.
- (10) Derry, M. J.; Smith, T.; O'hora, P. S.; Armes, S. P. *ACS Appl. Mater. Inter.*, **2019**, *11*, 33364.
- (11) Truong, N. P.; Quinn, J. F.; Whittaker, M. R.; Davis, T. P. *Polym. Chem.* **2016**, *7*, 4295.
- (12) Truong, N. P.; Whittaker, M. R.; Mak, C. W.; Davis, T. P. *Expert Opin. Drug Delivery* **2015**, *12*, 129.
- (13) Wen, X.; Tang, L.; Li, B. *Chem. Asian J.*, **2014**, *9*, 2975.
- (14) Qiu, H.; Hudson, Z. M.; Winnik, M. A.; Manners, I. *Science* **2015**, *347*, 1329.
- (15) Walther, A.; Hoffmann, M.; Müller, A. H. *Angew. Chem. Int. Ed.* **2008**, *47*, 711.
- (16) Warren, N. J.; Armes, S. P. *J. Am. Chem. Soc.* **2014**, *136*, 10174.
- (17) Massey, J.; Power, K. N.; Manners, I.; Winnik, M. A. *J. Am. Chem. Soc.* **1998**, *120*, 9533.
- (18) Zhang, L.; Eisenberg, A. *Macromolecules* **1996**, *29*, 8805.
- (19) Rodriguez-Hernandez, J.; Chécot, F.; Gnanou, Y.; Lecommandoux, S. *Prog. Polym. Sci.* **2005**, *30*, 691.
- (20) Finnegan, J. R.; He, X.; Street, S. T.; Garcia-Hernandez, J. D.; Hayward, D. W.; Harniman, R. L.; Richardson, R. M.; Whittell, G. R.; Manners, I. *J. Am. Chem. Soc.* **2018**, *140*, 17127.
- (21) Tao, D.; Feng, C.; Cui, Y.; Yang, X.; Manners, I.; Winnik, M. A.; Huang, X. *J. Am. Chem. Soc.* **2017**, *139*, 7136.
- (22) Zetterlund, P. B.; Kagawa, Y.; Okubo, M. *Chem. Rev.* **2008**, *108*, 3747.
- (23) Zetterlund, P. B.; Thickett, S. C.; Perrier, S.; Bourgeat-Lami, E.; Lansalot, M. *Chem. Rev.* **2015**, *115*, 9745.
- (24) Charleux, B.; Delaittre, G.; Rieger, J.; D'Agosto, F. *Macromolecules* **2012**, *45*, 6753.
- (25) Penfold, N. J.; Yeow, J.; Boyer, C.; Armes, S. P.; *ACS Macro Lett.*, **2019**, *8*, 1029.
- (26) Blanazs, A.; Madsen, J.; Battaglia, G.; Ryan, A. J.; Armes, S. P. *J. Am. Chem. Soc.* **2011**, *133*, 16581.
- (27) Kaga, S.; Truong, N. P.; Esser, L.; Senyschyn, D.; Sanyal, A.; Sanyal, R.; Quinn, J. F.; Davis, T. P.; Kaminskas, L. M.; Whittaker, M. R. *Biomacromolecules* **2017**, *18*, 3963.

- (28) Vu, M. N.; Kelly, H. G.; Wheatley, A. K.; Peng, S.; Pilkington, E. H.; Veldhuis, N. A.; Davis, T. P.; Kent, S. J.; Truong, N. P. *Small* **2020**, *16*, 2002861.
- (29) Zhang, L.; Yu, K.; Eisenberg, A. *Science* **1996**, *272*, 1777.
- (30) Achilleos, D. S.; Hatton, T. A.; Vamvakaki, M. *J. Am. Chem. Soc.* **2012**, *134*, 5726.
- (31) Pei, Y.; Lowe, A. B.; Roth, P. J. *Macromol. Rapid Commun.* **2017**, *38*, 1600528.
- (32) McCormick, C. L.; Sumerlin, B. S.; Lokitz, B. S.; Stempka, J. E. *Soft Matter* **2008**, *4*, 1760.
- (33) Rolland, M.; Truong, N. P.; Parkatzidis, K.; Pilkington, E. H.; Torzynski, A. L.; Style, R. W.; Dufresne, E. R.; Anastasaki, A. *JACS Au* **2021**, *1*, 1975.
- (34) Fielding, L. A.; Lane, J. A.; Derry, M. J.; Mykhaylyk, O. O.; Armes, S. P. *J. Am. Chem. Soc.* **2014**, *136*, 5790.
- (35) Ratcliffe, L. P.; Derry, M. J.; Ianiro, A.; Tuinier, R.; Armes, S. P. *Angew. Chem. Int. Ed.* **2019**, *58*, 18964.
- (36) Figg, C. A.; Simula, A.; Gebre, K. A.; Tucker, B. S.; Haddleton, D. M.; Sumerlin, B. S. *Chem. Sci.* **2015**, *6*, 1230.
- (37) Li, L.; Cui, S.; Hu, A.; Zhang, W.; Li, Y.; Zhou, N.; Zhang, Z.; Zhu, X. *Chem. Commun.* **2020**, *56*, 6237.
- (38) Lovett, J. R.; Warren, N. J.; Ratcliffe, L. P.; Kocik, M. K.; Armes, S. P. *Angew. Chem. Int. Ed.* **2015**, *54*, 1279.
- (39) Ratcliffe, L. P.; Couchon, C.; Armes, S. P.; Paulusse, J. M. *Biomacromolecules* **2016**, *17*, 2277.
- (40) Zhang, W.; Gao, C. *J. Mater. Chem. A* **2017**, *5*, 16059.
- (41) Phan, H.; Taresco, V.; Penelle, J.; Couturaud, B. *Biomater. Sci.*, **2021**.
- (42) Byard, S. J.; O'brien, C. T.; Derry, M. J.; Williams, M.; Mykhaylyk, O. O.; Blanz, A.; Armes, S. P. *Chem. Sci.* **2020**, *11*, 396.
- (43) Barton, A. F. *Chem. Rev.* **1975**, *75*, 731.
- (44) Figg, C. A.; Carmean, R. N.; Bentz, K. C.; Mukherjee, S.; Savin, D. A.; Sumerlin, B. S. *Macromolecules* **2017**, *50*, 935.
- (45) Hatton, F. L.; Derry, M. J.; Armes, S. P. *Polym. Chem.* **2020**, *11*, 6343.
- (46) Esser, L.; Truong, N. P.; Karagoz, B.; Moffat, B. A.; Boyer, C.; Quinn, J. F.; Whittaker, M. R.; Davis, T. P. *Polym. Chem.* **2016**, *7*, 7325.
- (47) Pochan, D. J.; Chen, Z.; Cui, H.; Hales, K.; Qi, K.; Wooley, K. L. *Science* **2004**, *306*, 94.

Future Outlook

The work presented in this thesis offers promising opportunities for future exploration. I would like to share my thoughts on potential avenues that could be pursued next.

Firstly, in relation to the oxygen-enhanced ATRP, further investigation can be conducted by analyzing the role of each component in the ATRP process. Different ATRP systems, such as conventional ATRP, ARGET ATRP, ICAR ATRP, and Cu(O)-RDRP, offer distinct advantages while utilizing different reaction components. Therefore, understanding the relationship between these components with oxygen will enhance our understanding of the system and facilitate optimization and simplification of the procedure. One possible approach is to explore the systems via an oxygen-probe (a simple device that can measure oxygen consumption), which would allow for the isolation and study of the relationship between each component and oxygen, as well as their synergistic effects.

The demonstration of photocatalytic depolymerization opens up numerous intriguing possibilities. For instance, exploring photo-RDRP, which is gaining popularity in 3D/4D printing, can provide significant advantages in printed polymeric materials. Similarly, the application of photocatalytic depolymerization in 3D/4D deprinting could be explored. This would further demonstrate the significant advantage of utilizing polymers with functional end-groups in printed polymeric materials and promote the modification of objects through depolymerization. Additionally, selective depolymerization of polymers from surfaces holds potential for photo-patterning applications and surface modifications.

Shifting the focus of polymer science towards more sustainable approaches is highly advantageous. Therefore, further exploration of both polymer synthesis and properties using renewable resources is of great interest. In this field, the sustainability cycle can be expanded by applying depolymerization techniques to polymers made from renewable resources. If this is feasible, it would enable the production of high-quality and controlled polymers from renewable resources, while also providing the possibility of ending their lifecycle by depolymerizing them back into virgin monomers.

Lastly, the *in-situ* characterization of polymeric nanoparticles can provide significant advantages. Exploring techniques such as *in-situ* cryo-EM and *in-situ* SAXS/SANS for the developed

transformer-induced metamorphosis strategy would enable the monitoring of morphological transformations in-depth. This would shed light on the underlying mechanisms and facilitate the observation/isolation of intermediate metastable morphologies, which could be of great interest.